Local mechanical stimulation based approaches for the study of cells

by

G. Monserratt López Ayón

Centre for the Physics of Materials

Department of Physics

McGill University, Montreal

August 2014

A Thesis submitted to McGill University in partial fulfillment of the requirements for the degree of Doctor of Philosophy

© G Monserratt Lopez Ayon, 2014

Contents

Abstract

Biology has traditionally focused on chemical cues to understand cell behaviour. New tools allow the influence of mechanical cues to be explored, as well as the mechanical properties of cells to be studied. In this thesis we use local mechanical stimulation techniques that operate at the single cell level to evoke active responses in cells.

We combine atomic force microscopy and fluorescence microscopy to investigate mechanotransduction resulting from different levels of microinjury (membrane deformation and membrane penetration) in bone cells, and we use pipette micromanipulation to investigate functional neural growth induced by controlled manipulation of adhesive contacts. We show that bone cell responses to local membrane deformation exhibit threshold properties when micro-injury is induced. We propose mechanisms by which the integrating signal, intracellular Ca2+, increases until it reaches the threshold concentration necessary to induce global response.

We have demonstrated for the first time that growth of functional neurites can be induced mechanically. To achieve this we developed and optimised a platform to initiate and elongate central nervous system (CNS) neurites and to precisely connect them to a desired target for assembly of new neuronal networks. We show that the newly extended connections are structurally indistinguishable from those naturally grown and have the capability to transmit an electrical signal. Finally, we speculate how such biophysical methods may contribute to the successful treatment of lesions to the central nervous system, which are presently considered incurable. Our results highlight the importance of mechanical cues in cellular biochemical responses and cell development.

Résumé

La biologie s'est traditionnellement concentrée sur les stimulations chimiques pour comprendre le comportement des cellules. De nouveaux outils permettent l'exploration de l'influence des stimulations mécaniques, ainsi que l'étude des propriétés mécaniques des cellules. Cela a permis d'apprécier l'importance des propriétés physiques et des stimulations mécaniques dans les processus physiologiques. Dans cette thèse, nous utilisons des techniques de stimulation mécanique locale qui opérent au niveau monocellulaire afin de provoquer des réponses actives dans les cellules.

Nous combinons la microscopie à force atomique et la microscopie à fluorescence afin d'investir la mécanotransduction résultant de différents niveaux de microtraumatisme (déformation de membrane et pénétration de membrane) dans les cellules osseuses, et nous utilisons la micromanipulation de pipette afin d'investir la croissance neurale fonctionnelle induite par la manipulation contrôlée de contacts adhésifs. Nous montrons que la réponse des cellules osseuses à une déformation locale de membrane présente un seuil lorsqu'un microtraumatisme est induit. Nous proposons des mécanismes par lesquels le signal intégré, la concentration de Ca2+ intercellulaire, augmente jusqu'à atteindre la concentration seuil nécessaire pour induire une réponse globale.

Nous avons démontré pour la première fois que la croissance de neurites fonctionnelles peut être induite mécaniquement. À cette fin, nous avons développé et optimisé une plateforme pour initier et élonguer des neurites du système nerveux central qui peuvent être connectées avec précision à une cible pour l'assemblage de nouveaux réseaux neuronaux. Nous montrons que les connections nouvellement établies sont structurellement indistinguables de celles crûes naturellement et ont la capacité de transmettre un signal électrique. Finalement, nous spéculons sur la façon dont de telles méthodes biophysiques pourraient contribuer au traitement efficace de lésions du système nerveux central considérées actuellement comme incurables. Nos résultats mettent en évidence l'importance des stimulations mécaniques dans la réponse biomécanique cellulaire et le développement des cellules.

Acknowledgments

First and foremost, I would like to thank my supervisor Dr. Peter Grutter for his advice and guidance, his support and encouragement to try new things. Thank you for providing me with such an incredible opportunity to learn and work on something I love surrounded by the best people.

Giant thanks to Svetlana Komarova, for making sure I did things to my full potential, for teaching me how to do science, for encouraging me to work hard and try new things. You are a wonderful person.

I would especially like to thank Margaret Magdesian for her friendship, her unconditional encouragement, support and love. Thanks for pushing me to do things to the best of my ability. Your example constantly reminds me to love and appreciate every minute of my life.

Thanks to my recently wedded and beloved husband David Oliver, for standing by me, being so wonderfully patient and supportive, as well as a brilliant scientist and colleague. I love you.

Thanks to Yves De Koninck for all your words of encouragement, your interest in what I do, your passion for learning and for lending me all the equipment.

Thank you all for being such incredible human beings. Thanks for your love, friendship, constant encouragement, support and all the lessons you taught me through this stage of my life.

Thanks also to Yoichi Miyahara, Robert Gagnon, John Smeros, Gula (Gulzhakhan Sadvakassova), Delphine Gobert, Ed Ruthazer, William Paul, Dominic Boudreau, Megumi Mori, Xue Ying Chua, Hussain Sanji, Jean François Desjardins, Paul Wiseman, Heng-Yen Liu, Stella Shu Xing, Osama Maria, Jeff LeDue, Mario Methot, Helene Bourque, Alexis Goulet-Hanssens, Christopher Barrett, Ricardo Sanz, Alyson Fournier, Zaven Altounian, Victor Yu, Mathieu Cesar, Sara Najem and all the members of the Grütter lab and everyone else who somehow collaborated, contributed or discussed with me to give me confidence and enable this work.

Thanks to the neuro-engineering program and other sources of funding.

To my mom and my sister.

Preface & Contribution of Authors

In this section the roles each author had in the preparation of the manuscripts presented in thesis Ph.D. thesis are described.

Article 1.

Deconvolution of Calcium Fluorescent Indicator Signal from AFM Cantilever Reflection

G. Monserratt Lopez-Ayon:
Designed and performed the experiments, developed the procedures to analyze and interpret the data and wrote the manuscript.

David J. Oliver:
Assisted in the development of the procedures to analyze the data and assisted in the result interpretation.

Peter H. Grutter
Supervised, assisted in the design of the experiments, in the result interpretation and revised the manuscript.

Svetlana V. Komarova
Supervised, assisted in the design of the experiments, in the result interpretation, revised the manuscript and responded to reviewers.

Article 2.

Local membrane deformation and micro-injury lead to qualitatively different responses in osteoblasts

G. Monserratt Lopez-Ayon:

Designed and performed the experiments, analyzed and interpreted the data and wrote the manuscript.

Heng-Yen Liu
Assisted in the performance of the control experiments, data analysis and revisions to the manuscript.

Shu Xing
Prepared samples and assisted in the performance of the experiments.

Osama Maria
Prepared samples and assisted in the performance of the experiments.

Jeffrey M LeDue
Assisted in the experimental design and assisted in the performance of the experiments.

Helene Bourque
Assisted in the experimental design and the result interpretation.

Peter H. Grutter
Supervised, assisted in the design of the experiments, in the result interpretation and revised the manuscript.

Svetlana V. Komarova
Supervised, assisted to the design of the experiments, in the result interpretation, revised the manuscript and responded to reviewers.

Article 3.
Rewiring neuronal networks using micromanipulation

G. Monserratt Lopez-Ayon (the first two authors share equal contribution)
Designed and performed the pulling experiments using pipette micromanipulation, designed the electrophysiology setup, performed the electrophysiology experiments, analyzed the electrophysiology data, interpreted the pulling and electrophysiology data and wrote the manuscript.

Margaret H. Magdesian (the first two authors share equal contribution)
Designed the experiments and developed the protocol for AFM pulling experiments and the imunofluorescence, analyzed and interpreted the data and wrote the manuscript.

Megumi Mori
Assisted in the performance of some of the pulling experiments

Dominic Boudreau
Assisted in the design of the electrophysiology setup

David Oliver
Assisted in the design of the experiments, the data analysis and the manuscript writing

William Paul
Assisted in the design of the electrophysiology setup

Ricardo Sanz
Provided samples for experimentation

Alexis Goulet-Hanssens
Designed the photo-release coating to release the adhesive contact

Yoichi Miyahara
Assisted in the design of the electrophysiology setup

Christopher J. Barrett
Supervised the design of the photo-release coating to release the adhesive contact

Alyson Fournier
Provided samples for experimentation

Yves De Koninck
Provided the instrumentation to perform electrophysiological recordings, assisted in the design of the experiments, the interpretation of the results and the data analysis.

Peter Grütter
Supervised, assisted to the design of the experiments, in the result interpretation, revised the manuscript

Publications

1.- G. Monserratt Lopez-Ayon, David J. Oliver, Peter H. Grutter, and Svetlana V. Komarova, "Deconvolution of Calcium Fluorescent Indicator Signal from AFM Cantilever Reflection", Microscopy Microanalysis, 18, 808–815, 2012

2.- Lopez-Ayon, G. Monserratt, Liu, Heng-Yen, Xing, Shu, Maria, Osama M, LeDue, Jeffrey M, Bourque, Helene, Grutter, Peter, Komarova, Svetlana V, "Local membrane deformation and micro-injury lead to qualitatively different responses in osteoblasts", F1000Research, 3:162, 2014

3.- Lopez-Ayon, G. Monserratt, Magdesian Margaret H, Megumi Mori, Dominic Boudreau, David Oliver, Alexis Goulet-Hanssens, William Paul, Ricardo Sanz**,** Yoichi Miyahara, Christopher J. Barrett, Alyson Fournier, Yves De Koninck, Peter Grütter, "Rewiring neuronal networks using micromanipulation", to be submitted

Mechanical forces act daily on living systems and are crucial for their proper growth and development. They can also cause injury and activate physiological repair mechanisms. Because mechanical stimuli are ubiquitous, sensation of mechanical cues could be one of the oldest sensory transduction processes that evolved in living organisms [1]. The cell membrane presents a major target to external mechanical forces that act upon a cell, and its sensitivity to the mechanical environment plays a key role in the physiological translation of mechanical cues into biochemical effects inside the cell.

For at least a century some people have speculated that mechanical forces are crucial for the morphology and functioning of tissues and cells [2]. However, most of the subsequent efforts were focused on understanding the effects of the chemical environment on the cellular activity. Still, many efforts are, but the belief that the mechanical environment affects the cellular behaviour has become more accepted. The perspective is shifting towards the fact that in addition to biochemical factors, mechanical signals also play pivotal roles in regulating cell behaviour. Take for example, the case of stem cells: it has been shown that mechanical stimuli can either work alone or together with chemical factors to regulate a stem cell's fate [3,4]. In vivo, cells receive environmental stimuli that guide them to differentiation and to grow towards specific cells or tissues. Mechanical forces have also been found responsible for modulating bone cell activity: microgravity directly affects bone cell mechanisms that regulate proper bone turnover [5], and mechanical stimulation of low amplitude and high frequency has been shown to stimulate bone formation [6].

Mechanical techniques such as cell indentation, manipulation, particle rheology and micro- or nanoneedle poking have enabled quantification of the mechanical responses which were only qualitatively described 100 years ago [2,7,8]. Using these techniques, it has become clear that the mechanical properties of live cells change during physiological processes and in diseases such as cancer [9–11]. Detection of these state changes through mechanical methods is one motivation for future development and application of nanomedicine and nanophysiology tools.

New experimental methods and technologies have recently enabled remarkable new discoveries. For example, aggressive cancer cells are softer than indolent cancer cells and they react differently to substrates with different stiffness [10,12–14]. The mechanical environment of many cell types can be used to detect, control and alter gene

expression [3,4,15,16]. It is possible to induce outgrowth of functional cellular processes by mechanical stretch [17–19]. It is even possible to access the intracellular environment to deliver, extract and perfuse intracellular components using cantilever based approaches [20–23].

The advent of techniques such as Atomic Force Microscopy [24] has allowed thorough systematic investigation of forces at a single cell level. Microfabrication techniques have enabled development of tools to alter the mechanical environment and even deliver well-defined forces to a single cell. In order to fully realize the potential of these and other mechanical tools, it is necessary to assess their capabilities. It is imperative to make sure they are robust and to understand the information that can be extracted and its limitations. Better appreciation of the strengths and weaknesses of these techniques will help elucidate how the mechanics of living cells and biomolecules, under physiological and pathological conditions, play a major role in health and disease.

Micro and nanomechanical techniques have most commonly been used to passively measure mechanical properties of cells and to detect biological status. By contrast, this thesis examines active responses of cells to mechanical stimulation. This includes signaling responses to mechanical stimulus (mechanotransduction), and even the generation of new cellular material in the case of neurons.

Nanoscale techniques, such as atomic force microscopy (AFM) allow us to provide localized mechanical stimulation at the single-cell level with precisely controlled forces. By further combining AFM with optical microscopy techniques, it is possible to correlate applied mechanical stimulation with simultaneous cellular biochemical response.

Chapter 4 of this thesis examines the strengths and weaknesses of the combination of atomic force microscopy and fluorescence microscopy to study living cells. The AFM operation causes significant artifacts on the fluorescence data that affect the results in an undesirable manner if not accounted for. We show how to correct for the artifact and show that it can in fact be used to establish more precise temporal correlations.

In Chapter 5 we use bone forming cells, osteoblasts; that are known for their robust mechanical sensitivity, to examine their responses to localized mechanical stimuli and obtain new insights into the complex dynamics of cellular responses to controlled application of forces of different magnitude. Such knowledge is important for better understanding the mechanisms of mechanical loading-induced bone formation, as well as micro-damage induced bone remodeling.

In Chapter 6, as a second part of this thesis, we study the intriguing possibility that mechanical cues can be used to manipulate the cell behaviour by directing the growth and extension of functional neuronal processes and generation of functional connections (i.e. rewiring) of neuronal networks. Traditionally, neuronal growth and the formation of connections are investigated within a molecular biochemical framework. In this work, we introduce and study the importance of mechanical forces for guiding rewiring of neurons. Our results demonstrate the importance of mechanical cues in fundamental processes of CNS axonal growth and repair, and open the door to the creation of artificial neuronal networks with predefined, controlled topology, the development of robust brain-machine interfaces as well as drug discovery platforms and therapies for traumatic CNS injury and other neurodegenerative diseases.

Chapter 2. Literature Review

The study of the mechanics of cells uses a wide variety of tools that have been adapted from the principles in physical sciences. These tools have enabled studies that help to elucidate the mechanical properties of cells, the nature of cellular forces, and the chemical mechanisms of response to the nature of the mechanical environment (mechanotransduction) [25]. The insights gained through these studies provide a better understanding of the complex processes that lead to the normal cell function and allow significant insights on the progression of mechanically related diseases.

2.1 Cell mechanics

2.1.1 The mechanical components of the cell

To understand how forces are transmitted throughout the molecular structures of the cell, and how they are transduced into biochemical reactions, it is first necessary to understand the morphology and mechanical properties of individual cellular components (Figure 1.1.1).

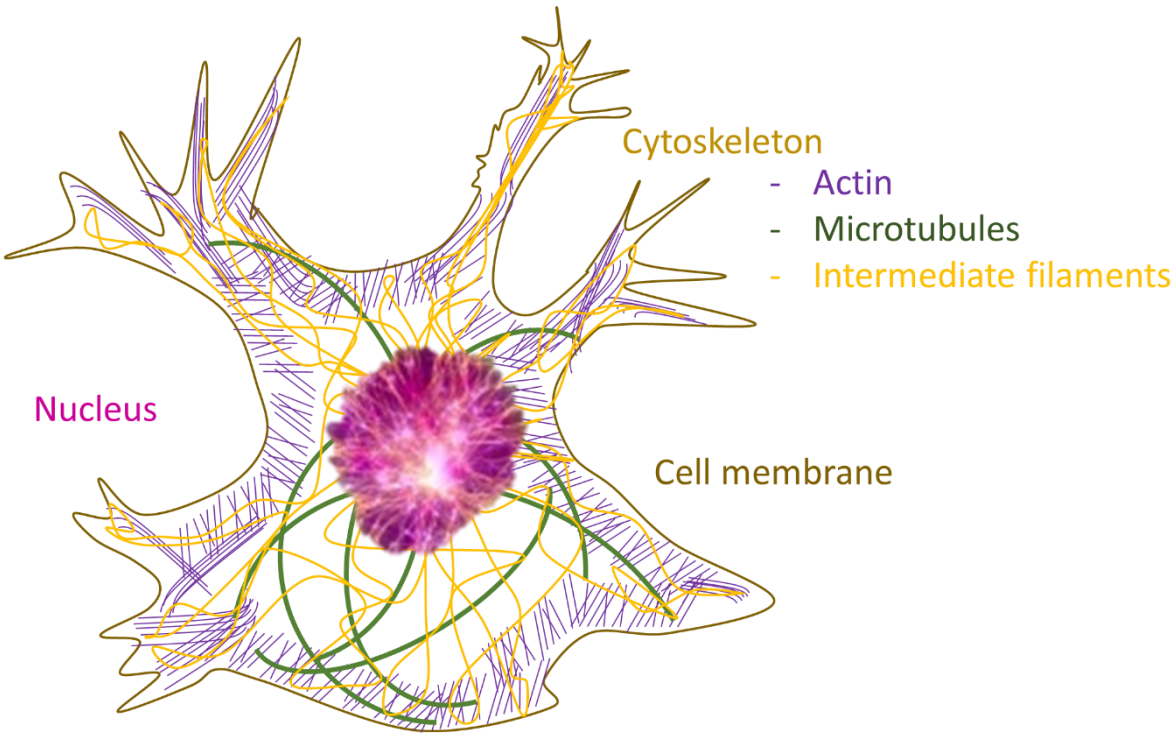

FIGURE 1.1.1 MAJOR STRUCTURAL COMPONENTS OF A CELL

Animal cells require specialized structures to maintain their cellular integrity. The mechanical properties and organization of the cytoskeleton determines, in large part, the

morphology and mechanical properties of the cell [26]. However, the cell membrane, nucleus, and cytoplasm also contribute to the mechanics of a cell.

The cell membrane acts as a barrier between the cell interior (cytosol) and the extracellular environment; it is mainly composed of a lipid bilayer, but also contains protein structures that act as receptors for signaling molecules, transport channels for ions, or linkers between a cell's cytoskeleton and the extracellular environment [27].

The nucleus lies within the central region of the cell, it protects the DNA and proteins with the nuclear envelope (a lipid bilayer similar to the cell membrane). The nucleus is robustly elastic and more rigid than the cytoplasm [28]. It provides structure to the cell and can contribute to its plasticity, but most importantly it detects molecules resulting from mechanotransduction and regulates gene expression [3,15].

The cytoplasm is the fluid that surrounds the nucleus and constitutes a crowded microenvironment of proteins and protein complexes. The density of proteins in the cytoplasm contributes to its rheological properties and influences the reactions taking place [29].

The cytoskeleton lies within the cytoplasm. It is a protein scaffold consisting of three major classes of filaments: microfilaments, microtubules and intermediate filaments (Figure 1.1.2, [26]). The cytoskeleton carries out three broad functions: it spatially organizes the contents of the cell; it connects the cell physically and biochemically to the external environment; and it generates coordinated forces that enable the cell to move and change shape. [30]. Each of the filaments in the cytoskeleton is built out of particular structural subunits that polymerize into different structures, determining strength and straightness. In the case of actin filaments and microtubules, the alignment of the subunits is parallel and unidirectional. This organization of the subunits makes the filaments polar, which influences the kinetics of polymerization [26].

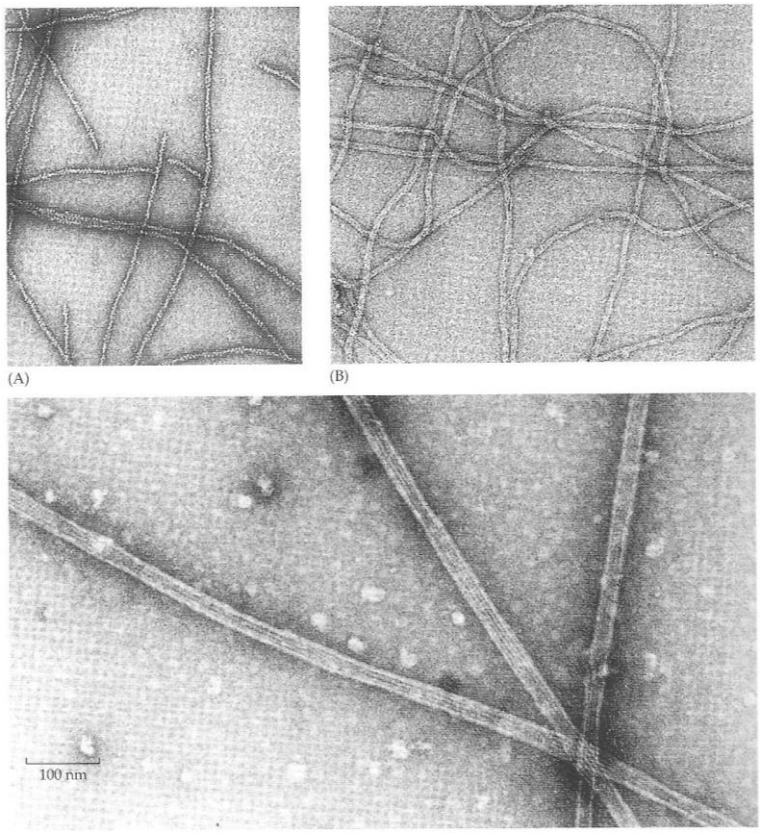

FIGURE 1.1.2 ELECTRON MICROGRAPHS OF NEGATIVELY STAINED CYTOSKELETAL FILAMENTS. (A) ACTIN FILAMENTS, (B) INTERMEDIATE FILAMENTS AND (C) MICROTUBULES. [26]. *ALL FIGURES HAVE THE SAME LENGTH SCALE.*

2.1.2 The contribution of the cytoskeletal filaments to the mechanical properties of the cell

Actin

Actin filaments, formed by actin monomers, are the primary structural component of the cytoskeleton and extend through the cytoplasm. These filaments are crucial for a functioning cell because they form a highly ordered structural network together with myosin proteins [31] and are the short-range transportation links in proximity to the cell membrane for transport and delivery of cargo [32]. Actin filaments are considered integral in creating and maintaining the forces required for cellular movement or contraction [33] and cell shape [34,35]. They have a diameter ranging from

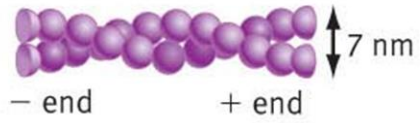

5 to 9 nm, persistence length on the order of tens of micrometers and elastic modulus of ~2 GPa [36].

Intermediate filaments

Intermediate filaments, formed by intermediate filament dimers, extend throughout the cytoplasm and inner nuclear membrane and provide strength, integrity, and organization for both. The genes responsible for expressing these filaments are variable, and this accounts for a great diversity in the types of structures they can form. [36] They have variable diameters (5-20 nm), a persistence length ~1 μm and elastic modulus of ~7 MPa [37], which conveys them a higher curvature (Figure 1.1.2).

Microtubules

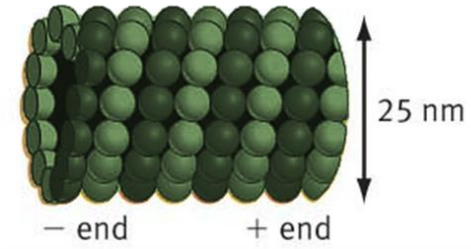

Microtubules, formed of tubulin heterodimers, are among the stiffest structural elements found in animal cells. They are hollow tubular structures [38], which serve as the long long-range transportation links for motor proteins and other molecules to shuttle cargo from the center to the periphery of the cell [32]. Microtubules form a rigid stable structure that is used by motor proteins to generate force and movement in motile structures such as neuronal growth cones. They display a resilience to shear and twist forces [39] and resist cellular compressive forces [40]. The diameter of a microtubule is generally about 24 nm, with a persistence length on the order of (~5 mm) millimeters and an elastic modulus of ~2 GPa [26]. Their larger cross-section and increased stiffness leads to their straight appearance in comparison to the other cytoskeletal filaments [36].

The mechanical properties of a cell are not a simple scalar quantity, but rather a function of the cytoskeletal components and how they respond to mechanical strains. Cells exhibit both viscous (time dependent) and elastic properties [41]. For such viscoelastic materials, the extent of mechanical deformation affects the interaction of the filaments; thus, the mechanical parameters depend upon the amount of deformation and the deformation rate. A good summary of how such polymer interactions are affected by the mechanical forces can be found in ref. [41]).

2.1.3 Cellular activity and mechanical stimulation

Just as mechanical forces can act on cells and lead to signaling cascades, cells which experience a change in their biochemistry can trigger changes in their mechanical properties and exert mechanical forces on their environment. In the former case, a force is applied or a mechanical stimulus is imposed on the cell, and changes in the cell's mechanical and/or biochemical response are observed, such is the case of endothelial cells which align in response to a directional fluid flow [42], whereas in the latter, biochemical changes induce changes in the mechanical properties of cells, for instance, hormonal changes regulate smooth muscle cells' mechanical properties [43]

In the coming section, different methods to examine how cells respond to external mechanical factors will be discussed.

2.2 Current nanoscience approaches for life cell studies

Advances in technology have allowed for the development of a number of different specialized approaches to estimate the cell's mechanical properties. Some of these techniques have also been used to determine cell mechanical and biochemical response in response to an applied force. It has been found that cells communicate with the external environment. They receive external signals that guide complex biochemical behaviours that lead to changes in adhesion [44,45], stiffness [46], electrical activity [47], motility [48,49], and, in some cases, gene expression and differentiation [3,4,16]. Whereas the contribution of chemical signals has long been studied and is to some extent understood, physical signals have only recently been recognized to be pervasive and powerful. In order to fully realize their potential, it is necessary to assess their capabilities in elucidating whether and how the mechanics of living cells and biomolecules, under physiological and pathological conditions, affect the cell.

Particularly helpful summaries of the techniques developed to determine the cell mechanical properties and the effects of an applied force in the mechanical and biochemical response can be found in [50–52]. A schematic representation which highlights the most

prominent techniques in the field is presented in following page (Figure 1.1.3) and is summarized below.

Substrate strain

Direct manipulation of the substrate to which cells adhere (substrate deformation, or SD) provides a means of mechanical stimulation by controlled uniaxial, biaxial or radial distortion of cells on a flexible surface. The strains applied are intended to mimic the physiological strain imposed on cells within the body. The approach has been adapted to impose static and cyclic deformation representative of in vivo conditions [50].

This technique has been widely applied to studies in bone cells and cartilage cells (chondrocytes) because they are known to react to mechanical stimuli [51,53]. Lately, it has been applied to developmental neurobiology studies to show that stretch can produce significant neurite outgrowth and induce neuronal differentiation [54]. It has been found that substrate stretching influences the morphology, genetic regulation, metabolic activity, injury, and cell phenotype [51].

Disadvantages of this technique include the anisotropy in the applied strain at the grip regions, and the inherent heterogeneity of the elastin substrates used in this technique.

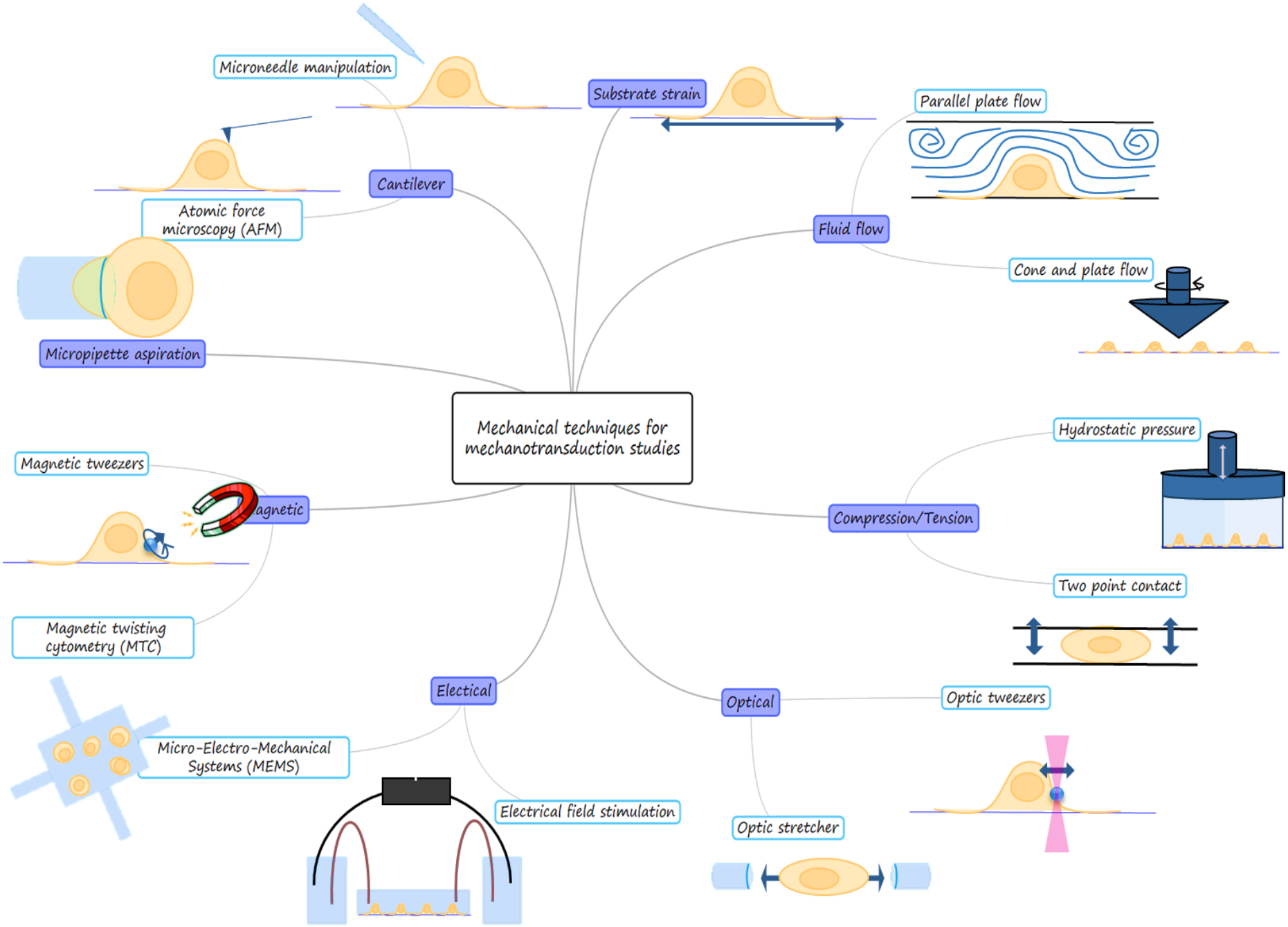

FIGURE 1.1.2 SCHEMATICS OF MECHANICAL TECHNIQUES FOR MECHANOTRNSDUCTION STUDIES

Fluid flow

For this technique, a flow of fluid is imposed on cells on a plate. Within these systems, cells can be subject to laminar, transitional, or turbulent flow profiles. The two most popular kinds of shear flow devices are the cone-and-plate system and the parallel plate flow chamber. They control the fluid dynamics by means of a top plate; the cone rotation controls the angular velocity, while the parallel plate controls the fluid shear rate, by means of the pressure differential between inlet and outlet. Using these systems, many different flow profiles can be achieved. The flows imposed are designed to mimic the fluid flow conditions in the human body in order to yield more physiologically relevant results.

There are a number of different cells resident within the human body that are subject to fluid flow. This technique has been widely applied to studies of vascular tissue [55–57] and bone [58–60].

Disadvantages of this system are the requirement for large amounts of reagents to control the cellular environment. It also assumes that the cell distribution is homogeneous, and in the case that there are discrepancies, the flow profile is likely affected.

Compression / Tension

Compression-tension systems act on the sample through either hydrostatic pressurization or direct contact. When they act on the sample through hydrostatic pressure, the cells are subjected to a homogeneous spatial compression or decompression through the fluid. It is appealing because it offers the ability to study either single cells or cell populations in two or three dimensions. In the case of compression through direct contact, two surfaces or contact points are required. Compression or tension is applied by changing the distance between the two contacts. In both cases static and/or transient loads can be applied. It is appealing because it offers a great versatility of application to a wide variety of samples [52].

Hydrostatic compression techniques have been widely applied to study the effect of compression in bone cells trying to simulate physiological loading [61–63]. Direct contact compression and tension has been widely applied to study the effect of compression and extension of bone and cartilage due to the similarities to in vivo loading by intra-articular

contact for *in-vitro* and *ex-vivo* studies [61,62] [64,65]. It has also been applied to nerves and neurons to simulate the effect of mechanical injury and bone lengthening interventions [47,66,67]. It can also serve to obtain the material properties of whole cells [68,69] and individual cell structures both in vivo [28] and purified [40].

Interestingly, when cells are subject to hydrostatic pressurisation, very similar to what happens with scuba divers, the partial pressure of the gases dissolved in the solution changes with the change in pressure, thus, compensatory treatments have to be performed in order to alleviate stress induced in the cells [63]. A significant disadvantage of having a direct contact of the surfaces is the limited nutrient exchange at the interface, which can lead to cell death. Another disadvantage is that the strain field is anisotropic and heterogeneous at the specimen–contact interface, and it is difficult to distinguish the effects of cell deformation and extracellular matrix mechanics. [52].

Optical techniques

Optical-mechanical systems employ photon trapping to manipulate and apply forces to whole cells, or a portion of a cell [70]. The two most common of these techniques are optical tweezers and optical stretching. Optical tweezers were originally developed to trap individual atoms, viruses, and bacteria [71,72]. This technique uses an infrared laser and a microscope to trap a nano or micron sized object, typically a transparent bead, and control its movements through a highly focused laser beam. The laser beam is focused at the center of the object and when the photons of the laser beam pass through the bead, there is a change in their direction based upon the object's refractive index. This results in a transfer of momentum to the bead. Imbalances in intensity between the center and the outside of the beam cause a net force on the bead acting towards the higher intensity part (by Newton's third law), thus moving the bead towards the center of the beam. [73–78] Thus when the beam moves, the bead is held in its centre, as in a pair of tweezers. Forces on the order of 50 pN can be applied.

An alternative use of the same principle, the optical stretcher, requires two lasers (not focused on the plane of the cell) shone on diametrically opposite portions of a cell in suspension. This technique affords maximum forces of several hundreds of pN [79]. In addition to the higher forces, the unfocused laser reduces the intensity and heat transmitted to the cell, such that high power lasers can be used without damaging the cell.

These optical techniques have been used to investigate single cell mechanics, by controlled displacement of dielectric objects that are either attached to the cell membrane or placed inside the cell [71,78]. A wide variety of cells have been tested using this technique: tumor cells [80,81], bone and cartilage cells [82], and stem cells [83]. Optical tweezers have also been used to determine mechanical properties of subcellular structures such as DNA and proteins and other intracellular structures [84,85].

In addition to this, there is a wide range of applications, of which one particularly interesting is the use of protein coated beads which are positioned at opposite ends of the cell and adhere to it. These beads act as the "grips" or "handles" by which the cell is manipulated [86,87]. Another remarkable application of this same principle is the capability of drawing plasma membrane nanotubes from live cells without the help of an intervening cell-surface attached microbead, but rather achieved by focusing the optical trap on the plasma membrane of the cell [17]. These focused laser approaches have shown the capability to guide neuronal growth [88].

The main disadvantages of the optical-mechanical techniques is the damage and heat they induce in the sample, as well as the relatively low forces that can be applied.

Electrical techniques

Electrical-mechanical systems employ electric fields to guide the organization of cells. They are based on principles of dielectrophoresis, which induces polarization of the cell via an applied electric field and then a non-uniform field to induce disparity in the Coulombic forces pulling on each end of the cell dipole to enable cell motion [89]. These electrical gradients are most often applied to cells cultured on flat substrates, but can also be applied to cells in three-dimensional scaffolds or tissues. MEMS combine mechanical, electrical and sometimes acoustic components onto micro-scale devices [50,90–92] and can be used to apply electrical fields to measure and control the cellular mechanics.

An old technique based on this principle that biologists use quite commonly is gel electrophoresis. It is applied to separate DNA strands (inherently charged) by application of an electric field. The different charges and (mass) of the DNA determine their speed of motion through the gel. Dielectrophoresis can also be used to stretch cells via electrical stresses generated by microelectrodes [90]. A particularly interesting application is the assembly of quasi one-dimensional organization of neurons in logical devices [93].

One disadvantage of this technique is that the electrical fields can be non-uniform and may cause anisotropic stimulation to the sample. Another disadvantage is that high resolution is difficult to achieve due to the spatially delocalized character of the field [50].

Magnetic techniques

Magnetic techniques apply forces to a cell using ferromagnetic beads. The most prominent magnetic techniques used for studies in cell mechanics are magnetic tweezers [94] and magnetic twisting cytometry [95]. The bead's movement is manipulated by a magnetic field produced by an electromagnetic coil probe in proximity to the bead, the magnitude of the force applied to the bead depends on the magnetic field and the proximity to the sample. In addition to the application of normal and lateral forces, the beads can be twisted thus enabling the application of torsional forces. The applications of this techniques are very similar to optical tweezers, and they can be used for almost any cell type, within most materials and media types. They have the added advantage that the majority of cells and media fluids have relatively small magnetic susceptibility and compared to optical techniques, this prevents sample damage by illumination or heat. [50,70,96]

Early applications of the magnetic beads technique include manipulation of individual cellular components, by either endocytosis [97,98] or specifically linked particles [99]. They have been used to study focal adhesion proteins [100,101], mechanical properties of DNA [102], lipid bilayers [103], cell receptors [104] whole cells [105] and even membrane nanotubes [106].

One of the limitations of this technique is that when micron sized beads are inserted into the cytoplasm, the presence of an external object can be destructive to the cell and undefined interactions of the bead with the intracellular components can lead to an incorrect estimation of the mechanical properties [107].

Micropipette aspiration

Micropipette aspiration is a classic technique for quantifying the mechanical properties of cells. This technique uses a micropipette to contact a cell and apply slight suction in order

to deform a portion of it [70]. The cell is deformed by a known force or stress, and its deformation (strain) is measured.

This technique has been widely used to measure the mechanical viscoelastic properties of all kinds of cells in suspension. [70,96,108–111] It has also been used to study the nuclear mechanisms by gently extracting the nucleus from the cell for testing [22]. By introducing a second pipette, the strength of specific ligand-receptor bindings [112] and cell junctions [113] have been tested. One of the most important contributions of this technique is that it enables the assessment of the electrophysiological activity of electrically excitable cells by precise manipulation of the pipette with a micrometer sized opening [114–116].

Due to the geometry of the experiment, the applied stress is complex and various models have been used to extract the mechanical and functional characteristics of the cell deformed by aspiration [117–120]. The disadvantage is that the model chosen dramatically affects the value of fitted parameters and the calculated viscoelastic characteristics. In addition to this, the cells are tested in suspension, which, for many cells, is far from physiological.

Cantilever Manipulation

The two most prominent techniques within this category applied to the study of cell mechanics are microneedles and atomic force microscopy (AFM). As these are key techniques employed for this thesis, the operating principles and limitations will be briefly outlined here and explained with more detail in the following chapter.

Both techniques use a spring to locally deform a cell with a calibrated force by making use of Hooke's Law (the fact that the deflection of a spring is proportional to the force acting on it). In the case of the microneedle, the induced needle displacement is measured via optical images [121,122] and in the case of the AFM, the deformation is measured via the reflection of a laser off of the back of the cantilever-shaped spring onto a position-sensitive photodiode [24]. Since the cantilever spring constant of these systems can be calibrated, the force applied to the sample can be determined.

Microneedles and cell pokers are commonly used to tug or push on a cell or a subcellular structure [8] and investigate the subsequent response of cells to this cytoskeletal indentation [121]. They have been refined to enable determination of the mechanical properties of cells [123–125]. In addition, microneedle manipulation techniques have been

applied to study many aspects of mechanotransduction [31,126,127], intracellular delivery of DNA [20], and neuron growth and development under tensile forces [19,128–130].

Although this technique is one of the simplest and most effective tools in cell mechanics, the approach is somewhat data-limited because individual cells have to be tested and experiments are not always repeated enough to reach statistical significance. Development of automated, high-throughput devices for poking cells could provide a more data-rich approach [131].

The AFM technique was originally developed as a tool for nanoscale imaging of the topography of solid substrates, but has shown great impact for force based probing of biological materials [132,133]. Generally, a silicon or silicon nitride flexible cantilever with a fine tip at its end is scanned laterally or vertically on top of the sample with high resolution using a piezoelectric positioner. Cellular structures can be imaged [134], and probed to assess their viscoelastic properties and adhesion [3,45,135–140]. Recently, advancements in AFM have enabled simultaneous imaging and temporal assessment of the viscoelastic properties of the sample during different physiological processes [141–144], and even cell contraction and motility [45,49,145–147] . In addition, AFM can be applied to assess cell response and resistance to injury [35,148,149], aspects of mechanotransduction [150–155], intracellular delivery [156,157] and the strength of single molecule interactions [135,140,158–163]. It has recently been reported that membrane nanotubes can be elicited through manipulation of adhesive contacts using this technique [106,164,165].

AFM has been exploited as a research tool by the biophysics community because this technique affords high imaging resolution, positioning accuracy, the ability to image and mechanically manipulate biological structures and molecules and the potential to track biological processes in near-physiological environments over time. One of the main disadvantages of AFM is that it can be quite invasive: the imaging force can be too high and damage the cell. In addition, estimation of the elastic properties depends on the shape of the AFM tip, as well as the location of the indentation, and therefore results are not easily transferable between experiments employing different AFMs [166,167].

One of the major issues forced when using this technique is the maintenance of cellular viability because the sample environment is very difficult to control with the AFM instrumentation in place. This is one of the main reasons that many AFM-bio studies have limited biological relevance. Cells require careful culturing under physiological and aseptic conditions. They are very sensitive to changes in temperature, osmolarity, pH and to

bacterial infections commonly present in the atmospheric environment out of the culture room. Experiments with cells require saline solutions to maintain the cells in a physiologically relevant environment, which greatly reduces the useful life of the expensive equipment used. The evaporation and residues of solutions can ruin the delicate electronics.

Chapter 3. Experimental techniques

This chapter will describe the operation and principles of the key experimental techniques used and developed in this thesis. The first and most central technique is AFM, which was used in this study to induce membrane deformation and microdamage in bone cells, and to artificially initiate and extend connections between neurites of mature CNS neurons (mature, in this context refers to their capability to make synapses). In the second part, we will describe the techniques developed and tested to enable release of the newly-formed neuronal connection, the environmental factors critical to keep the cells alive for the duration of the experiments, and the assessment of the calcium dynamics in response to deformation and the structural cytoskeletal proteins in the newly created neuronal connections through fluorescence microscopy. Lastly, the assembly and operation of the patch-clamp setup to test the functionality of the artificially created connection will be described.

3.1 AFM and micropipette manipulation techniques

AFM is a scanning probe technique in which a sharp tip attached to the end of a cantilever is used to probe the sample. It was developed by Binnig, Quate & Gerber in the 1980s as an extension of scanning tunneling microscopy (developed by Binnig, Gerber, Weibel and Rohrer early in the same decade) allowing non-conducting samples to be imaged [24]. It measures the tip-sample interaction forces by determining the deflection of a cantilever attached to the tip. The cantilever will deflect by an amount d, proportional to the force experienced by the tip, $F = k \cdot d$, where k is the spring constant of the cantilever. The deflections of the cantilever are typically measured by optical beam deflection. Piezoelectric tubes are used to scan a sample relative to the tip as they allow very precise control of the tip height and X-Y position relative to the sample, thus allowing imaging with vertical nm resolution and lateral resolution limited by the tip size. Originally developed to scan solid surfaces in air and vacuum, AFM has been extended to enable atomic and molecular resolution measurements of biological systems in liquid environments [136,137,167–169] making it a useful tool to study living cells in nearly physiological environments without prior fixing, labeling or other chemical treatment, as required by many other bio-imaging techniques. AFM techniques can additionally be

combined with a variety of optical microscopy techniques, further expanding their applicability.

The following section highlights the central features of the AFM techniques employed for experiments described in subsequent chapters.

3.1.1 Bio-AFM design

The experiments in this work are conducted in a commercial AFM MFP-3D-BIO AFM instrument (Asylum Research, Santa Barbara CA) mounted on an Olympus IX-71 inverted optical microscope, designed specifically for life sciences applications. The reader is referred to the user manual provided by the manufacturer for specific design features, calibration procedures and basic operation.

In a typical bio-AFM experiment, a silicon or silicon nitride cantilever is mounted in the AFM head. Cantilevers for bio applications typically have two shapes: rectangular and "V"-shaped. The cantilever back face (not in contact with the sample) is usually coated with a thin metallic layer (typically Au) in order to enhance the reflectivity and thus signal to noise. The details of the cantilevers used for the different experiments preformed in this thesis are indicated in the relevant sections.

The AFM head is mounted on the stage of the inverted optical microscope so the sample can be simultaneously probed from above with the AFM tip while optically viewed from below, thus, combining optical imaging methods and force-based measurements. In this integrated approach, either the sample or the tip can be translated in X and Y. If the sample is fixed, then the tip is actuated in XY and Z. In our microscope, the sample is scanned via X and Y piezo actuators and the tip is scanned in Z (Figure. 3.1.1).

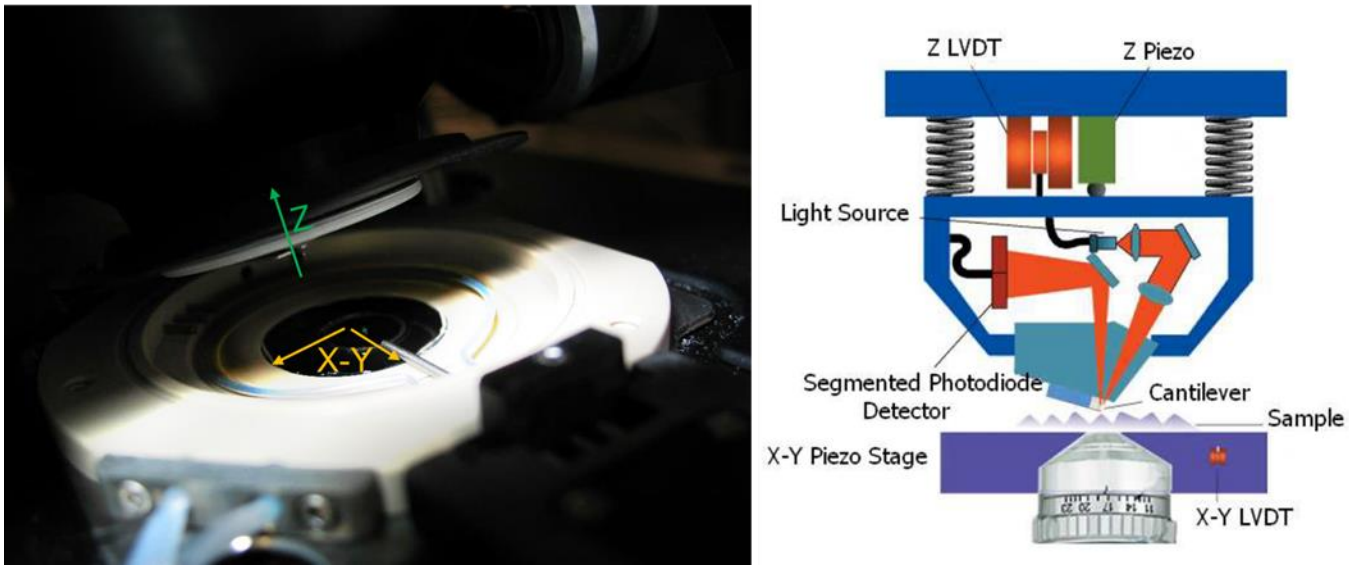

(FIGURE. 3.1.1) AFM HEAD AND SCHEMATICS SHOWING PIEZO ACTUATION SYSTEMS. THE USE OF THE LINEAR VARIABLE DIFFERENTIAL TRANSFORMER (LVDT) SUPRESSES THE HYSTERESIS OF THE PIEZO MOTION AND REPORTS A MORE ACCURATE POSITION.

To minimize the acoustic vibrations that contribute noise, the microscope is located on a damping table (Herzan TS-Series Table Stable) inside an acoustic insulation enclosure (BCH-45) (Figure. 3.1.2 left).

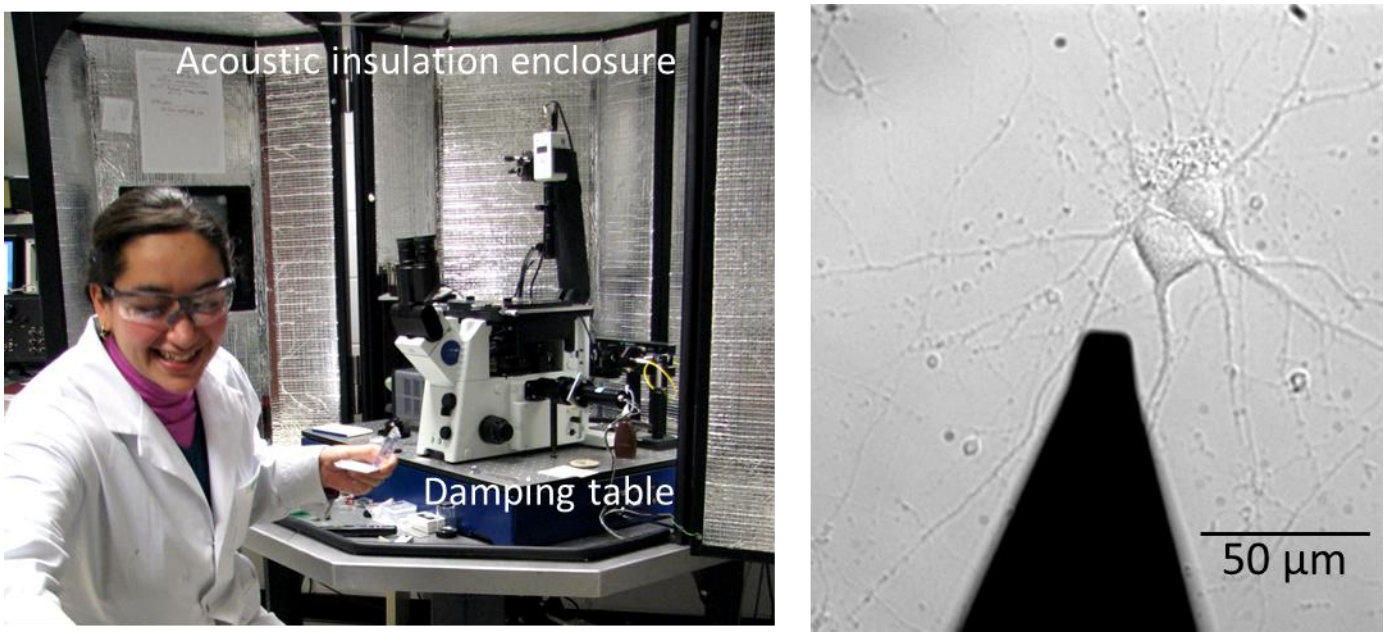

(FIGURE. 3.1.2) ISOLATION SYSTEM FOR AFM AND OPTICAL REPRESENTATIVE IMAGE OF AFM EXPERIMENT IN LIVE CELLS (40X OBJECTIVE).

The samples must be accessible to direct contact with the AFM tip. Although the design of the microscope enables some versatility, live cell experiments are most often performed on dissociated culture cells plated on glass coverslips to allow easy identification of individual cell bodies and processes (Figure. 3.1.2 right).

At the time of the experiments the coverslips are mounted on the closed fluid cell dish with optional heating capability (Figure. 3.1.3). The samples are held magnetically to the stage. When the experiment requires physiological temperatures the sample is warmed up to 37 °C using a heating element. Temperature control is specified for the experiments where it was used. In the case that the sample temperature is elevated, the duration of the experiment is limited by two factors: increased evaporation rates, and cantilever drift. To prevent evaporation, a Viton membrane which mates to the standard MFP-3D cantilever holder serves as an evaporation shield (Figure. 3.1.3 left). Because the lever is coated with a metallic thin layer (crucial to enhance the reflectivity), it is extremely sensitive to temperature variations, due to the bimetallic effect. The cantilever deflection will therefore change while the temperature changes and a new thermal equilibrium is reached which might take several minutes.

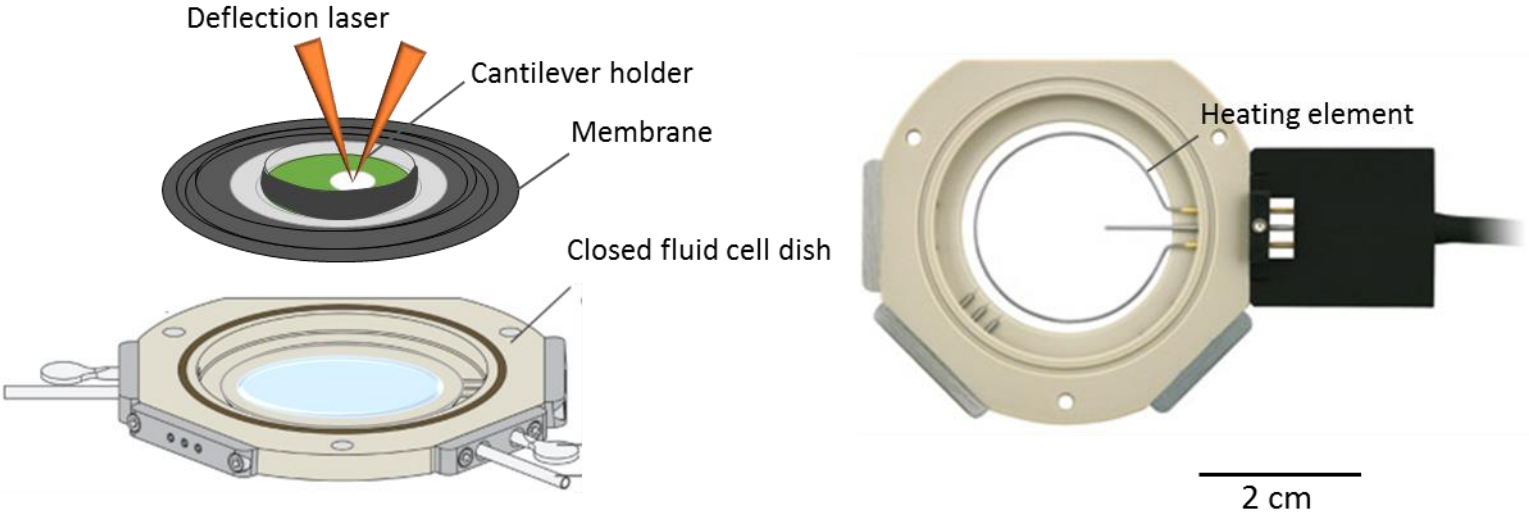

(FIGURE. 3.1.3). SCHEMATICS OF SAMPLE HOLDER AND CANTILEVER HOLDER AT THE LEFT AND HEATING SYSTEM AT THE RIGHT

3.1.2 AFM techniques for life science application

Although AFM is well known for imaging and generating a surface profile of the scanned sample, many other modes have been developed. Some of them enable the study of tip-sample forces as a function of z-separation with pN resolution [170], [138], [171], [172], [173] [174] [175]. This will be discussed in the next section.

It is important to realize that the AFM can also be used as a micromanipulation tool, opening up new ways of monitoring cell biomolecules and biomechanics in real time. Such is the case with single cell DNA transfection [157], mRNA extraction from live cells [156], mechanotransduction of bone cells [150] (further studied in chapter 5) and adhesive contact manipulation to induce new neuronal branching sites and artificially connect separate populations of neurons (studied in chapter 6).

Static force-distance curves

The following section will discuss what information can be extracted from force-distance curves. A static force-distance measurement is typically influenced by sum of forces arising from short range chemical interactions, van der Waals interactions and electrostatic forces, hard repulsion or viscoelastic deformation, and non-specific surface adhesion or specific molecular extension [176].

When a static force-distance measurement is performed on a very stiff sample with respect to the cantilever (Figure. 3.1.4), the cantilever engages towards the surface with zero deflection (A), and when in close proximity, it may bend upwards due to repulsive interaction (electrostatic or hydration forces) (B), jump in to contact due to short range strong attractive forces such as van der Waals forces and (C) be then repulsed by Pauli forces until a maximum force (or deflection) is reached and the cantilever is retracted (D). Often, upon retraction, adhesive forces appear as negative forces with respect to the zero-force baseline deflection (E). Adhesion can be an indication of electrostatic interactions, specific or non-specific tip-sample interactions or (in air) capillary forces due to moisture condensation on the surface. During contact, as the tip is pushed into the rigid surface (D),

there is a linear correspondence of the cantilever deflection with the motion of the z-piezo. Note that this is how the optical beam deflection is calibrated to relate the cantilever deflection to the voltage registered in the photo-detector, which, together with a calibrated spring constant of the cantilever, allows quantitative forces to be determined or applied.

In saline solutions used for live cell experiments, the long range electrostatic forces are usually negligible and the cantilever appears to enter smoothly into contact with no jump.

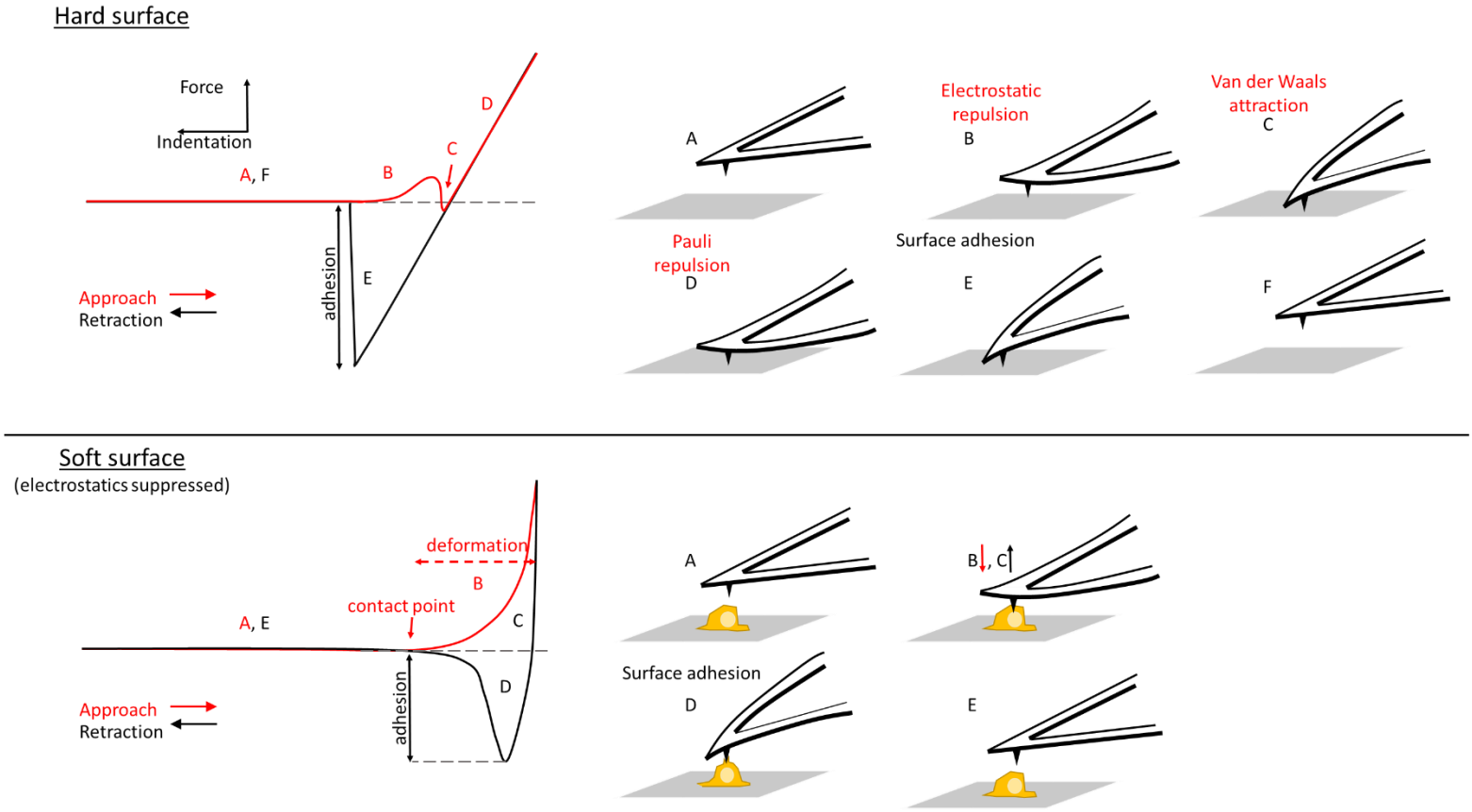

(FIGURE. 3.1.4) SCHEMATICS OF FORCE-DISTANCE CURVES AND TIP-SAMPLE INTERACTION ON HARD AND SOFT SURFACES.

In live cell experiments, because the sample's flexibility is comparable to the cantilever spring constant (Figure. 3.1.4 bottom), the force applied by the cantilever induces a non-linear deformation response (B). This nonlinearity arises because as the tip is indented, the area of the tip in contact with the sample increases. Since the transition from non-contact to contact is so smooth, determination of the contact point on soft samples is sometimes difficult [138].

After a programmable maximum set force is reached, loading ceases and the AFM probe is retracted and the impinging force is decreasing. Due to the tip-cell adhesion, the

interaction force (deflection) may become negative. This negative deflection indicates adhesive interactions between the tip and the sample, which results from sample molecules that bonded to the tip during the contact and are being pulled apart by the retraction (D). [137].

Although the AFM is very versatile and provides very good control of the probe position, maximum force applied, loading/unloading speed, indentation frequency and the use of different probe geometries (spherical, pyramidal, conical), the interpretation of the data obtained in AFM force-distance curves on living cells can still be difficult. In the following we will discuss how the elastic modulus can be estimated from force-distance curves and what are the assumptions and limitations of such estimations.

Force-distance curves used in conjunction with appropriate mathematical models describing the tip-sample contact mechanics can be used to estimate the Young's modulus and other material properties [138,177,178]. One of the most widely applied contact mechanics models derived from linear elasticity for determination of the Young's modulus is the Hertz model [91,110,179,180]. In this model the geometry of the indenter and the sample are taken into account to calculate the resulting force as a function of the sample displacement induced by the tip and sample elastic properties. Some example geometries are shown in Figure 3.1.5 alongside the corresponding equation for force:

Here *Ecell* and *Etip* are the respective elastic moduli of the cell and the tip (*Etip* =150 GPa for silicon and 3.5 GPa for polystyrene), γcell and γtip are the Poisson ratios with values $\gamma cell$ = 0.5 (incompressible; a reasonable assumption given that cells are mainly composed of water) [133], and γtip =0.17 for silicon and γtip =0.34 for polystyrene [181,182]. δ is the indentation depth calculated as: $\delta = z - d$, with z the piezo motion and d the deflection signal relative to the non-contact, free deflection, and *Dcell* and *Dtip* are the diameter of the bead and the cell respectively. In the cylindrical case, *K*, -1/*e* and *dE/de* result from complete elliptic integrals and corresponding values can be found elsewhere [179] By fitting this Hertzian model to the experimental force-distance curve, it is possible to estimate *Ecell*.

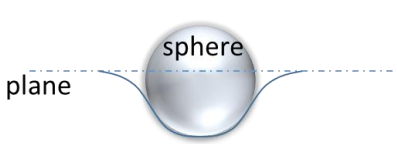

$$F = \left[\frac{(2\delta)^{3/2}}{3\pi \left(\frac{1-\gamma_{tip}^2}{E_{tip}} + \frac{1-\gamma_{cell}^2}{E_{cell}} \right) \left(\frac{1}{D_{tip}} \right)^{1/2}} \right]$$

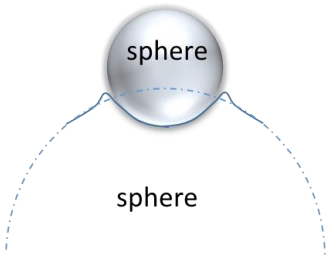

$$F = \left[\frac{(2\delta)^{3/2}}{3\pi \left(\frac{1-\gamma_{tip}^2}{E_{tip}} + \frac{1-\gamma_{cell}^2}{E_{cell}} \right) \left(\frac{1}{D_{tip}} + \frac{1}{D_{cell}} \right)^{1/2}} \right]$$

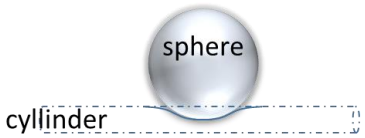

$$F = \left[\frac{(\delta)^{3/2} \left(\frac{2\pi}{3} \right)}{\left(\frac{1-\gamma_{tip}^2}{E_{tip}} + \frac{1-\gamma_{cell}^2}{E_{cell}} \right) \left(\frac{K}{-\frac{1}{e}\frac{dE}{de} D_{tip}} \right)^{1/2}} \right]$$

(FIGURE 3.1.5) HERTZ MODEL FOR DIFFERENT TIP-SAMPLE GEOMETRIES.

It is particularly interesting to point out the fact that for these three geometries, the force is proportional to $\delta^{3/2}$ and they differ only by the corresponding geometric factor. Not taking into account the geometry could lead to significant errors that can differ by as much as one order of magnitude. For this reason, it is important to determine the appropriate geometric contact model if one wants to extract quantitatively elasticity data from the force curves.

The Hertz model assumes that:

- the elastic limits of the materials are not exceeded
- the tip and sample materials are homogeneous
- the sample is much thicker than the indentation depth
- there is no adhesion within the contact area

In general, these conditions are not fully met in experiments with live cells.

In the following paragraphs, we will discuss some important factors that should be taken into account before being able to compare the elastic modulus of living cells.

The tip shape determines the regime of elasticity

To assure the elastic limits of the material are not exceeded, blunt and spherical tips are often used. When the sample probed by the usual commercial cantilevers carrying sharp pyramidal tips, local strains are typically induced that far exceed the linear material regime. High local strains can introduce significant errors in the Young's modulus estimation that can go up to a two-fold increase [11,183]). Studies have shown that, using beaded cantilevers, good agreement can be obtained with macroscopic measurements of the same material within some range of applied load [184]. However, the spatial resolution is compromised.

The tip-sample geometry

One other reason the tip geometry is important is that, since the radius appears in the force equation, any error in the radius will translate to an error in the calculated force. Therefore, knowing the geometry of the tip is important and when possible the cantilever tips should be inspected to know its exact dimensions. In addition, it is also useful to know the sample dimensions and have an estimate of the shape. Depending on the dimensions of the tip and how they compare to those of the sample, the appropriate Hertz model should be selected. For instance, for experiments in chapters 5 and 6, pyramidal blunt tips were used to indent cells; the blunt pyramid was modeled as spherical tip for small indentations (smaller than radius of the tip 0.5± 0.1 μm) as suggested by [185]. The cells were indented on top of the nuclei (with approximate radius of 10± 5 μm), in this case, the indentations were modeled as that of a sphere (the tip) on a plane (the cell). In a study preliminary to chapter 7, beaded cantilevers were used to study the axonal resistance to injury [148]. Beaded cantilevers (with a typical radius of 10 ± 1 μm) were used to indent neuronal branches and bundles of branches axially aligned (with a radius of 1.5± .5 μm), in which case, the indentations were modeled as a sphere on a cylinder.

The cellular structure is not homogeneous

Live cells are not homogenous, but constituted of multiple subcellular components which undergo complex physiological processes; due to the heterogeneity inside the cell, sub-cellular components are often probed with the tip. As we previously discussed, the membrane, the nucleus and the different cytoskeletal components have different mechanical properties [186]. This can introduce a variability of up to one order of magnitude among the estimated values [41,187].

The indentation depth is much smaller than the sample thickness

For a proper estimation of the mechanical properties, it is important to separate the contribution of the sample from the contribution of the substrate on which it is plated. The Hertz model assumes that indentation is not influenced by the substrate. In other words, the sample is infinitely thick compared to the indentation depth, and in cases where the substrate influences the indentation, large errors may result [188–190]. To avoid these errors, a common rule of thumb is that indentations have been empirically estimated to be kept below 10% of the total height of the sample at the indentation site [191]. Alternatively, modified Hertz models to account for finite thickness can be applied [183,192,193].

Adhesion forces within the contact area

Adhesion of the tip with the sample, is often observed when upon retraction, the force curve presents negative deflection. As mentioned before, this negative deflection can be attributed to the presence of substantial adhesive forces at the tip–sample interface. These adhesive forces are sometimes prevented by appropriately coating the tips (often with silicone) [194,195], however, the presence of additional coating chemicals may introduce undesired cell reactions. Alternatively, other contact models can be used, such as the Johnson, Kendall, Roberts (JKR), which take adhesive interactions into account. It has been shown that using this model the differences in elastic modulus at different peak loads could be reconciled [196].

In addition to not following the assumptions of the Hertz model, other factors related to the indentation and the sample response have to be taken into account in order to appropriately estimate and compare the Young's modulus. The following paragraphs will discuss some of the main considerations.

The uncertainty in the contact point

The indentation response for soft samples exhibits a smooth increase in the cantilever deflection. This smooth transition appears because the area of contact between the tip and the sample increases with the indentation. Because the transition is smooth, the estimation of the contact point is difficult and can introduce a significant error in the determination of the Young's modulus. Studies have shown that measured values can differ by more than an order of magnitude for the same sample because of this contact point uncertainty [183,197].

The applied load and the loading rate affect the cell response

Several studies have shown that the maximum applied load affects the estimation of the elastic modulus. The apparent increase in the elastic modulus is thought to occur because of the viscoelastic nature of the cells: at higher indentation loads, viscous effects are more apparent and lead to a stiffer response [11,198]. This increase in stiffness can also be related to the fact that deeper indentations are more likely influenced by the substrate and/or the cells are inhomogeneous and sub-membrane cellular components are being probed by the indentation [41]. Lastly, it is also possible that at the indentation site, finite thickness effects are coming into play or the deformation exceeds the elastic limits of the material [190].

In addition to the applied load, it is important to remember that the cell's resistance to deformation depends sensitively on the speed of deformation; because of their viscoelastic nature, cells are stiffer and more elastic in response to rapid (short time-scale) indentations, compared with less stiff more viscous responses to slower (longer time scale) indentations. [41,199]. There are alternate models to the Hertzian that take viscoelasticity into account (and can calculate storage and loss moduli) [178,199].

Thus, it is evident that performing experiments and analysis unaware of the limitations of the contact model used leads to significant errors that can go as far as several orders of magnitude in the calculations. The most important limitations for application of the Hertz model are the uncertainty in the contact point, the inexact estimation of the tip dimensions and thus contact geometry and indentations that exceed the elastic limits of the sample (frequently because of the finite sample thickness).

The quantification of the elastic modulus of cells and subcellular structures clearly represents a challenge. Different studies report different values due to systematic errors [200]. All the measurements within one study may have the same (unknown) systematic error, and be comparable one to the other, but there is no meaning in comparing them either to absolute modulus values or to other studies with different sets of errors. For estimation of absolute values, other analysis methods such as finite element modeling.

For our experiments, we made sure that indentations were not greater than 10% of the total height of the sample at the indentation site, and that the tip used had a well-defined geometry and dimensions (which required custom-designed or modified tips, as illustrated in the following section). The main focus of our studies is the relative comparison of the results and analysis of variable speed and load of the indentation and their effect on the cellular response.

Custom designed probes

Nowadays, AFM probes are commercially produced using Microfabrication techniques for many applications. However, probe modifications are sometimes necessary, such is the case of the tips used in this thesis. Our interest in modifying our tips was to have a better defined geometry and to distribute the applied load over a larger surface area, thus, reducing the strains induced by sharp tip indentations. Excessive strain leads to puncturing of the cell membrane. We produced two different types of tips: Type A with a plateau (Figure. 3.1.6), used for studies in deformation and microinjury, and Type B with a functionalized bead (Figure. 3.1.7), to induce adhesion after gentle contact with the cell. For the former, pyramidal cantilever tips were etched down to a 1 μm^2 diameter at the tip using the focused ion beam (FIB) microscope (model FEI DB235, Ecole Polytechnique de Montreal).

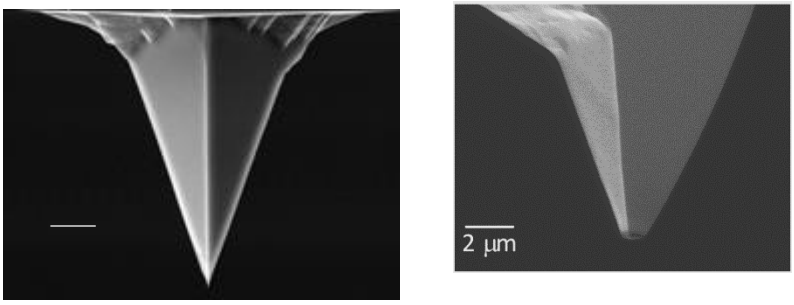

(FIGURE. 3.1.6) SCANNING ELECTRON IMAGE OF AFM TIP BEFORE AND AFTER MILLING WITH FIB

For the beaded tips, triangular cantilevers were used and 10 or 20 µm microspheres were attached to the tip of the cantilever using epoxy adhesive (Loctite®E-30Cl). The following beading procedure was developed (Figure. 3.1.7): 1) a 50 µl drop of 4, 10 or 20 µm carboxylate microspheres (Polysciences) diluted in water (1:500) was deposited on a square coverslip and let dry in the oven at 37 °C. The beads were loosened from the glass with a blade. 2) Epoxy adhesive (Loctite®E-30Cl, in yellow) was dabbed onto one edge of a square coverslip. Both coverslips are fixed at opposite sides of a microscope slide using vacuum grease 1 cm apart, with the dab of glue facing towards the center of the slide. The slide is set onto the optical microscope. 3) A MLCT (k = 0.01 N/m) (Bruker) cantilever mounted in the AFM head and positioned on the optical microscope stage. The AFM tip is brought in contact with the glue and retracted using the manual coarse approach mechanism leaving a small droplet of glue on the tip. 4) The slide is shifted onto the coverslip with the released beads, and the AFM tip is positioned a few microns above a single bead. The AFM

tip with glue is then brought in contact with the bead and lifted away. Bead attachment is optically confirmed. The cantilever is cured overnight in an oven at 37 °C.

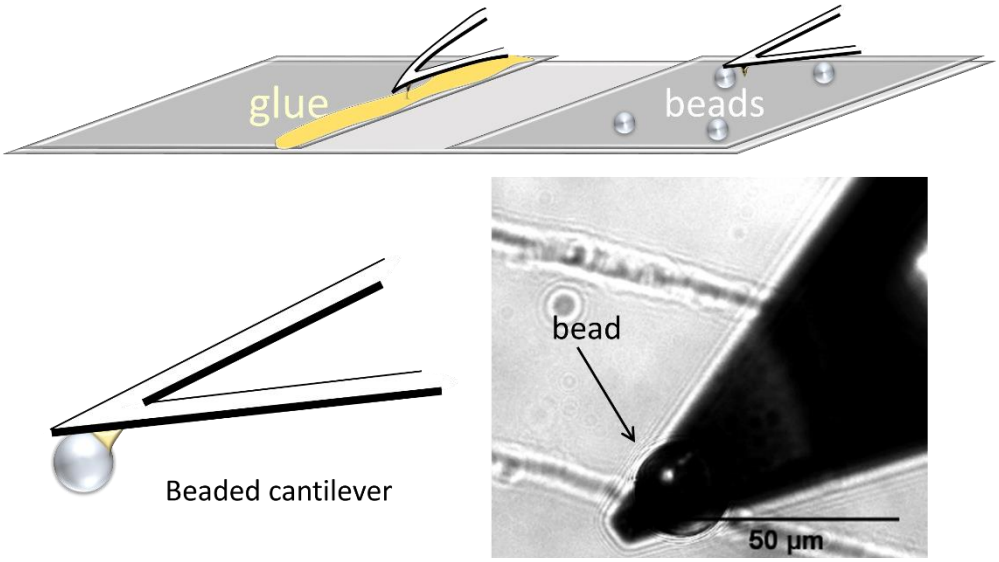

(FIGURE. 3.1.7) SCHEMATICS OF CANTILEVER BEADING PROCESS AND REPRESENTATIVE IMAGE OF BEADED PROBE

3.2 Cell culturing

To produce the samples used in this thesis, cells were cultured by experienced people following established protocols (specified where necessary, see later). Dr G Sadvakassova (Faculty of Dentistry, McGill University) and Dr M Magdesian (Montreal Neurological Institute), who cultured the cells, provided training to evaluate morphologically whether the cells were viable for experimentation.

For experiments in this thesis, the cells were either cultured on pure glass (in the case of the bone cells) or poly-D-lysine coated glass coverslips (in the case of the neurons) in medium containing the appropriate nutrients to maintain the particular cell type alive (details in respective section). This solution is also known as cell media. Cells are kept in an incubator at 37 °C, 5 % CO2 – 95 % air and 100 % relative humidity to maintain an environment similar to in vivo.

For AFM experiments, dissociated cells cultured on glass coverslips are most often used to allow easy identification of individual cell bodies and processes (Figure. 3.1.2 right).

This is the case for the samples in Chapters 4 and 5. However, cells with a specific spatial distribution may be required for different experiments. The growth and distribution of the cells can be controlled if the cells are cultured in microfluidic chambers. Microfluidic chambers are polymer devices with a specific channel structure, which can be assembled onto a glass coverslip. These chambers guide and thus determine the geometric pattern of cells grown cells on the glass substrate. The polymeric chambers can be removed from the coverslips after cell growth for the experiment to enable AFM access to the sample. The microfluidic chambers used for studies in Chapter 6 were designed and produced by ANANDA (URL, McGill University).

As an example of one of the chamber designs used in this thesis, a culture chamber for isolating neuronal processes from cell bodies is used (Figure. 3.2.1 top). This design is such that only neurites grow through a series of microgrooves, leading to a large number of parallel, spatially separated individual neurites. In the other design (Figure. 3.2.1 bottom), four culture chambers are separated by walls 100 – 200 µm wide. This leads to four spatially separated cell populations.

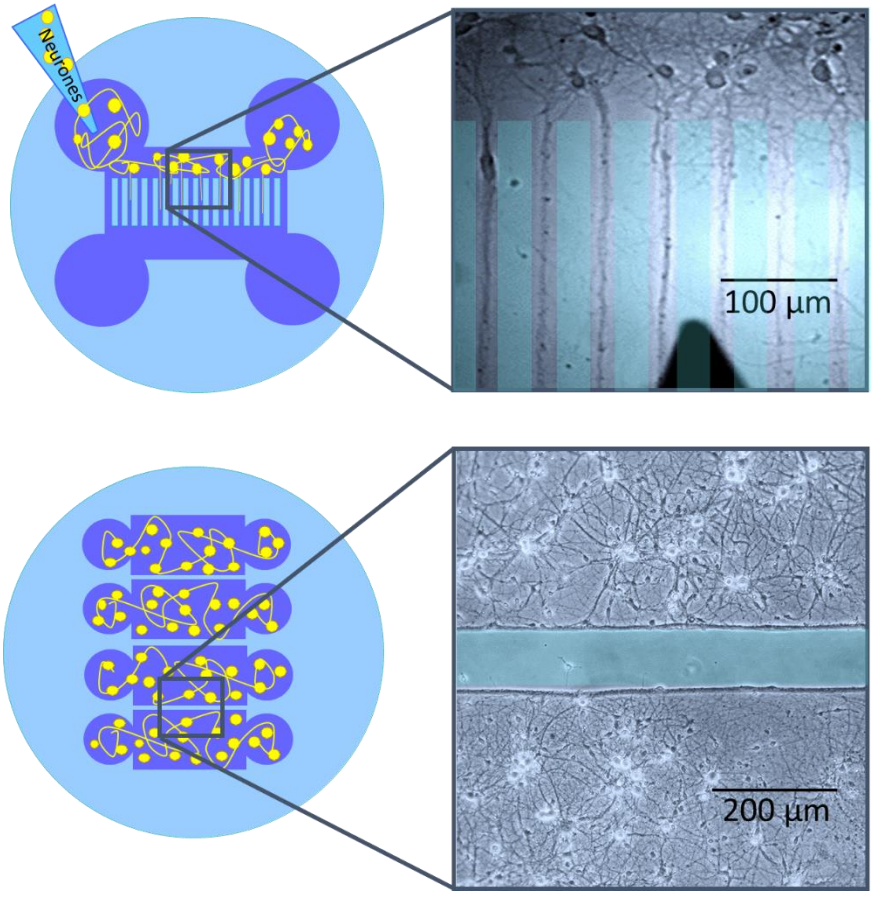

(FIGURE. 3.2.1) SCHEMATICS AND REPRESENTATIVE IMAGES OF CELLS (YELLOW IN THE SCHEMATICS) PLATED IN MICROFLUIDIC CHAMBERS FOR NEURONAL STUDIES

3.2.1 Maintaining cell viability

No useful data can be extracted from observations in contaminated or dying cells, as these are not in well defined, reproducible states. It is extremely important to evaluate the health of the cultures critically if meaningful experiments are to be performed.

For the experiments described in this thesis, the cells are removed from the incubator, placed in the sample holder and set in the microscope stage. Often biological microscopes are designed so that the sample environment can be regulated; however, our setup is not provided with this capability. Since the environment in the microscope is quite different from that inside the incubator, the properties of the media change. When the cell solution is exposed to normal atmosphere, the reduced percentage of CO_2 dissolved in the media, the metabolism of the cells induce pH changes [201].I In addition to this, the humidity and temperature gradient induce evaporation. However, the correct pH and the osmolarity of the solution are essential to maintain the cells alive and growing [202,203]. Thus, when out of the incubator the cells are often kept in saline buffers containing HEPES (4-(2-hydroxyethyl)-1-piperazineethanesulfonic acid), a buffering agent that helps maintaining physiological pH despite changes in CO2 concentration. To reduce the evaporation rate and maintain the osmolarity, it is necessary to either perfuse fresh solution or to keep the sample sealed. Sometimes, the sample can be heated to reach physiological temperature (37 °C). However, the osmotic changes under these conditions are even more dominant due to enhanced evaporation rates and the cells degrade faster. The following figure shows degradation of the cell at the top left due to osmotic changes over the course of a few of hours (sample at room temperature).

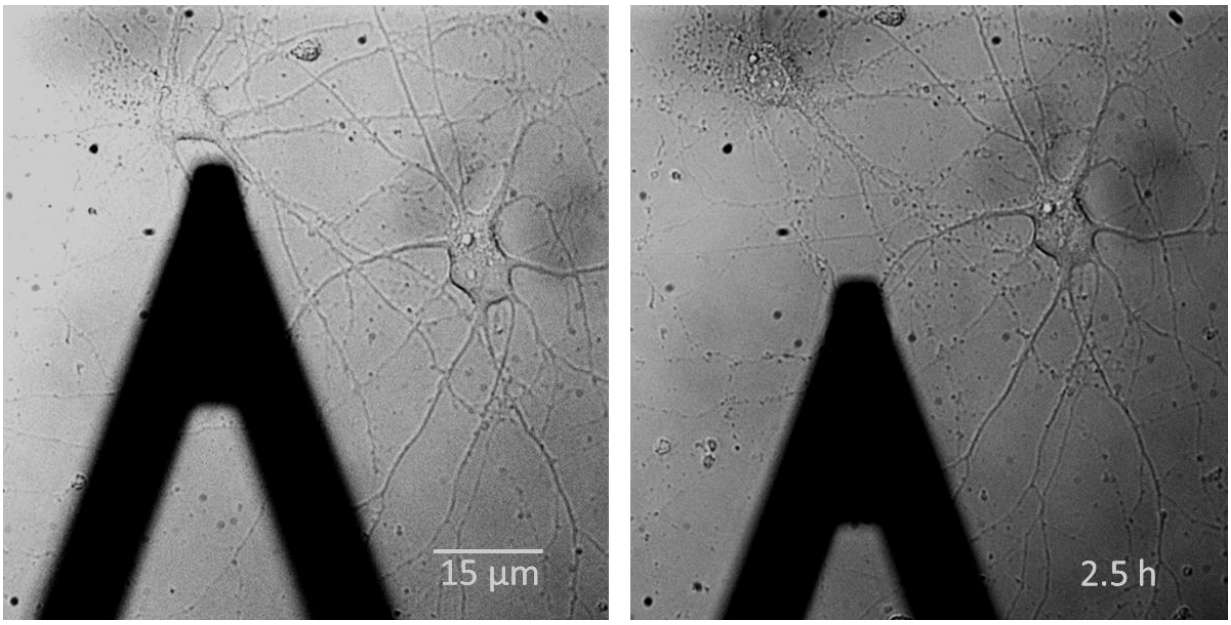

(FIGURE. 3.2.1) REPRESENTATIVE IMAGES SHOWING CELL DEATH INDUCED BY OSMOTIC CHANGES (SEE TEXT FOR DETAILED EXPLANATION)

Cell death via necrosis typically involves irreversible changes, such as the loss of cytoplasmic structure, dysfunction of various organelles and cytolysis (when the cell bursts due to an osmotic imbalance), as a result of strong swelling [204]. In the image above, the cell at the top left has died due to cytolysis after 2.5h out of the incubator, death is apparent because the cytoplasmic structure is lost, the membrane is discontinuous and only debris from that cell is left. Thus, it is crucial keep the duration of the experiment below the time in which the cell health is safely maintained outside of the incubator (~30 mins in the case of heated samples) as is the case for the experiments in chapter 4 and 5. In some cases, however, 30 minutes is too short to perform a full experiment as is the case of experiments in chapter 6. In order to prolong the cell life and health over several days that our experiments required, we had to perform exhaustive experimentation to a viable procedure. In these experiments, the cells need to be kept for a few hours outside the incubator, followed by overnight incubation and then again taken out for a few more hours. To maintain the cell environment that would enable these experiments to be carried out with minimal stress for the cells, multiple solutions were systematically tested. The following table summarizes the solutions tested, the experimentation times and our findings.

Condition	Solutions		Experiment Duration	Trials	Findings
AFM pulling	bead contact, filament extension and connection:	Hibernate E	6 h	36	the cells deteriorate within a few hours outside of the incubator
Pipette micromanipulation	bead incubation: filament extension and connection:	Hibernate E	4 h	8	the use of the heater augments the deterioration rate
	bead incubation: filament extension and connection:	Cell media Hibernate	2 - 3 h	18	
	bead incubation: filament extension and connection:	Cell media Perfusion: 1:1 cell conditioned media: neurobasal bubbling 5% CO_2	2 - 3 h	2	constant perfusion enables the osmolarity to stay stable over a longer period of time
	bead incubation: filament extension and connection:	Cell media Perfusion: saline buffer bubbling Oxygen	2 - 3 h	28	the pH of the solutions can be maintained stable when bubbling CO_2 or O_2 depending on the solution

TABLE 3.1. SUMMARIZES THE DIFFERENT SOLUTIONS TESTED TO PROLONG THE CELL LIFE AND HEALTH OVER THE EXPERIMENT DURATION

For the experiments shown in Chapter 6, the cells were perfused a rate of 0.5-1ml/min with saline buffer containing HEPES bubbled with oxygen at room temperature. Although some cellular processes may cope differently at room temperature, many of these processes can be reversed when the conditions return back to normal physiological temperatures (37 °C). Moreover, experience of extreme temperatures activates processes of plasticity that feed back to tune the circuit parameters and the homeostatic processes such that subsequent exposures can be tolerated more easily [205–207]. From this perspective, "what doesn't kill you, makes you stronger". Thus, physiological temperatures can be compromised in order to maintain the osmolarity. When possible, exchange or perfusion of fluid during an experiment is recommended, but care has to be taken to not mechanically disturb the measurement with the fluid flow (crucial in AFM experiments).

3.3 Techniques for artificial neurite initiation, extension and connection

As was previously mentioned, AFM can also be used as a micromanipulation tool. Suarez described in his Ph.D. Thesis and associated papers [208–210] how poly-D-lysine (PDL) coated beads can be used to stimulate the formation of artificial synapses. He also observed that these artificial synapses form adhesive contacts. For experiments in chapter 6, we thus use beaded cantilevers in order to trigger adhesive contact formation which we further manipulate to induce new neuronal branching sites and artificially connect separate populations of neurons. To connect neurites, a PDL functionalized beaded cantilever was used. For functionalization, the beaded cantilever was incubated overnight in a solution of PDL, following procedures in [208]. The region of contact is localized (green), the bead is gently pushed to contact the neurite and becomes resistant to detachment within a few minutes (less than 20 min) of contact. To assure a good physical contact that would reliably result in an adhesion site between the bead and the neurite, the deflection of the cantilever was monitored while the neurite was optically guided and positioned below the tip. Using the AFM allowed manipulation of the bead upon adhesion. Gentle displacement of the bead

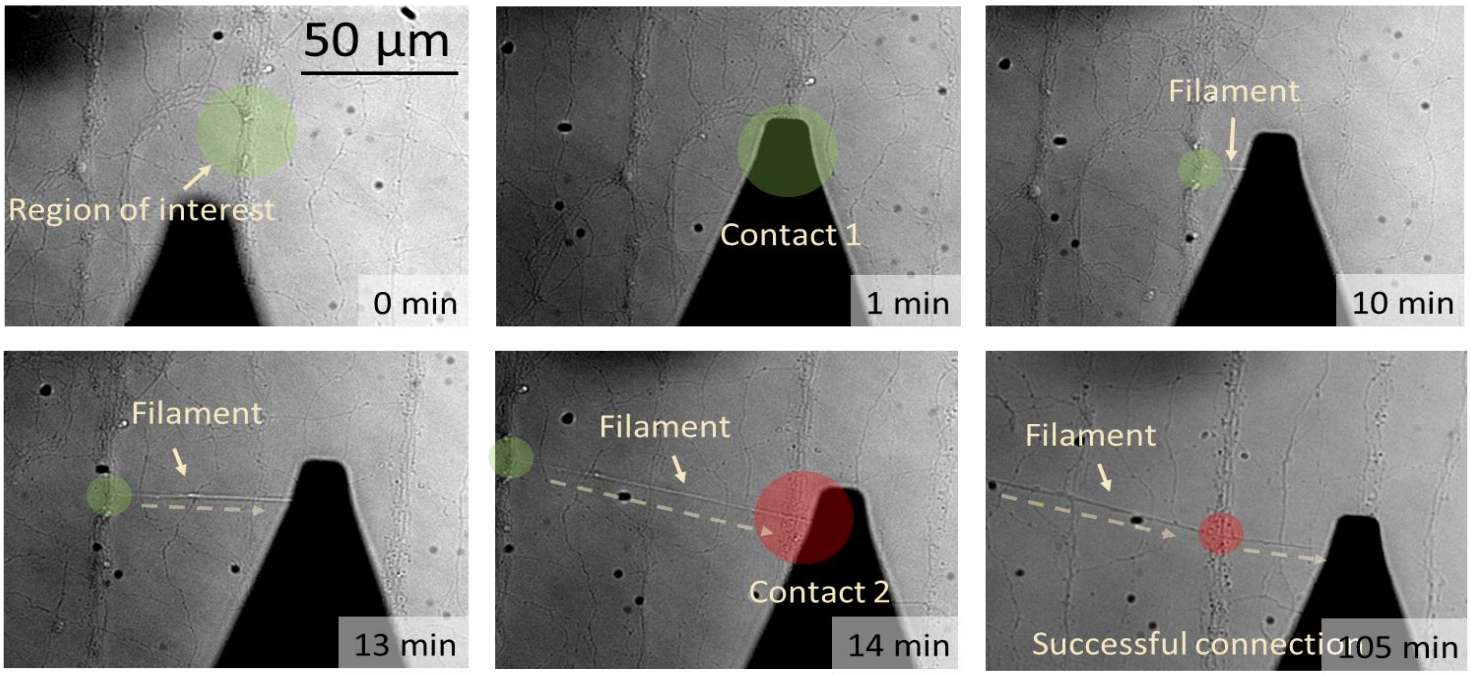

(FIGURE. 3.3.1) REPRESENTATIVE IMAGES DEPICTING THE PROCESS OF FILAMENT EXTENSION AND CONNECTION USING A BEADED AFM TIP (THE BLACK SPOTS ARE MARKS NOT MEANT TO BE THERE, THEY ARE DUST PARTICLES SOMEWHERE ON THE OPTICAL PATH)

initiates formation of a new neurite filament extending from the contact site, which can be

artificially elongated for several hundreds of microns. Upon full filament extension, the cantilever was reengaged with another neurite (red), and a new adhesive contact was formed with the filament. The figure above illustrates this process (Figure. 3.3.1).

3.3.1 AFM bead release after connection

To enable the functionality of the artificial connection to be tested, the AFM head has to be removed, given that the PDL functionalized bead is glued to the cantilever and the adhesive contact between the filament and the bead, triggered by the PDL, persists. The table below summarizes the methods developed and tested for this purpose. It is important to keep in mind that live cells and particularly primary neurons (extracted by dissecting the brain of an animal) are quite delicate, and damaging the connection during the release process is likely to impair its functionality.

Bead release experiments

Method	Execution	Success rate	Reproducibility	Comments
Rastering the bead into other cells	Release possible	2 out of 5	40%	Filament damaged and retracted upon release
Removal of cantilever with wedge	Release possible	1 out of 8	13%	Filament damaged and retracted upon release
Photorelease of PDL coating with UV light exposure	Release possible	3 out of 12	25%	Both filament and sample were severely damaged by UV light exposure
Pipette suction and expulsion of the bead	Release possible	50 out of 60	83%	Successful connection and release: Filament integrity is maintained during release. Connection stable over more than 1 hour in 34 out of 60 experiments

(TABLE 3.2.) SUMMARY OF DIFFERENT TECHNIQUES DEVELOPED FOR BEAD RELEASE FROM THE AFM TIP.

The release of the connection from the AFM head via a mechanical approach (ie. rastering/crashing the bead into the cells or removing/breaking off the cantilever or the bead attached to the cantilever with a wedge), resulted in detachment of the connection, the bead or the cantilever. These mechanical methods were not reliable. The filament was often damaged during the release process. This is likely due to the sudden rapid pulling on

the neurites, which likely disrupted the filament [211] [129]. The example in the figure below (Figure. 3.3.2) shows removal of the bead from the cantilever using a wedge.

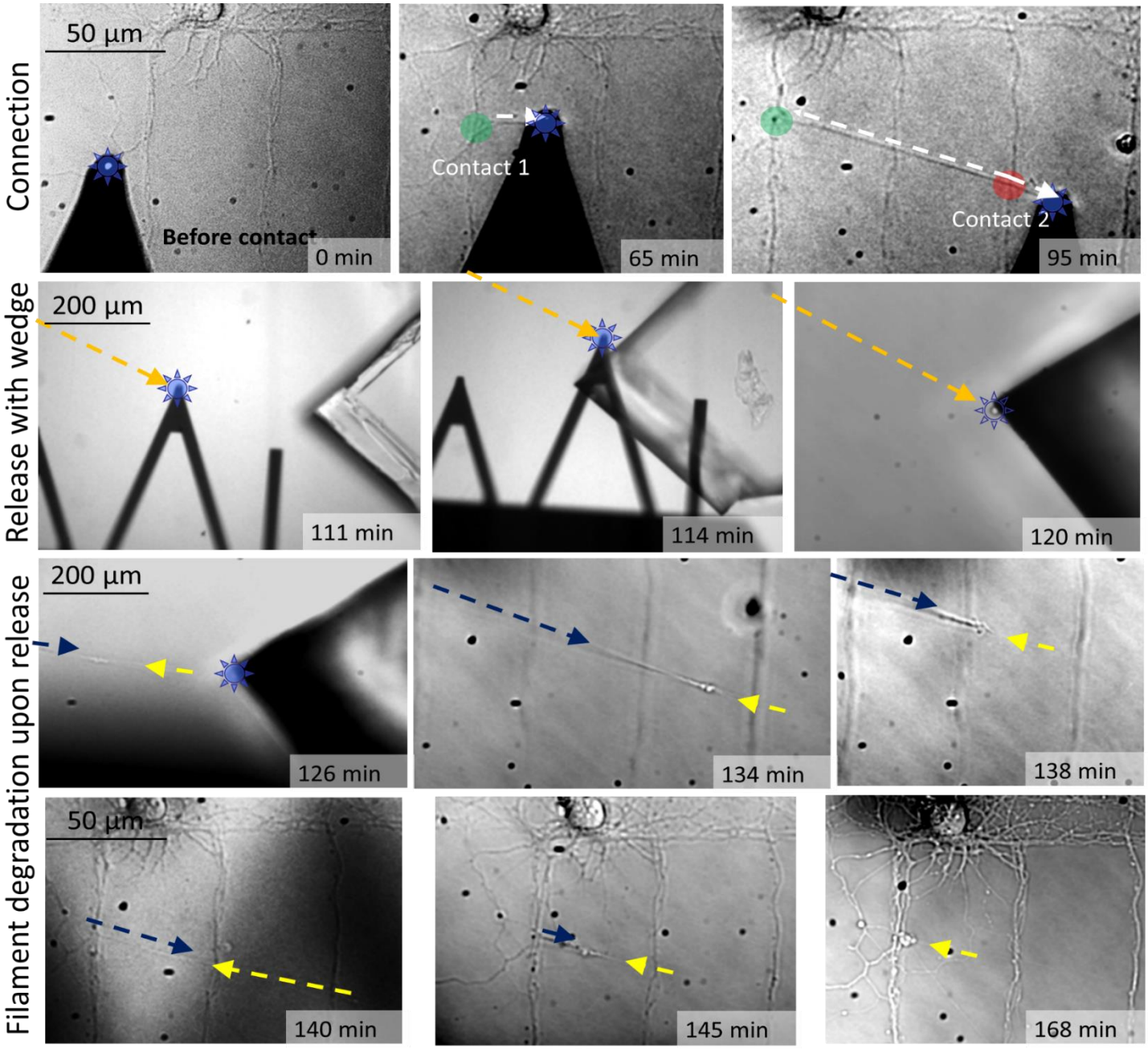

(FIGURE. 3.3.2) REPRESENTATIVE IMAGES DEPICTING THE PROCESS OF ATTEMPTED FILAMENT RELEASE USING A WEDGE TO REMOVE THE AFM CANTILEVER OR TIP

In this case the bead (indicated by the blue star) was released at the corner of the wedge. In order to mechanically remove the bead from the cantilever, a wedge of glass was placed in the sample prior to experimentation. After positioning the bead for attachment and posterior extension to the connection site (indicated by the white arrow), the cantilever along with the bead and the filament was moved in the direction of the wedge (indicated by the orange arrow). Once the cantilever had reached the wedge, it was slightly brushed against its edge in order to mechanically release it. Upon release, the filament degraded and retracted back to the original extension point (indicated by the blue and yellow arrows). This indicates that directly after pulling the filament is under considerable tensile stress.

Photo-release of the PDL coating via ultraviolet light exposure was a method developed by Alexis Goulet-Hanssens in Christopher Barret's lab, at McGill University. The approach consisted of coating the beaded cantilever with an azobenzene-based photocleavable sidegroup layer that would react by breaking bonds upon irradiation with ultraviolet light [44,212,213]. This approach had the potential to work and seemed quite elegant, but unfortunately the cells were severely damaged by exposure to UV light before release was observed (Figure. 3.3.3).

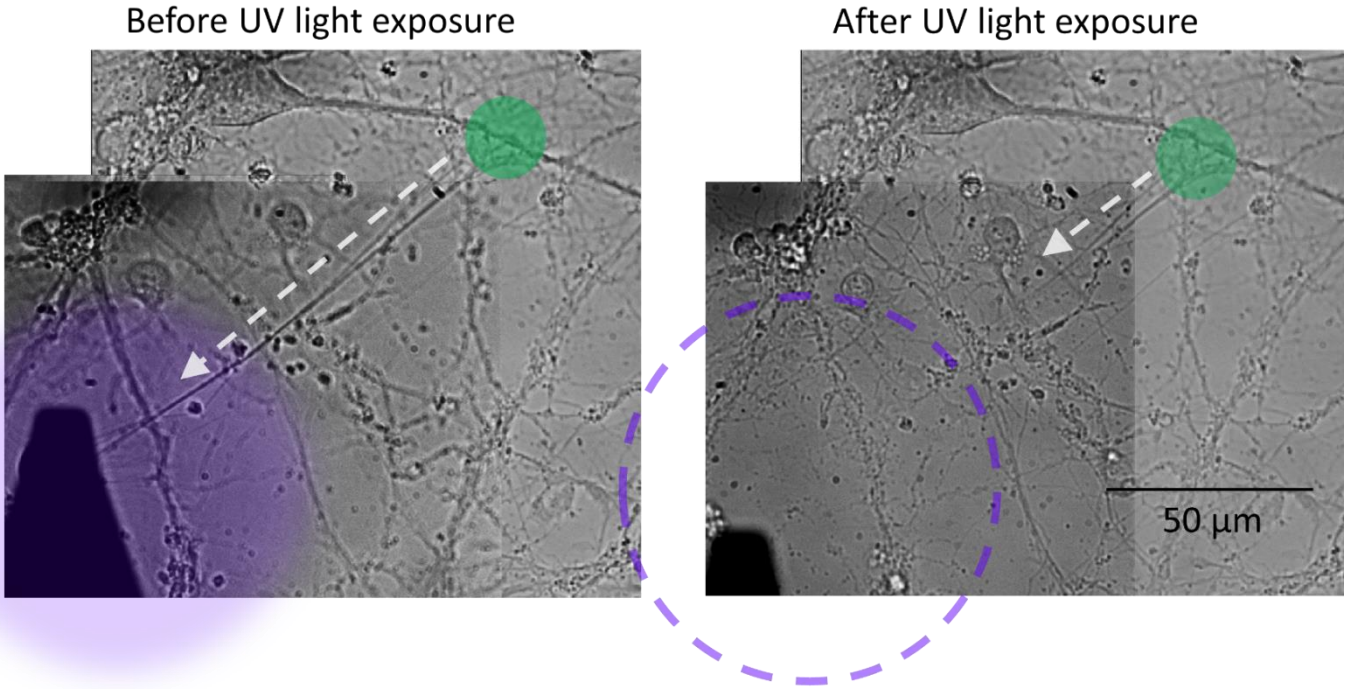

(FIGURE. 3.3.3) IMAGES DEPICTING THE PHOTO-RELEASE PROCESS OF THE FILAMENT USING UV LIGHT. CELL DAMAGE INDUCED IN THE REGION OF UV LIGHT EXPOSURE

3.3.2 Micropipette manipulation enables extension, connection and release of the filament

Since release of the complete bead from the cantilever proved to be complicated, we attempted using a pulled pipette with a tip diameter smaller than the average bead size prepared from a glass capillary tube. The pipette opening would be used for suction and expulsion of the bead. At this point, AFM was not used anymore for manipulation; instead, a micromanipulator was employed to control the pipette's 3D motion. The bead could then be manipulated via the pipette and the filament integrity would be kept upon release. This experiments were done on the same stage as the AFM. Details on the incorporation of the micromanipulators and the pressure control system used can be found in section 3.5.1.

As previously observed, pulled filaments are under tension. In order for released filaments to remain in place and not retract (thus breaking the newly established connection), the newly extended filament had to be maintained under tension. When the adhesive force of the bead upon release at the contact site (green) was not strong enough, the bead retracted back to the original extension site (Figure. 3.3.4). This observation adds an additional requirement to the successful release of the filament: the adhesion force of the bead at the connection site must be higher than the tensile retraction force of the filament.

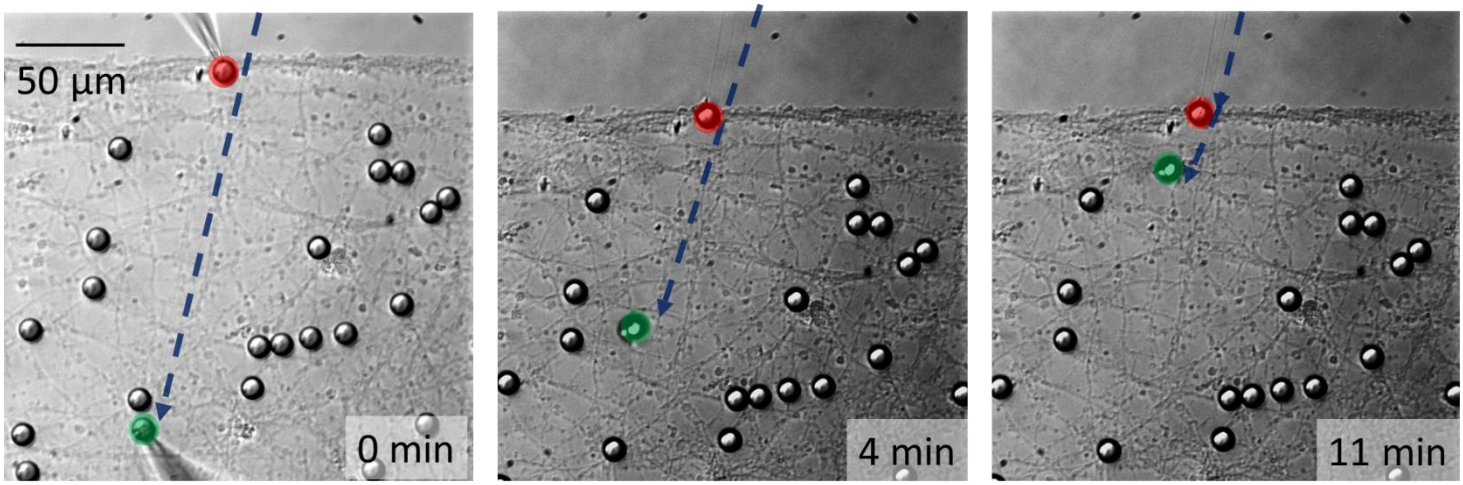

(FIGURE. 3.3.4) REPRESENTATIVE IMAGES DEPICTING UNSUCCESSFUL ATTACHMENT AND RETRACTION OF THE (GREEN) BEAD UPON FILAMENT RELEASE

In detail, the functionalized beads were added to the sample and incubated at 37 ºC and 5% CO2 for one hour prior to experimentation. This initiated adhesion of the beads to the sample. The sample was transferred to the microscope stage and a pipette was used to capture and manipulate a bead of interest, enabling extension of the filament. For these

experiments, the cells were plated in microfluidic chambers to culture spatially separated populations in order to enable connecting previously unconnected groups of neurons. The filament was extended across the gap onto the new population of neurons. To assure a good physical contact between the artificially extended filament and the population of neurons across the gap, an additional pipette was used to manipulate a second bead or group of beads (red) and bring the filament in contact with this region of the sample. The strong adhesion of the pulled filament to the previously cultured neurons is stronger than the tensile retractile force, leading to a stable filament. Upon full filament extension and connection, the bead was carefully released at the connection site by applying positive pressure in the pipettes. The following figure (Figure. 3.3.5) shows a successful experiment. Upon release, the bead adhered strongly to the connection site, enabling the filament to remain fully extended under tension. The connection was mechanically stable, allowing subsequent incubation of the sample overnight to enable formation of a stable connection including neurite typical structural components such as actin, tubulin and neurofilaments. Incubation is also needed to increase the chances of synapse formation.

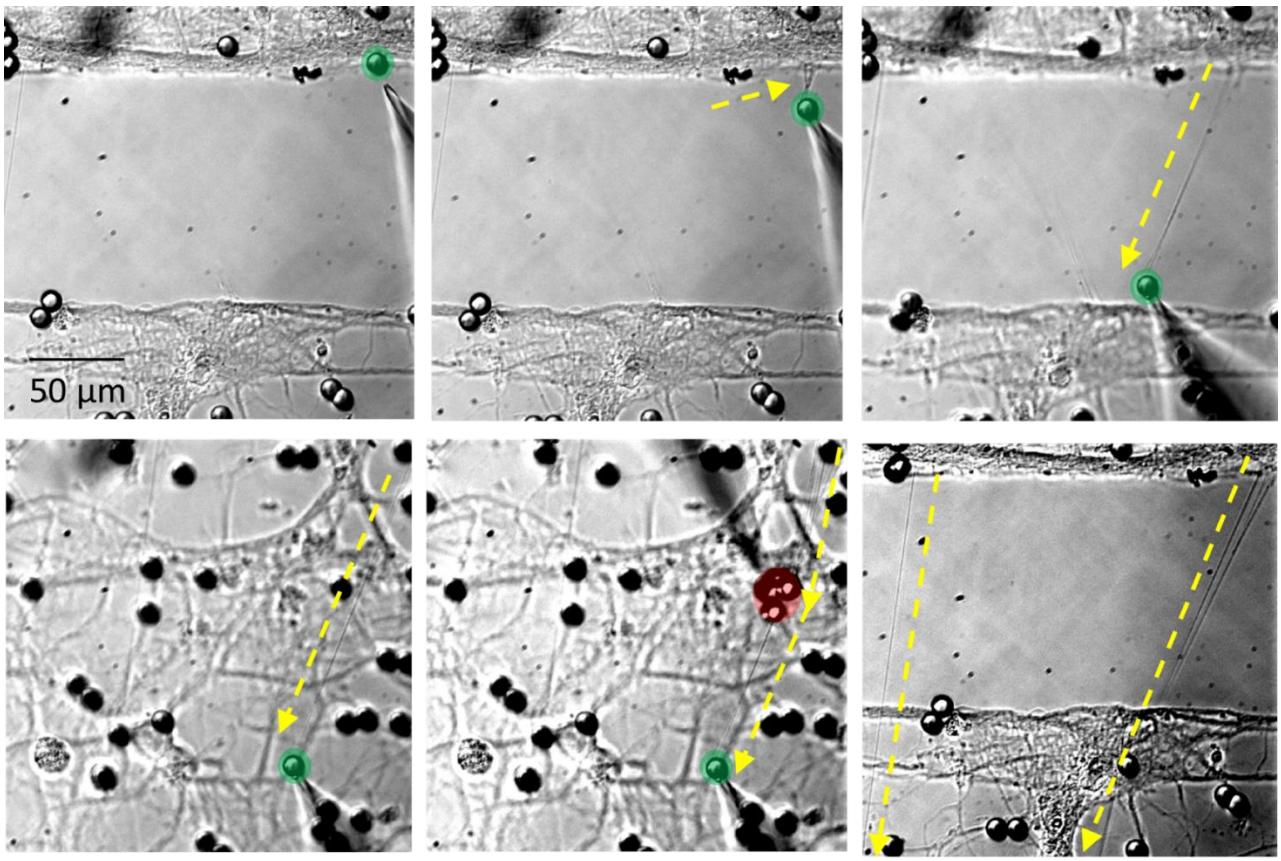

(FIGURE. 3.3.5) REPRESENTATIVE IMAGES SHOW PROCESS OF SUCCESSFUL EXTENSION, CONNECTION AND RELEASE OF FILAMENTS

3.4 Fluorescence microscopy

The invention of fluorescence microscopy as we know it today was the result of a series of largely uncorrelated but fortunate discoveries that culminated at the beginning of the 20th century. Long before, in the 16th century, the properties of various minerals and plant extracts to either emit light when kept in the dark (phosphorescence) or reflect a certain color and transmit a different one when illuminated with sunlight (fluorescence) were well known [214]. However, it wasn't until 1856 that a scientific explanation of this phenomenon was first provided by George Stokes. Stokes named this phenomenon "fluorescence" [215].

Fluorescence is the property of atoms and molecules (called fluorophores) to emit light following excitation by an outside source of energy such that the wavelength of the light emitted is lower than that used for excitation. Few techniques have been more widely developed and applied to biology than fluorescence techniques. It relies on chemical staining of molecules involved in cellular processes both in live and fixed samples. Live samples are often labeled with fluorescent indicators which change their fluorescence properties in response to active processes. Fixed samples are often treated with immunofluorescence labels, which use the highly specific binding of an antibody to its antigen (much like a key in a lock) in order to selectively label proteins or other molecules within the cell. [216]. A fluorescence microscope captures an image of the fluorescence of the sample to study its properties. Simple epifluorescence set ups use common bright field optical microscopes slightly modified to capture a 2D image, while more complicated designs such as confocal microscopes enable optical sectioning of the sample to get 3D imaging and better resolution. [217]

Fluorescence microscopy was used in this study to examine the dynamics of intracellular calcium in response to mechanical stimulation in live osteoblasts and to examine the structure of the artificially connected filaments in neurons after fixation. For the experiments in chapters 4 and 5 the fluorescence recordings were carried out using the Olympus IX-71 inverted optical microscope that serves as a platform for the AFM. Images were captured using a cooled Cascade II camera mounted on a side port of the microscope and stored using Image Pro 6.2 software. Confocal imaging was used for imaging of the structures of studies in Chapter 6.

3.5 Patch clamp electrophysiology

The field of electrophysiology started with the scientific breakthrough of Galvani in 1780, who discovered that muscle movements could be evoked by applying electrical stimuli to dead frogs legs' [218]. As recordings of the electrical activity in animals became more sophisticated, in 1963, Hodgkin and Huxley won the Nobel Prize in Physiology for their intracellular recording experiments on the squid giant axon using a micropipette. These experiments led to an understanding of the mechanisms underlying the generation of action potentials in neurons [219]. In 1976, Neher and Sakmann realized that a tight seal could be formed between the cell membrane and the micropipette opening which was stronger than the cohesion of the membrane. Applying a pressure pulse thus could break the membrane around the patch but keep the seal intact. This breakthrough enabled recording of single ion channel currents (on the order of pA) in cells. Neher and Sakmann were awarded the Nobel Prize in 1991 for this invention [220]. Shortly after, they developed the patch clamp technique as we know it today [114]. Conventional patch-clamp recordings use a microelectrode (a term often used to designate a complete electrode/micropipette/pipette-holder assembly) to record or induce electrical activity from/in an excitable cell. The microelectrode tip opening is pushed against a cell membrane, and gentle suction is applied to draw a piece of the membrane (the 'patch') into the microelectrode tip; the glass tip forms a high resistance (on the order of GΩ) 'seal' with the cell. This configuration is the "cell-attached" mode, and it can be used for studying the activity of the ion channels that are present in the patch of membrane [221]. However, in order to both detect and control the activity of the whole cell, additional suction is applied so that a small patch of membrane in the electrode tip can be removed, leaving the electrode sealed from the extracellular environment and in direct contact with the cell interior. The figure below depicts this process (Figure 3.5.1). While this technique enables control of the cytosolic environment through the solution in the pipette, the fluid inside the cell mixes with the solution inside the recording microelectrode, and so some important components of the intracellular fluid may be perfused.

In the following sections, details of the set-up construction and the specifics of the patch-clamp technique and recording modes used are described. The setup was developed according to procedures in [222–226], while Dominic Boudreau (from Prof. Yves De Koninck's lab at Laval University) provided hands-on training to perform patch clamp recordings.

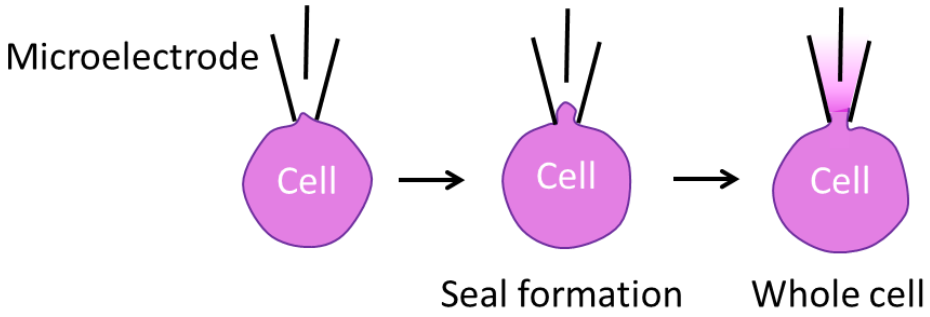

(FIGURE 3.5.1) SCHEMATICS OF WHOLE CELL PATCH

3.5.1 The patch-clamp set-up

Because patch clamping involves the placement of the opening of a glass micropipette against a cell to form a tight seal, experiments require a platform with minimal mechanical interference. Our electrophysiology setup was placed on the same platform as the AFM. The inverted optical microscope was used to visually identify the cells and optically guide the electrodes onto the region of interest. Bright field illumination was used. The image brightness and contrast were optimized using the camera software during live view to enable observation of the pipette-cell contact during approach and seal formation. Two micromanipulators (a MX7600R from SD Instruments and a PCS-5000-series from Burleigh) were magnetically attached to the damping table and the microscope stage to access the sample and position the micropipette tip against the cell membrane in a controlled manner.

When the pipette approaches the cell, positive pressure on the pipette fluid is required to protect the tip from contamination. Once the cell membrane deflects due to the presence of the pipette close to it, delicate suction needs to be applied for formation of the seal. For these reasons, pressure control at the tip of the pipette is required. The system must be able to provide constant pressure (a syringe) and a switch to oral pressure control (through the

mouthpiece). The patch pipette holders usually feature an auxiliary port which can be connected to tubing to precisely enable this pressure control. A diagram of our system is presented in the figure below (Figure 3.5.2).

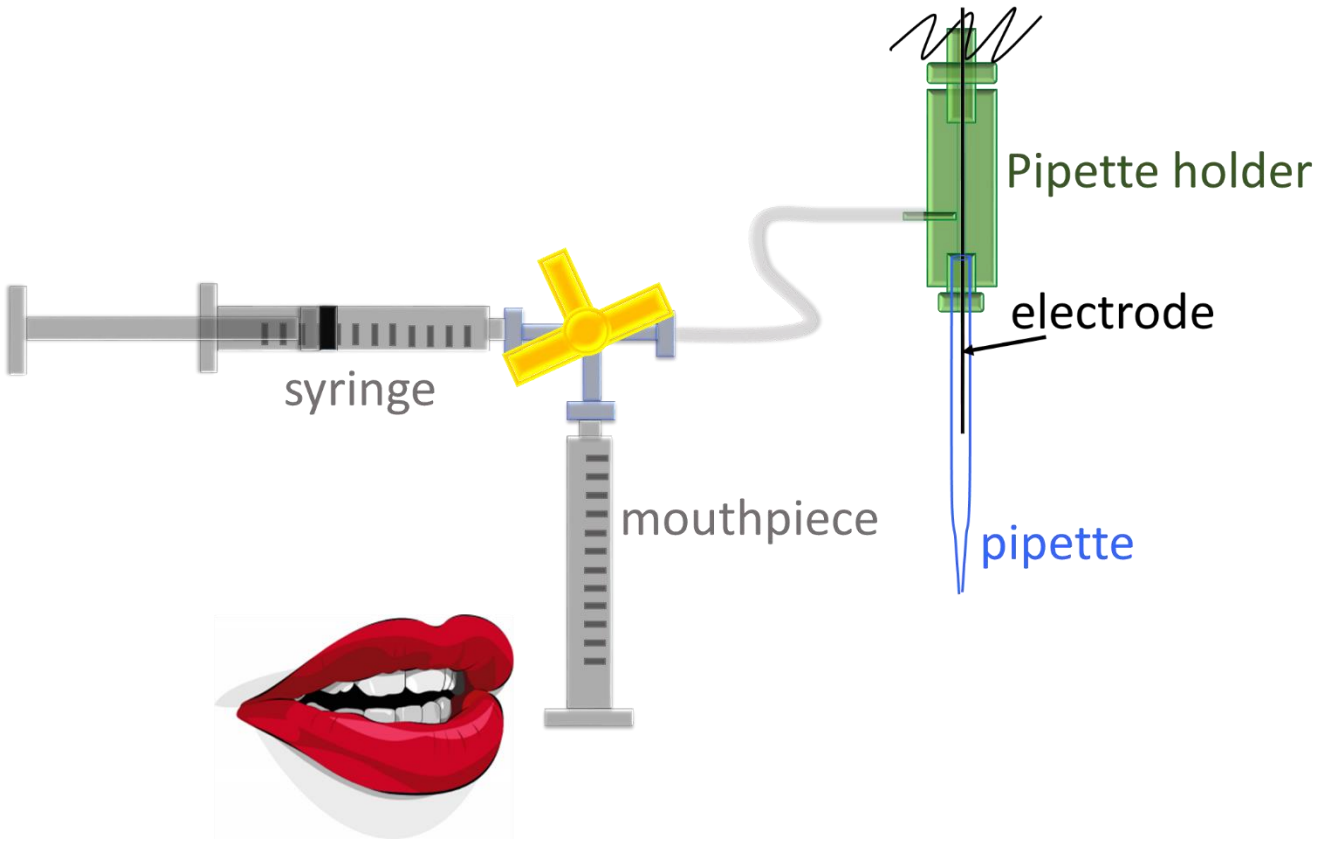

(FIGURE 3.5.2) SCHEMATICS OF MICROPIPETTE PRESSURE CONTROL SYSTEM

In our experiments, a perfused bath of fresh solution was necessary. The perfusion system should not obstruct the access of the micropipettes to the preparation. A special sample mount for the perfusion inlet and outlet was designed. To ensure flow, the inlet was drained by gravity and the outlet drained by negative pressure using a manually controlled syringe at an average rate of 0.5-1 ml/min. To prevent oxygen deprivation in the culture, the solution was bubbled with oxygen and perfused at room temperature. A schematics of the system is shown below (Figure 3.5.3).

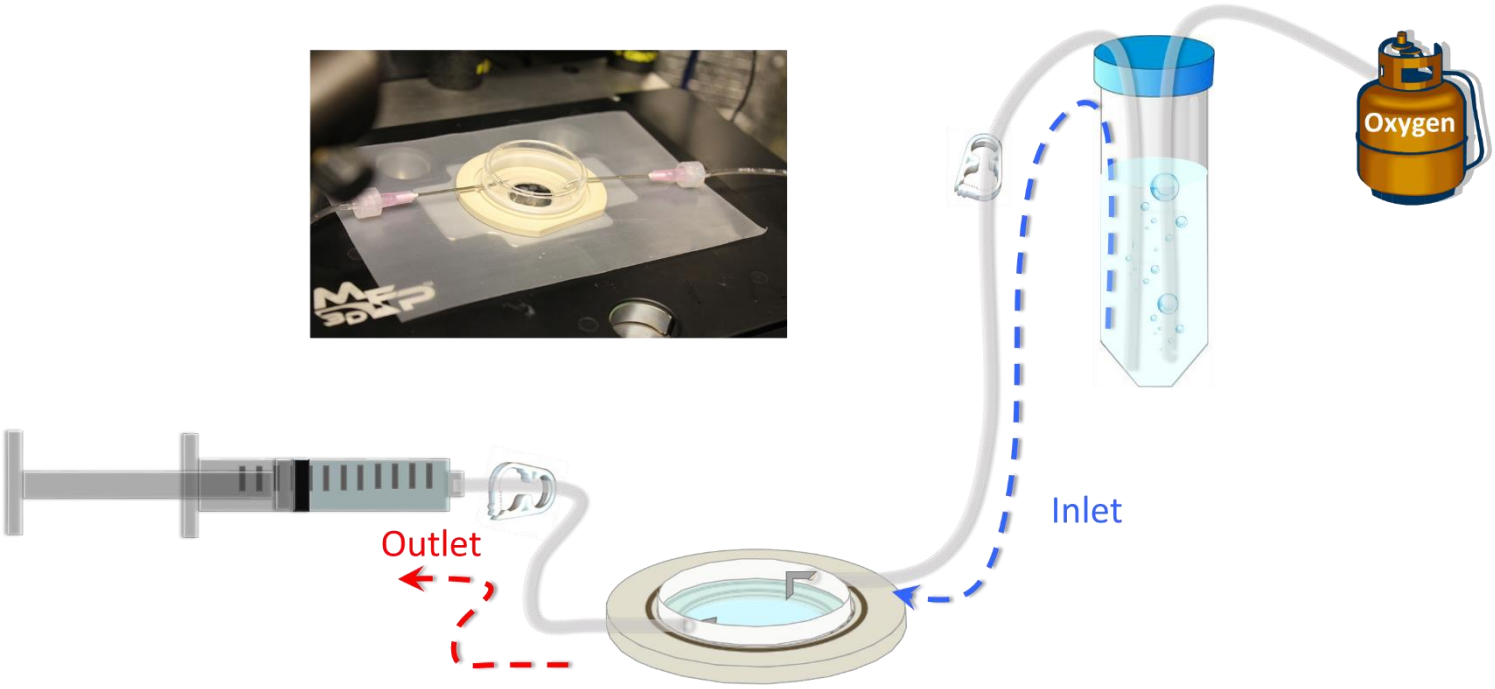

(FIGURE. 3.5.3) SCHEMATICS AND INSET IMAGE OF SAMPLE PERFUSION SYSTEM.

In patch-clamp, two electrodes are usually used: the pipette electrode and the bath electrode (reference electrode). Due to the voltage difference applied between the electrodes, the ionic solution in which they are immersed can polarize and thereby delay or even nullify the charge transfer. Additionally, at the metal-liquid interface, redox reactions (electron transfer) between the metal and the salt solution will induce a potential between the two media. To minimize these effects, materials with low redox potentials and weak polarization properties are used. Silver chloride (AgCl) electrodes are an ideal candidate and are often prepared by immersing the silver wire into neat household bleach: the bleach reacts with the silver and forms an AgCl layer on the outside of the wire. The AgCl layer on the electrode is easily rubbed off when the pipette is changed, so new electrodes have to be prepared every few days depending on the use.

For whole cell patch clamp, the membrane opening brings the electrode in contact with the inside of the cell, thus, the micropipettes have to be filled with saline solution with similar characteristics as the intracellular solution. Additionally, the glass pipettes used to make the patch onto the membrane have to be microscopically small, therefore, pipettes are commonly tapered down to a micrometer size aperture using a micropipette puller available in our lab (Flaming/Brown, model P-87, [227]) (Figure 3.5.4).

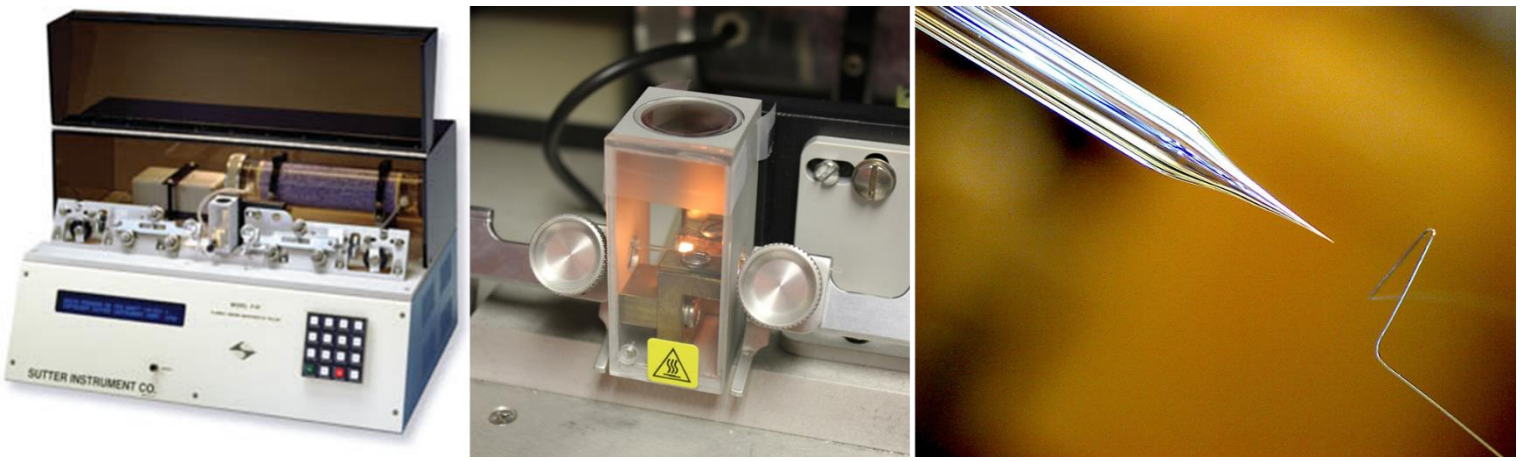

(FIGURE 3.5.4) SUTTER PIPETTE PULLER AND REPRESENTATIVE IMAGE OF PULLED PIPETTE.

FROM LEFT TO RIGHT: THE PIPETTE PULLER, THE ENVIRONMENTAL CHAMBER TO PROTECT THE FILAMENT THAT IS HEATED UP IN ORDER TO PULL A PIPETTE AND AN EXAMPLE OF A PULLED GLASS PIPETTE USING THIS SETUP.

Once in the patch, the electrode can be used to excite or detect electrical activity in the cell. The electrical signals coming from a cell are an effect of single or multiple ion channels being activated. The currents recorded from a single cell are typically very low (~pA) and a high impedance circuit is required to detect them. The electronic circuits need to detect the small single cell currents make patch clamping instruments prone to electrical interference. To assure an electrically quiet environment, all wires, instruments and metal pieces should be connected to the same ground (to avoid ground loops). Additional shielding of the stage is sometimes necessary to lower the noise amplitude. For our experiments, a Faraday cage was built and placed over the stage to bring the noise amplitude down to acceptable levels (~5pA) for whole cell (patch-clamp) measurements (Figure 3.5.5).

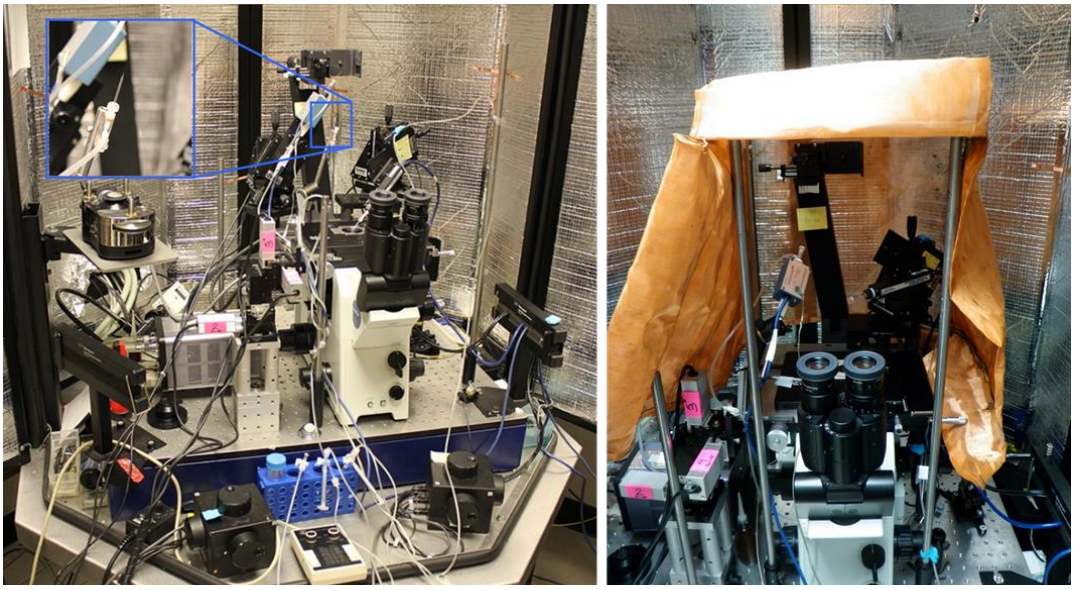

(FIGURE. 3.5.5) IMAGES OF THE PATCH CLAMP SETUP AND FARADAY CAGE.

The patch-clamp amplifier is the central component of the set-up, containing the measuring and clamping circuitry. Patch clamp amplifiers have a head-stage (with a high impedance preamplifier) which connects directly to the pipette holder and placed as close as possible to the sample. The basic control commands (current/voltage clamp selection, current offset, capacitance compensation, holding potential, gain and others) can often be regulated through the amplifier. Specific clamping and stimulation signals are programmed through the computer to which the amplifier is connected. The application dictates the type of amplifier required. In the experiments presented in this thesis, whole cell patch-clamp recordings were performed and two Axopatch amplifiers (Axopatch-200A and -200B amplifiers, Axon Instruments) were employed. For whole cell signal recording, the amplifier settings include a low-pass filter to enable clear visualization of biological signals and lower the noise due to high frequencies. The filter settings in the amplifier are essential to avoid aliasing or losing important data. The amplifier filters the signal using a 5 kHz lowpass Bessel filter set according to recommendations made in the manufacturer's manual [222,223].

To provide commands and acquire data, signals must be converted from analogue to digital (AD) format, and vice versa. The device to perform these tasks is the AD/DA converter or interface. The quality of conversion depends on optimization of temporal and amplitude resolution. According to the Nyquist–Shannon sampling theorem, if a function x(t) contains no frequencies higher than B Hz, it is completely determined by giving its ordinates at a frequency of 2B Hz [228]. In our setup the bandwidth was set to 5 kHz by

the amplifier Bessel filter. A sufficient sample-rate for the digitizer is therefore 10 kHz. In practice this should be larger in the presence of noise. In our setup, the signals were digitized using a USB-6218 (National Instruments) coupled to a personal computer running WinWCP V4.7.3 software (from the University of Strathclyde Science). The WinWCP software controlled the electrical stimuli provided, the signals were sampled at 10 KHz.

3.5.2 The cell as an electric component

To understand electrophysiology, the cellular components need to be described in terms of their electronic representation. Animal cells are enveloped by a plasma membrane that acts as a barrier between the cytoplasm and the extracellular space. This membrane forms a very effective barrier for charged molecules. It is constituted of a lipid bilayer that embeds different proteins with a variety of functions such as communication, structure and homeostasis. When the membrane proteins are active, small currents (~pA) can cross the membrane, which can be modeled as a resistive component of the cell. Due to the way these proteins function to maintain the cell homeostasis, the charges on either side are not in balance; the inside of all cells is more negatively charged than the outside, and the difference causes a "negative" membrane potential (*Em*). Every ion has an equilibrium potential (*Eion*) associated with its concentration ([*ion*]) across the membrane that can be determined by the Nernst equation [229]:

$$E_{ion} = \frac{RT}{zF} \ln\left(\frac{[ion_{in}]}{[ion_{out}]}\right)$$

Where *T* is the temperature of the system and *R*, *z* and *F* are the gas constant, the ionic valence and the Faraday constant respectively. If the membrane of the cell was permeable to only one ion, then *Em* would be equal to *Eion*. In reality, the channels, pumps and transporters (proteins) embedded in the membrane are permeable to different ions and every ionic potential contributes to the resting membrane potential (*Em*) and can be calculated using the Goldman equation [230,231]. The Goldman equation is limited because it assumes that Em is constant. An intuitive understanding of the temporal evolution of the system in response to a change in *Em* can be obtained when the cell is modeled as its equivalent electrical circuit.

Say there is a difference between the equilibrium potential (*Eion*) and the membrane potential *Em*, then a driving force (*Em – Eion*) will provoke the ions to move across the membrane. Following Ohm's law, the current across the membrane can be expressed as follows:

$$E_m - E_{ion} = R_{m,ion} \cdot I_{ion}$$

The driving force provokes an ionic current *Iion* through the proteins permeable to that ion *Rm,ion*. Due to the lipid content of the membrane, it is able to store charge and can be modeled as a capacitive element (*Cm*). The amount of charge (*Q*) stored can be expressed as:

$$Q = E_m C_m$$

The physical dimensions of the membrane are important in determining the capacitance: cells with a bigger surface area (A) can accumulate more charge. The following figure (Figure 3.5.6) shows the cell membrane composed of ion permeable elements and the lipid membrane and its equivalent electrical circuit.

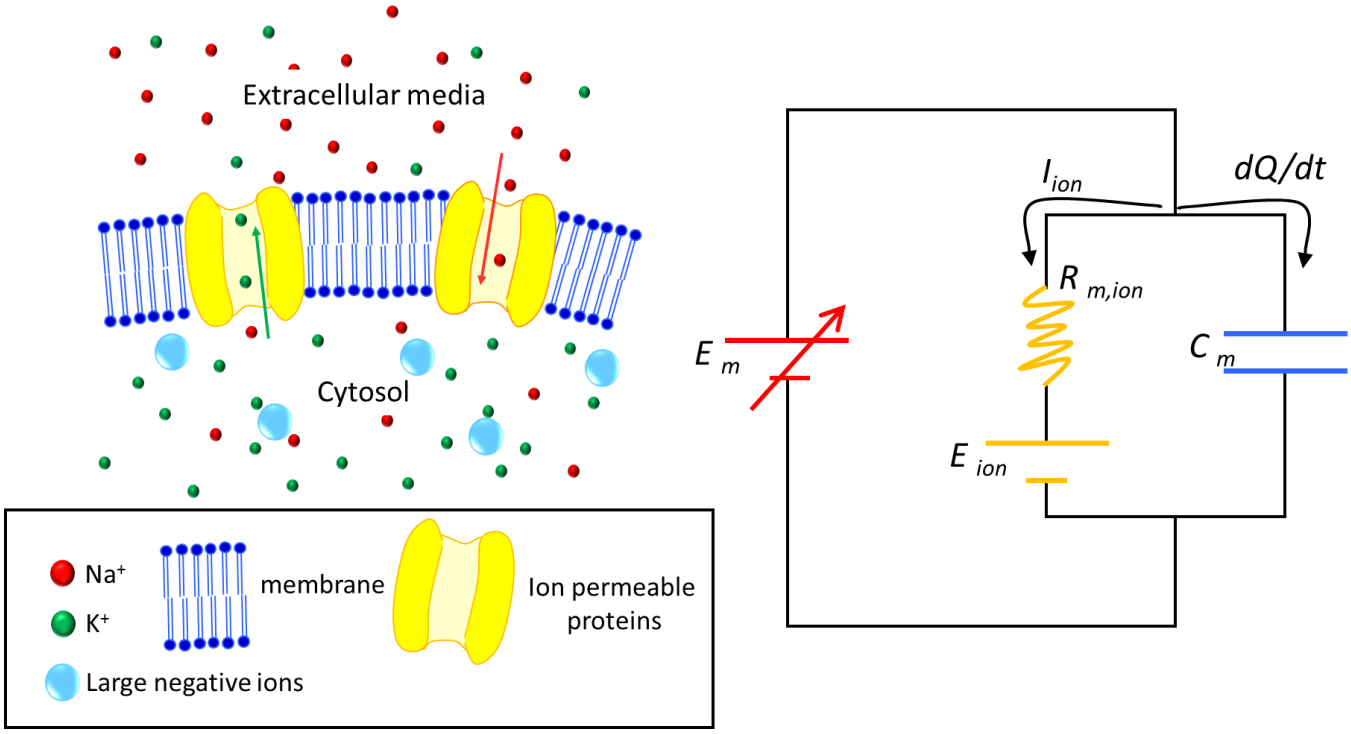

(FIGURE 3.5.6) SCHEMATICS OF THE CELL MEMBRANE AND EQUIVALENT CIRCUIT.

3.5.3 Patch clamp modes

Broadly speaking, electrophysiological techniques record ion fluxes across a membrane. The particular technique used (whole cell patching) records ionic currents while the microelectrode is in contact with the cytosol of the cell of interest. In "*voltage-clamp*" mode, the applied pipette potential extends into the cell to control the membrane potential and record the membrane current. Voltage (potential) control and current measurement use the same pipette. To keep the voltage constant, the current feedback must be instantaneous, thus, low-resistance pipettes are required to avoid long RC delays in the response. By convention, outward excitatory currents always are considered positive and are shown as upward deflections, whereas inward inhibitory currents are considered negative and are shown as downward deflections (Figure 3.5.7, left). Because the output signal in "*voltage-clamp*" mode is the current required to keep the voltage constant, the excitatory activity (outward currents) experienced by the cell will be counteracted by negative currents in the feedback circuit, and the inhibitory (inward currents) will be shown as positive currents in order to keep the clamping voltage constant. Alternatively, the amplifier could be used to inject a fixed current into the cell to "*current-clamp*" the cell membrane , with voltage allowed to vary. The resulting voltage change can be used to estimate Rm and Cm. Additionally, this mode can be used to measure the membrane potential Em, (typically -65 mV) which is useful to check the quality of the patch on the cell or inject a slightly depolarizing current and bring it closer to the action potential threshold (Figure 3.5.7, right). Schematics of the whole cell patch clamp equivalent circuit can be found in appendix A.

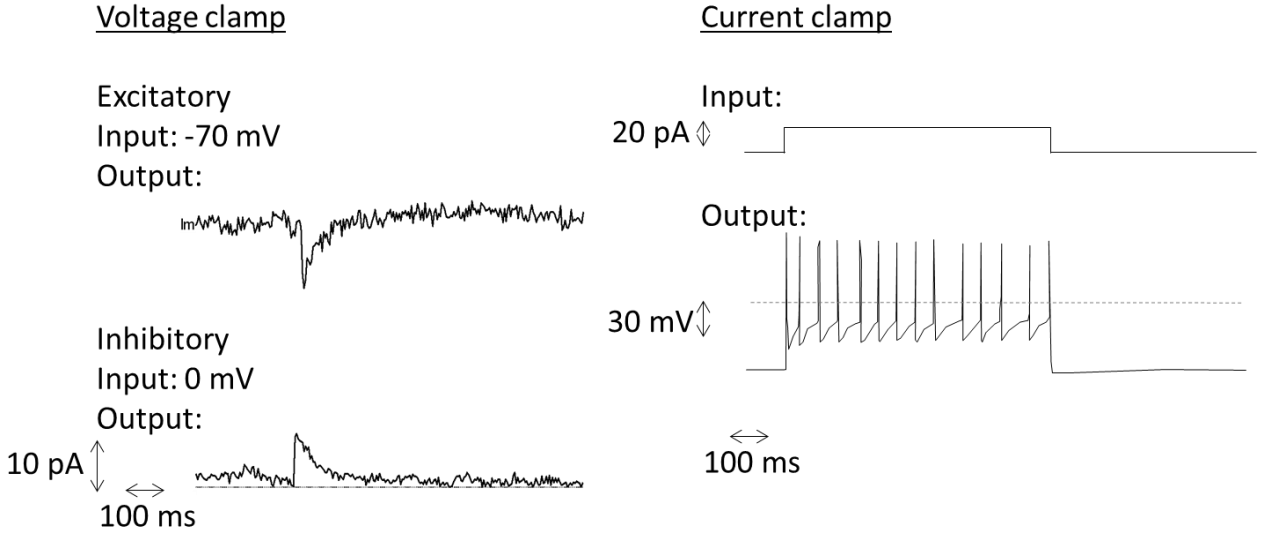

(FIGURE 3.5.7) SAMPLE TRACES DEPICTING VOLTAGE AND CURRENT CLAMP MODES

3.5.4 Paired patch clamp recordings

For the experiments in Chapter 6, paired whole cell patch–clamp recordings using two sets of electrodes were used to study communication between individual neurons. This method was first developed in Aplysia neurons in vitro [232]. It is a powerful and versatile tool allowing the study of many basic properties of neuronal communication in brain circuits. Particularly, it enables the study of synaptic interaction between neurons and their characteristics [233–236]. In the experiments described here all solutions were prepared following recommendations by Dr Boudreau and described in [234,237]. Typically, a pair of connected neurons is selected and one of the neurons is stimulated while currents are detected in the other neuron. The first neuron (presynaptic or input) is stimulated in current clamp, which enables action potentials to be triggered, while in the second neuron (postsynaptic or output) currents are recorded in voltage clamp. Pre- and postsynaptic traces are continuously recorded. A typical trace of a connected pair examined using this technique is shown in the figure below (Figure 3.5.8)

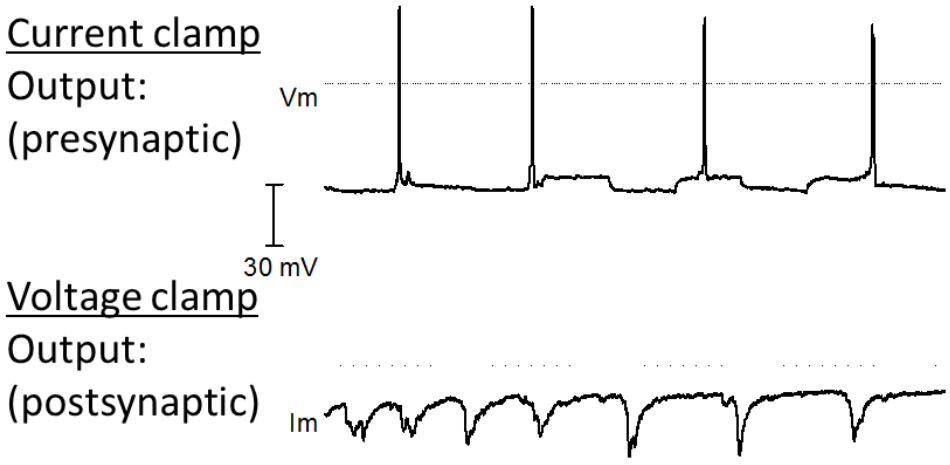

(FIGURE 3.5.8) SAMPLE TRACES SHOWING OF A PAIRED RECORDING. THE PRESYNAPTIC CELL HELD UNDER CURRENT CLAMP EXHIBITED ACTION POTENTIALS (TOP) WHILE THE POSTSYNAPTIC CELL, HELD IN VOLTAGE CLAMP MODE EXHIBITED EXCITATORY POSTSYNAPTIC ACTIVITY (BOTTOM)

After recording, the data was exported for offline analysis. The traces were aligned with respect to the time course of onset of the presynaptic action potentials and the evoked postsynaptic activity were detected and plotted following protocols in [238] (Figure 3.5.9).

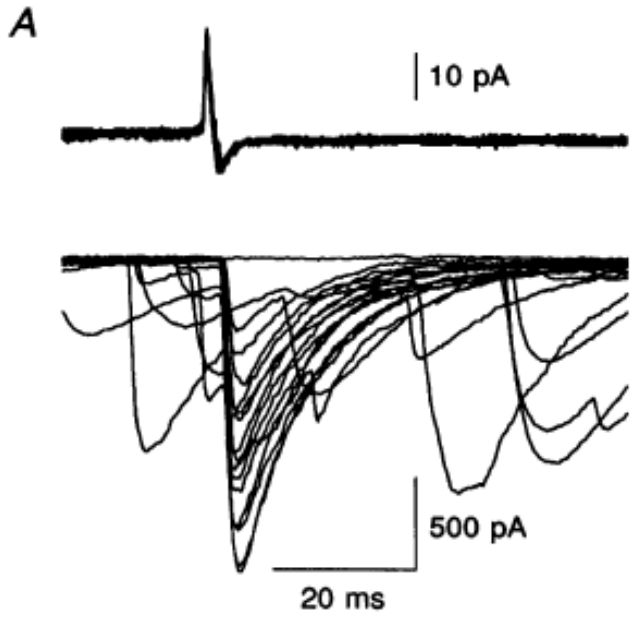

(FIGURE 3.5.9) FIGURE DEPICTING SPIKE TRIGGERED ACTIVITY (TAKEN FROM: (VINCENT & MARTY, 1996), FIGURE 1.)

The analysis of these traces is detailed in the corresponding section.

Chapter 4. Deconvolution of Calcium Fluorescent Indicator Signal from AFM Cantilever Reflection

The development of techniques to apply and quantify mechanical forces in a controlled manner has enabled investigations of a wide range of biological samples and environments. Many of these techniques use optical imaging and microscopy to enable quantification [9,64,94,128,239–241].

It is particularly common to combine many of these mechanical approaches with fluorescence microscopy due to its wide application and profound impact in our current understanding of biology. The combined approach enables complementary simultaneous visualization of dynamic changes in specific structures of the cell in response to changes in the mechanical environment. This is particularly useful for studies of mechanotransduction [15,150,240], assessment of the properties of specific cellular structures [127,207,242], and kinetics of single molecules [157,243], providing a more complete understanding of the physiological processes taking place.

The simultaneous combination of AFM and fluorescence is a particularly useful approach. In this chapter, we demonstrate the importance of understanding each of the instruments used and the potential interactions between them because they may lead to artifacts in the measurements that need to be accounted for or corrected. On the upside, we found that the coupling artifacts in our experiments can also be used for a more precise temporal correlation of the measurements

Deconvolution of calcium fluorescent indicator signal from AFM cantilever reflection.

Short Title: ***AFM reflection in fluorescent channel***

Gabriela M Lopez A[1]*, David J Oliver[1], Peter H Grutter[1]and Svetlana V. Komarova[2]

[1] Center for the Physics of Materials and the Department of Physics, McGill University, 3600 University, Montreal, Quebec Canada, H3A 2T8, Canada.

[2]Faculty of Dentistry, McGill University, 740 Dr. Penfield Ave, 2201, Montreal, Quebec Canada, H3A 1A4, Canada

*Corresponding author**: Gabriela M Lopez A; Tel: (514) 398-1629, Fax: (514) 398-8434, email: lopezm**@physics.mcgill.ca

Keywords: ***AFM, fluorescence artifacts, mechanical stimulation, calcium signaling, fluo-4***

*Abbreviations**: AFM, $[Ca^{2+}]_I$, MEM, DMEM, C2C12, BMP-2, HEPES***

Abstract

Atomic force microscopy (AFM) can be combined with fluorescence microscopy to measure the changes in intracellular calcium levels (indicated by fluorescence of Ca sensitive dye fluo-4) in response to mechanical stimulation performed by AFM. Mechanical stimulation using AFM is associated with cantilever movement, which may interfere with the fluorescence signal. The motion of the AFM cantilever with respect to the sample resulted in changes of the reflection of light back to the sample and a subsequent variation in the fluorescence intensity, which was not related to changes in intracellular calcium levels. When global calcium responses to a single stimulation were assessed, the interference of reflected light with the fluorescent signal was minimal. However, in experiments where local repetitive stimulations were performed, reflection artifacts, correlated with cantilever motion, represented a significant component of the fluorescent signal. One needs to separate this reflection artifact from the cantilever induced cell stimulation. We developed a protocol to correct the fluorescence traces for reflection artifacts, as well as photo-bleaching. An added benefit of our method is that the cantilever reflection in the fluorescence recordings can be used for precise temporal correlation of the AFM and fluorescence measurements.

Introduction

The development of Atomic Force Microscopy (AFM) has enabled investigations of a wide range of samples and environments, from single atom manipulation in ultrahigh vacuum to studies of individual molecules, proteins, nucleic acids and different structures of living cells in buffered solutions (Muller, 2008). AFM imaging is fundamentally different from conventional microscopy in that it allows localized, highly controlled invasion and manipulation of nano- and microscopic structures. These qualities have rendered it a technique of wide application in biology. By combining AFM with fluorescence microscopy, a technique widely used in biology, it provides simultaneous ability to locally manipulate the sample (such as in force spectroscopy and nano-manipulation techniques) and to visualize the associated, dynamic changes in cell status properties or signalling as reported by labeled molecules (Sanchez & Wyman, 2010), (Barfoot et al., 2008), (Oh et

al., 2008). The combined setup enables a complementary examination of the sample and a better understanding of the physiological processes than either of the techniques alone can deliver. However it is important to understand potential interactions between different instruments and be prepared for the possibility of artifacts in the measurements.

AFM imaging allows local, controlled and quantifiable mechanical or chemical interactions with the cellular and molecular structures, which enables experiments that require high resolution imaging, determination of local mechanical properties or the application of mechano-chemical stimuli. These techniques involve the use of a tip integrated at the very end of a cantilever. Interactions between the tip and the sample are controlled by controlling the deflection of the cantilever. Thus, during experiments the tip moves relative to the sample to perform the measurement. The AFM application of particular interest to us is its use to study cell sensitivity to mechanical deformation of cell membrane (Ehrlich & Lanyon, 2002), (Charras & Horton, 2002), (Guo et al., 2006).One of the most prominent first cellular responses to mechanical stimulations of different nature is transient elevation of cytosolic free calcium concentration ($[Ca^{2+}]_i$) (Duncan & Turner, 1995). Several fluorophores have been developed and successfully used to study changes in $[Ca^{2+}]_i$, including fura-2, fluo-3 and fluo-4 (Molecular probes, 2011). Fluo-3 and -4 can be used in the situations where only visible spectrum excitation light source is available and fluo-4 is brighter and more stable compared to fluo-3 (Molecular Devices, 2010). Our goal was to establish a combined AFM and fluorescence microscopy setup to measure the changes in $[Ca^{2+}]_i$ (indicated by fluorescence of fluo-4-loaded osteoblastic cells) in response to mechanical stimulation performed by AFM. Since mechanical stimulation using AFM is associated with cantilever movement, we hypothesized that this motion may potentially interfere with the fluorescence signal.

Materials and Methods

Mechanical stimulation of a single cell using AFM: C2C12 cells stably transfected with BMP-2 were kindly provided by Dr M. Murshed, McGill University. Cells were cultured in in Dulbecco's Modified Eagle Medium (DMEM, from Invitrogen) supplemented with 2 mM of L-glutamine, 100 IU of penicillin, 100 μg/ml of streptomycin and 10% of fetal bovine serum (Wisent) on round 25 mm No.1 glass coverslips (Matteck corporation) at 5% CO_2 at 37°C. The media was changed every third day. Cells were cultured to 50-70% confluence to allow easy identification of individual cells. The experiments were conducted using an MFP-3D-BIO AFM (Asylum Research, Santa Barbara CA) mounted

on an Olympus IX-71 inverted optical microscope. The sample placed in the closed fluid cell was left undisturbed for 15 min to achieve thermal equilibrium at 37°C. A 60X oil immersion objective with 1.45 NA (Olympus) was put into contact with the coverslip allowing optical access from the bottom and AFM probe access from the top of the sample. The region of interest over the nucleus of the cell was located and aligned with the cantilever tip using bright field and fluorescence images. Cells were mechanically stimulated using an NCLAuD cantilever (Nanosensors), with a spring constant (k) of 40 ± 8 N/m. The tip end was etched a 1 μm^2 area using a focused ion beam microscope (FEI DB235) to have a well-defined truncated pyramid shape, allowing the local pressure to be determined. The cantilever deflection and distance the probe moved were monitored and plotted in a deflection-distance curve. The force ($F = k \cdot deflection$), the range (the net extension of the piezo element in a deflection-distance curve), the speed and the number of indentations were controlled.

Intracellular calcium measurements: The cells were loaded with 1.5 µl of Ca^{2+}-sensitive dye Fluo4–AM (Molecular Probes) in culture media for 40 minutes at room temperature. The dye was washed twice with physiological buffered solution (130 mM NaCl; 5 mM KCl; 10 mM glucose; 1 mM MgCl2; 1 mM CaCl2; 20mM) containing 2% 1M HEPES (pH 7.4)) (Kemeny-Suss et al., 2009), the coverslip was assembled on to the peak fluid chamber (Asylum Research) and physiological buffered solution (1.5 ml) was added. The cells were illuminated with a 488 nm argon laser and the emitted light was collected with a CCD camera (Cascade II; Liquid from Photometrics). In each experiment 200 images were acquired in a sequence. The exposure time was set to 250 ms and minimum time between frames was selected. The average time per frame was calculated to be 335 ±10 ms.

Analysis: Data are presented as representative traces, representative images, or means ± standard error of the mean (SEM). AFM data was acquired using Igor Pro software package, fluorescence images were collected using Image-Pro Plus (Version 6.2.) and saved as *.tif files. Matlab was used to extract, combine and analyze fluorescence intensity data, calculate the fast Fourier transform (FFT) and analyze the power spectrum. Power spectra peaks were fitted using least squares regression to a power law. Fluorescence and force spectroscopy measurements were correlated using Igor Pro.

Experimental Setup

Calcium (Ca^{2+}) signaling has been shown to be the prominent first response of osteoblastic cells to any type of mechanical stimulation (Chen et al., 2000), (Hung et at., 1995*a*, 1996*b*). As a model of osteoblastic cells, we used C2C12 cell line stably transfected with BMP-2 and cultured for 2-6 days (Li et al., 2011). Cells exhibiting osteoblastic morphology (strongly adhered mono-nucleated cells with a relatively large body and several filopodia) were chosen for mechanical testing. Post-experiment, the cells were fixed and stained for osteoblast marker alkaline phosphatase. Cells exhibiting osteoblastic morphology were also stained positive for the alkaline phosphatase (Fig. 1 A). Mechanical stimulation was performed with AFM force spectroscopy using a 1 μm^2 diameter tip. We analyzed Ca^{2+} transients in response to two different regimes of mechanical stimulation: *i*) low load indentation in which only membrane deformation was induced (Fig. 1 B, C, green trace) and *ii*) high load indentation in which the membrane was penetrated after deformation (Fig. 1 B, C, blue trace). The membrane penetration event is easily identifiable on the deflection-distance curve as a decrease in the force required to continue to move the probe.

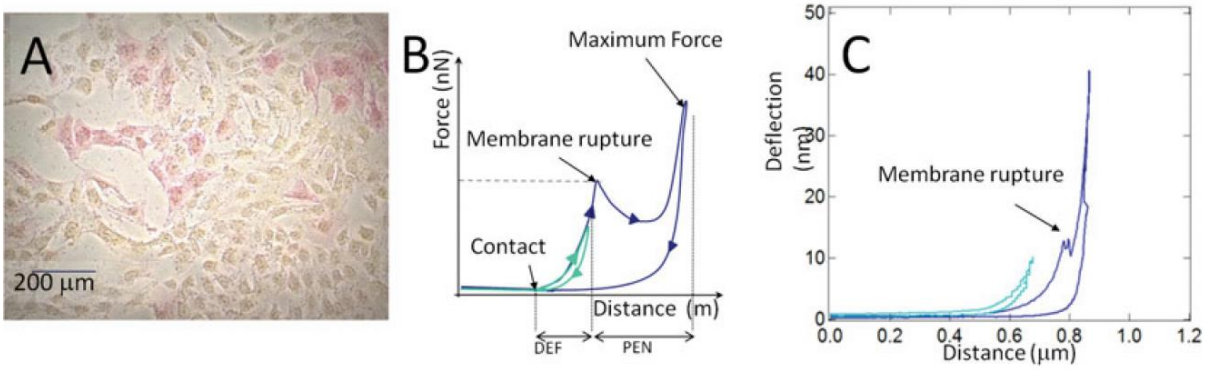

FIGURE 1. Testing mechanosensitivity of bone cells using atomic force microscopy (AFM). C2C12 cells stably transfected with BMP-2 were cultured for 2-6 days to obtain osteoblastic phenotype. A) Representative image of C2C12 culture stained for osteoblast marker, alkaline phosphatase (red). B, C) A single cell was indented using a cantilever with a blunt tip of 1 mm^2. The force exerted by the probe and the distance the probe moves were monitored and plotted as a deflection-indentation curve. B) Schematic representation of events observed using deflection-indentation curve: a) the contact point of the tip is evident as increase in force required to move the probe; b) when membrane rupture force is reached, the tip penetrates the cell (apparent by a decrease in the cell resistance); c) when a predetermined maximum force, is reached, probe retraction is initiated. The maximum force was set to be either below (green) or above (blue) the membrane rupture force. C) The examples of deflection-distance curves from the experiments in which membrane deformation only (green) or deformation plus penetration (blue) were induced.

Photo-bleaching of Fluo-4 fluorescence

Because $[Ca^{2+}]_i$ transients are elicited in response to mechanical stimulation, we used Ca^{2+}-sensitive fluorescent dye Fluo-4-AM (Molecular Probes, 2011) to study Ca^{2+} responses to mechanical stimulation. First, to assess photo-bleaching, we monitored Fluo-4-loaded cells for the period required to perform the indentation experiment. Photo-bleaching was evident as a decrease in fluorescence intensity in the field of observation over time (Fig 2, A). The cells in the field of view were individually selected with the assistance of bright field image (Fig 2, A, *white ellipses*) and the average intensity for each cell was plotted as a function of the frame (Fig 2, B *solid lines*). As described by Vicente and colleagues (Vicente et al., 2007), the traces were fitted with a mono-exponential decay function ($I(t) = Ae^{-at}$), resulting in a = 228 ± 28 s (Fig 2, B *dotted lines*). Photo-bleaching was also evident in the experiments where mechanical stimulation was induced (Fig. 2 C-F). When high load indentation resulting in membrane deformation and penetration was induced (Fig. 2 C), the cell exhibited a global increase in fluorescence intensity, indicating a $[Ca^{2+}]_i$ transient (Fig. 2 D). When the cells were indented with forces leading to membrane deformation only (Fig. 2 E), the cell exhibited local elevations in fluorescence intensity, which were only apparent at the point of contact with the indenting tip (Fig. 2 F). Multiple increases in fluorescence intensity were observed in response to multiple consecutive stimulations (Fig. 2 F).

The movement of AFM cantilever affects sample illumination.

During analysis of the experiments in which multiple consecutive membrane deformations at 0.1 Hz were performed, we noticed regular oscillations of the background signal (*Supplementary information I, video*). We plotted the average intensity over an ellipse surrounding the total area of the stimulated cell (*Cell 1*) and non-stimulated cells (*Cell 2-4*) as a function of time (Fig. 3 A). Changes in fluorescence intensity of non-stimulated cells are synchronized with those in the stimulated cell, therefore it is unlikely that these changes are biological in nature. The characteristic frequencies of the fluorescence signal of the non-stimulated cells were assessed using Fast Fourier Transform and the peak frequency of the power spectrum was found to be 0.128 ± 0.001 Hz (Fig. 3B). The deflection curves were plotted as a function of time and the average duration of each indentation was found to be ~8 s, resulting in a frequency of 1/8 = 0.125 Hz, which closely corresponds to the oscillation frequency in fluorescence traces (Fig. 3C). Next, for the experiments performed at different indentation speeds, the peak frequency of the

fluorescence intensity traces was calculated and plotted as a function of the average duration of a corresponding deflection curve. A $f = 1/t$ relation was obtained by fitting a power function to the data set (R^2=0.998) (Fig. 3D). Thus, the frequency (f) of the oscillations observed in fluorescence traces corresponds to a period ($1/f$) with which the indentations were performed. We concluded that the motion of the AFM cantilever affects the sample illumination due to reflection of laser light from the cantilever, producing changes in the fluorescence intensity of non-stimulated cells that are un-related to changes in the $[Ca^{2+}]_i$ of stimulated cells, as schematically summarized on Figure 3E.

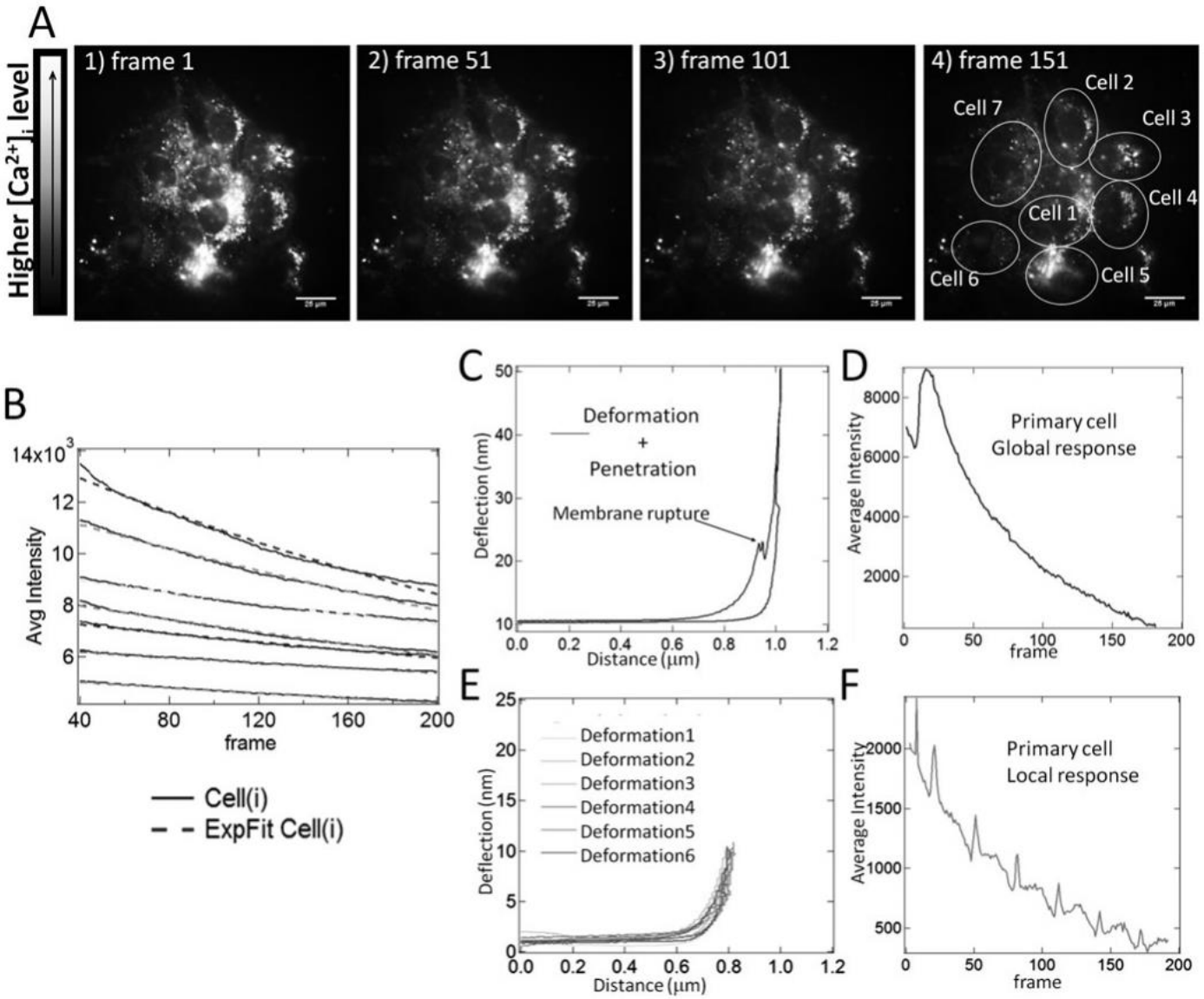

FIGURE 2. Photo-bleaching of the calcium-sensitive fluorescent indicator fluo-4 AM. A, B) Osteoblastic cells were loaded with 1.5 μl of Ca^{2+}-sensitive dye Fluo4 –AM and changes in fluorescence intensity over time were assessed. A) Overall decrease in fluorescent intensity is evident over the image sequence taken at ~ 3 frames/s. No mechanical stimulation was performed. Image frames are indicated at each image. Scale bar is 25 μm in all images. Different cells were identified with the assistance of bright field image and are indicated by white ellipses. B) The average fluorescence intensity of each cell was determined and plotted as a function of frame (solid traces). The intensity trace of each cell was fitted with a mono-exponential decay function (dotted lines). C-F) Photo-bleaching is evident in fluorescence traces acquired while mechanical stimulation was performed. C, D) Deformation leading to membrane rupture induced global increase in fluorescence intensity. C) Deflection-distance curve of stimulation leading to membrane rupture. D) The average fluorescence intensity over the total area of indented cell was plotted as a function of frame. E, F) Low level membrane deformation induced local increase in fluorescence intensity. E) Deflection-distance curves for the six consecutive stimulations performed in the same position in a single cell. F) The average fluorescence intensity over 5 μm diameter circle centered at the indentation site was plotted as a function of frame.

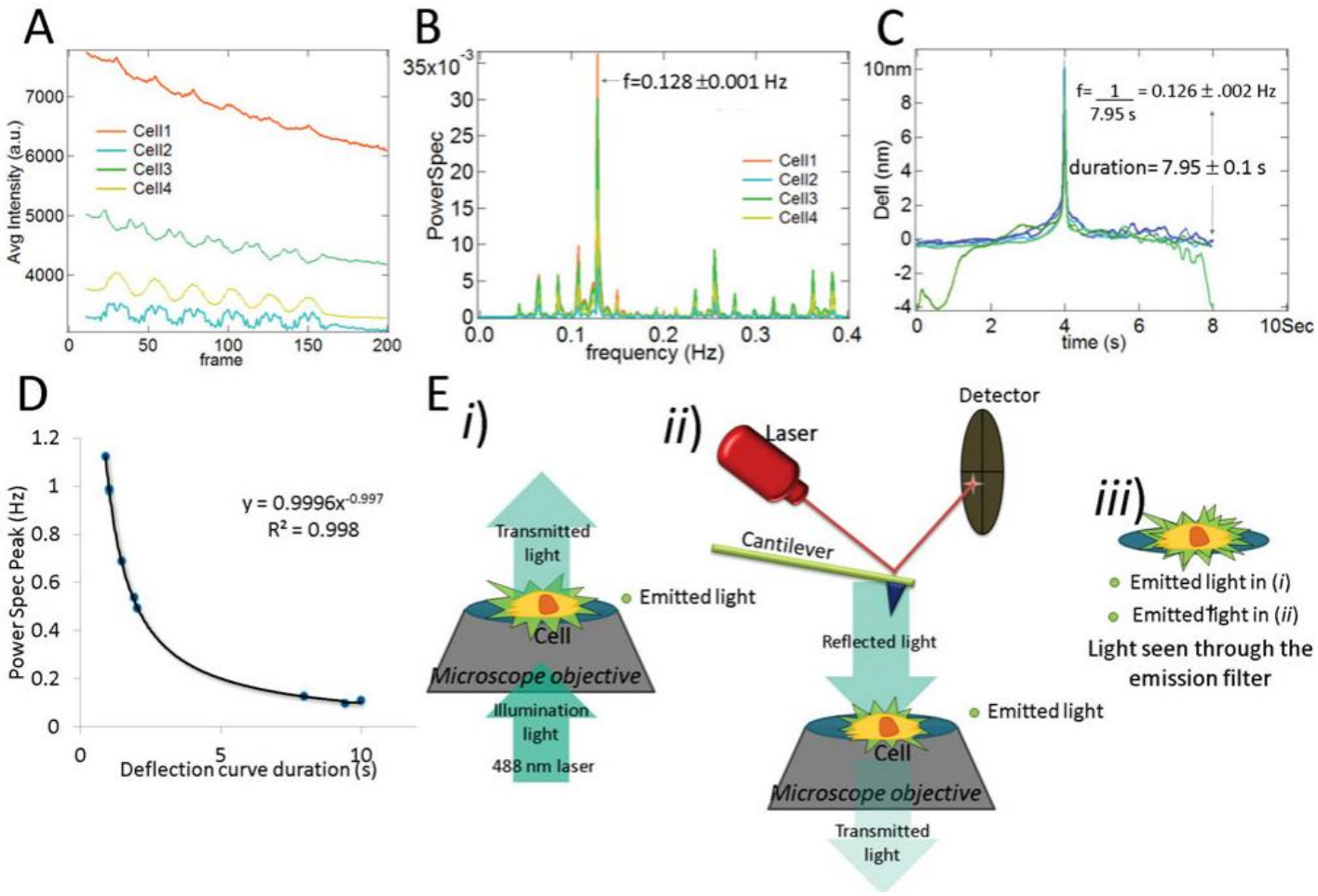

FIGURE 3. The motion of AFM cantilever affects sample illumination resulting in changes in fluorescence intensity unrelated to changes in $[Ca^{2+}]_i$. Osteoblastic cells were loaded with Fluo4 –AM and changes in fluorescence intensity in response to multiple consecutive AFM stimulations were assessed in stimulated and non-stimulated cells. A) The average fluorescence intensity over the total area of indented cell (Cell 1) or non-stimulated cells (Cell 2-4) was plotted as a function of frame. Oscillatory fluorescence intensity changes in non-stimulated cells are evident. B) The Power spectrum (PowSpec) of the Fast Fourier Transform for each cell trace in (A) was calculated and is plotted as a function of the frequency. A frequency peak appears at 0.012 Hz. C) The deflection-time curves acquired for the same experiment are plotted as a function of time. D) The power spectrum was calculated for non-stimulated cells in experiments performed at different indentation speeds, the peak frequency of the power spectrum for each experiment is plotted as a function of the duration of the deflection-time curves. A power fit was calculated and a relation ~ 1/f was obtained with R^2=0.998. E) Schematics of the effect of the presence of the cantilever on the sample illumination: *i*) The incident light in the sample is partially absorbed by the sample, and partially transmitted through the sample (green arrow). The fluorophores that absorbed light at the excitation wavelength are now excited and decay back to their lower energy state, emitting light at a longer wavelength (emitted light in *i*). *ii*) The light transmitted continues its optical path and is then reflected by the cantilever, which is located a few microns above the sample. The back-reflected light is again partially absorbed by the sample and thus, more fluorophores are excited emitting additional light (emitted light in *ii*). *iii*) The light emitted by the fluorophores is detected (emitted light in *i* + emitted light in *ii*).

Protocol for signal correction for bleaching and cantilever reflection

To correct for the cantilever motion and bleaching artifacts, raw fluorescence traces were processed using Matlab (*Supplementary information II, Matlab code 1*). The image sequence was loaded into the program, and ellipses surrounding different cells were manually selected (Fig 4 A, D). The spatially-averaged intensity for each selected cell was calculated for each frame, and the frame evolution of the average fluorescence intensity was plotted (Fig 4 B, E).

For the experiments in which global increase in fluorescence intensity (an average intensity higher than 4-fold the average noise) were observed (Fig.4 A-C), the curves were processed as follows (*Supplementary information III, Matlab code II*). First, we assessed if the changes in fluorescence intensity can be due to changes in sample illumination. We assumed that changes in sample illumination are evident in the fluorescence traces of non-stimulated cells, therefore, if we can find a linear combination of the fluorescence profiles of the *n* non-indented cells *Cell*(i) ($Cell1 = \sum_{i=2}^{n+1} a(i) \cdot Cell(i)$) such that the *Primary* cell profile will be obtained, then, the increase in fluorescence intensity in the *Primary* cell is due to changes in sample illumination and not in $[Ca^{2+}]_i$. If the *Primary* trace (Fig. 4C) and the *linear combination* (Fig. 4C) are different, specifically at the peak of the fluorescence increase, we concluded that the *Primary* cell exhibited a *Global* Ca^{2+} response to mechanical stimulation.

Next we corrected the *Global* Ca^{2+} response for photo-bleaching. A new linear combination of non-stimulated cells (Fig. 4C, *ExtrLinComb*) was fitted to the initial (before stimulation) and final (last 25 frames of recording) extremes of the *Global* response trace (Fig. 4C), and approximated with a mono-exponential decay curve (Fig. 4C, *ExpFit).* *Global* trace was divided by the *ExpFit* curve resulting in the final bleaching-corrected (i.e. normalized) *Global* Ca^{2+} response (Fig. 4C, *UnbGlobal*). Although we sometimes see reflection artifacts in stimulated and non-stimulated cells, in all cases they appear before the onset of global Ca^{2+} response. Therefore, when the post-stimulation time-frame is selected for analysis, no additional procedure is required to correct for these artifacts in the experiments with global calcium responses.

For the experiments in which multiple consecutive low load membrane deformations were performed (Fig. 4 D-F), the traces were processed as follows (*Supplementary information IV, Matlab code III*): In addition to the spatially-averaged fluorescence intensity profile over the whole cells in the field of view (Fig. 4 D, *white circles*), we took the spatially-

averaged intensity over a circle of 5 μm in diameter centered on the point of indentation (*Local*) (Fig. 4 D, *black circle*). To correct for photo-bleaching, the *linear combination* ($Cell1 = \sum_{i=2}^{n+1} a(i) \cdot Cell(i)$) of traces from non-stimulated cells was calculated and approximated with a mono-exponential decay curve. The *Primary Global and Local* traces, as well as the *linear combination* were corrected for bleaching by dividing them by the mono-exponential decay curve. Once corrected for bleaching, the *Local* (Fig. 4 F, *UnbLocal*), the *Global* (Fig. 4 F, *UnbGlobal*) and the *linear combination* (Fig. 4 F, *UnbLinearCombination*) profiles were compared. Although we observed oscillatory changes in fluorescence intensity of *Global* profile they were similar to oscillations in the *linear combination* trace, and corresponded to the frequency of mechanical stimulation allowing us to conclude that the *Global* Ca^{2+} response is absent; this signal is cantilever displacement induced. However, in the *Local* fluorescence trace both oscillatory changes present in the *Global* profile and sharper fluorescence spikes (changes in fluorescence intensity higher than 4-fold the average noise) are evident (Fig. 4F). Therefore, we attribute these *Local* elevations to a cellular Ca^{2+} response to mechanical stimulation. To correct the *Local* response for illumination artifacts, we subtract the bleaching-corrected *Global* Ca^{2+} trace (*UnbGlobal)* from the bleaching-corrected *Local* Ca^{2+} trace *(UnbLocal),* resulting in bleaching- and reflection-corrected *Local* Ca^{2+} response (Fig. 4F, *UnbResp*).

Using the cantilever reflection as a means to correlate the force and fluorescence signals

Although both deflection-distance data and fluorescence sequences can be time-stamped, different programs are used for data collection, which may be operated on different computers, resulting in uncertainty with the small offsets between the indentation and fluorescence measurements. Presence of cantilever reflection within the fluorescence data set allows for precise alignment of these independent data sets. Using Igor Pro software the deflection-time traces (Fig. 5A, *black*) and the fluorescence trace of the non-stimulated cell that exhibited the most prominent oscillations were plotted on the same graph (Fig. 5A, *grey*), matching the specific events in the deflection-time curves (the time between the maximum deflections for curves one and five), to specific positions in the fluorescence trace (the first and the fifth minima in the fluorescence trace). This procedure allows the temporal component of the fluorescence recording of the stimulated cell to be overlaid with the force spectroscopy measurements (Fig. 5B).

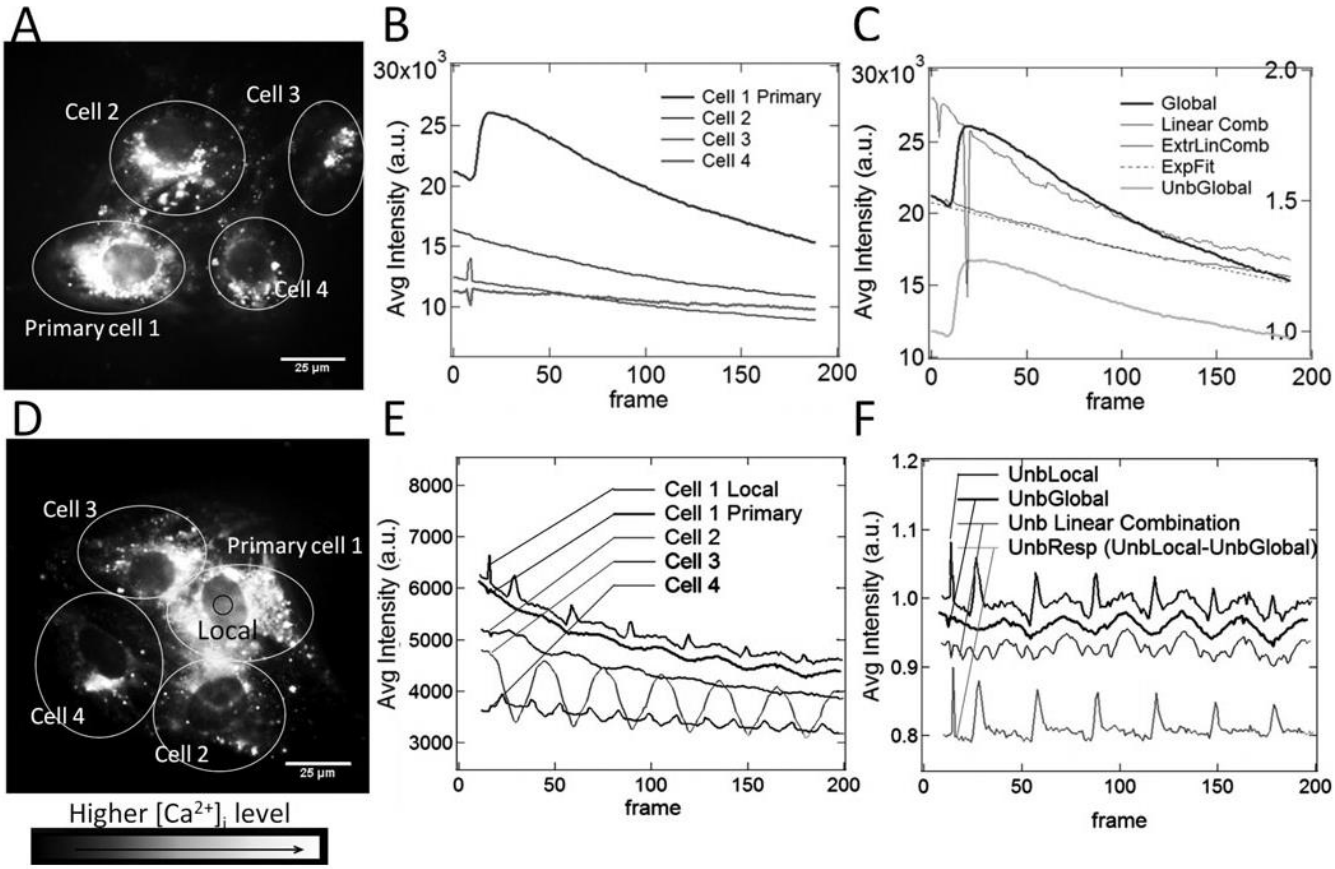

FIGURE 4. Correction of bleaching and cantilever reflection artifacts in Ca^{2+} responses. Osteoblastic cells were loaded with Fluo4-AM and $[Ca^{2+}]_i$ changes in response to AFM-induced mechanical stimulations were assessed. A-C) A single high level indentation leading to membrane penetration was performed and fluorescence intensity was recorded at ~3 frames/s. A) With the assistance of bright field image, the cells in the field of view were identified for analysis as a) Primary cell 1, which was subjected to AFM indentation and b) non-stimulated Cells 2-4. B) The average fluorescence intensity in each of the selected regions (*white ellipses* in A) was plotted as a function of frame. C) The linear combination of non-stimulated cells (*Linear Comb*) was fitted to the Global Ca^{2+} response trace of the Primary cell (*Global*), or to the initial (before stimulation) and final (last 25 frames of recording) segments of the Global response trace (*ExtrLinComb*). An exponential fit (*Exp. fit*) of the later curve was calculated. The Global response trace was divided by the calculated exponential fit resulted in bleaching-corrected Global response trace (*UnbGlobal*). D-F) Multiple consecutive indentations inducing low level deformation of the cell membrane were performed in the single cell (*Primary*) and fluorescence intensity was recorded at 3 frames/s. D) With the assistance of bright field image, the cells in the field of view were identified for analysis as a) Primary cell 1, which was subjected to AFM indentation and b) non-stimulated Cells 2-4 (regions of interest are shown as *white ellipses*). An additional Local region (*black circle*) was selected as a 5 µm diameter circle centered at the site of indentation. E) The average fluorescence intensity of the selected regions (*white ellipses* and *black circle* in D) was plotted as a function of frame. F) The linear combination of non-stimulated cells was fitted to the Global response trace, an exponential fit of this curve was calculated and the traces of global response, local response and linear combination of non-responding cells were divided by the calculated exponential fit resulting in unbleached traces (*UnbLocal*: unbleached local response, *UnbGlobal*: unbleached global response, *Unb Linear Combination*: unbleached linear combination of non-responding cells). To isolate reflection artifacts, the global response was subtracted from the local resulting in bleaching and reflection-corrected Local response trace (*UnbResp*).

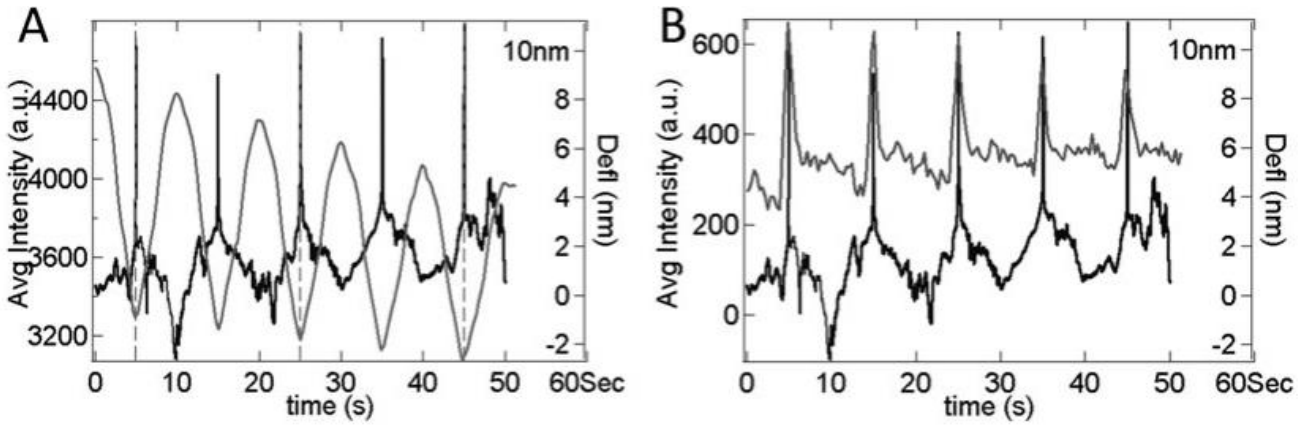

FIGURE 5. The reflection time-stamp in the fluorescence recording can be used to correlate it with the force-spectroscopy measurements. Osteoblastic cells were loaded with Fluo4 –AM and changes in $[Ca^{2+}]_i$ in response to multiple consecutive mechanical stimulations of a single cell were assessed. A) The average fluorescent intensity of a non-indented cell (*grey trace*) was overlaid to the force-spectroscopy measurements in the same experiment (*black traces*) to achieve the best match of fluorescent minima with the points of maximum extensions of the cantilever in a force spectroscopy measurement (*dotted lines*). B) The overlay of bleaching- and reflection-corrected fluorescence trace of a stimulated cell (*grey*) with the force-spectroscopy measurements (*black*).

Conclusion

Fluorescence is one of the most common optical techniques used for the characterization and quantification of biological systems. Combining fluorescence measurements with other microscopy techniques allows achieving better understanding of the molecular and cellular processes. However, it is important to understand potential coupling of signals from the different instruments, and be prepared for the possibility of resultant artifacts in the measurements. We have used the combination of AFM micro-indentation with fluorescence measurements of cytosolic free Ca^{2+} levels. In our experimental setup, the motion of the AFM cantilever with respect to the sample resulted in reflection of light back to the sample and thus changes in the fluorescence intensity profiles that were not related to changes in intracellular calcium levels. We developed a protocol to correct the fluorescence traces for this coupling artifact. In addition, we demonstrate that the coupling of the different tools, when corrected for artifacts, can in fact be used for advanced data analysis, such as more precise temporal correlation of AFM and fluorescence measurements.

Acknowledgements

The authors are grateful to Dr. M. Murshed for the C2C12-BMP-2 cell line. The authors thank O. Maria, S. Xing and Dr. G. Sadvakassova for their help providing the cell cultures used in this study. The authors also thank Drs. H. Bourque, G. Brouhard and W. Reisner for helpful discussions. G.M.L.A. was supported by the Principal's Graduate Fellowship, Chalk-Rowles Fellowship, NSERC Graduate Excellence Fellowship and McGill University. SVK holds Canada Research Chair. This work was supported by Natural Sciences and Engineering Research Council of Canada Discovery grants to SVK and PHG.

References

BARFOOT, RJ., SHEIKH, KH. & JOHNSON, BRG, COLYER, J., MILES, RE., JEUKEN, LJC., BUSHBY, RJ. & EVANS, SD. (2008). Minimal F-actin cytoskeletal system for planar supported phospholipid bilayers. Langmuir: the ACS journal of surfaces and colloids. 24(13):6827-36.

CHARRAS, GT. & HORTON, MA. (2002). Single cell mechanotransduction and its modulation analyzed by atomic force microscope indentation. Biophysical Journal, 82(6), p.2970-2981.

CHEN, N. X., RYDER, K. D., PAVALKO, F. M., TURNER, C. H., BURR, D. B., QIU, J., AND DUNCAN, R. L. (2000). Ca(2+) regulates fluid shear-induced cytoskeletal reorganization and gene expression in osteoblasts. American journal of physiology Cell physiology *278*, C989-C997.

DUNCAN, R. L., &TURNER, C. H. (1995). Mechanotransduction and the functional response of bone to mechanical strain. Calcified Tissue International 57, 344-358.

EHRLICH, PJ. & LANYON, LE. (2002). International Review Article Mechanical Strain and Bone Cell Function : A Review. Transformation, 13(9), p.688-700.
FA Note 2-6.

GUO, XE., TAKAI, E., JIANG, X., XU, Q., WHITESIDES, GM., YARDLEY, JT., HUNG, CT., CHOW, EM., HANTSCHEL, T., AND COSTA, KD. (2006). Intracellular calcium waves in bone cell networks under single cell nanoindentation. Molecular cellular biomechanics MCB 3, 95-107.

HUNG, C. T., ALLEN, F. D., POLLACK, S. R., AND BRIGHTON, C. T. (1996). Intracellular Ca2+ stores and extracellular Ca2+ are required in the real-time Ca2+ response of bone cells experiencing fluid flow. Journal of Biomechanics *29*, 1411-1417.

HUNG, C. T., POLLACK, S. R., REILLY, T. M., AND BRIGHTON, C. T. (1995). Real-time calcium response of cultured bone cells to fluid flow. Clinical Orthopaedics and Related Research *313*, 256-269.

KEMENY-SUSS, N., KASNECI, A., RIVAS, D., AFILALO, J., KOMAROVA, S. V., CHALIFOUR, L. E., AND DUQUE, G. (2009). Alendronate affects calcium dynamics in cardiomyocytes in vitro. Vascular Pharmacology *51*, 350-358.

LI, J., KHAVANDGAR, Z., LIN, S.-H., AND MURSHED, M. (2011). Lithium chloride attenuates BMP-2 signaling and inhibits osteogenic differentiation through a novel

WNT/GSK3- independent mechanism. Bone *48*, 321-331.

MOLECULAR DEVICES. (2010) Comparison of the Ca 2 + -Sensitive Dyes Fluo-3 and Fluo-4 Used with the FLIPR ® Fluorometric Imaging Plate Reader System.

MOLECULAR PROBES. (2011) Fluo calcium indicators, Product information.

MULLER, DJ. (2008). AFM: A Nanotool in Membrane Biology. Biochemistry, 47, 7986–7998
OH, YJ., JO, W., LIM, J., PARK, S., KIM, YS. & KIM, Y. (2008). "Micropatterning of bacteria on two-dimensional lattice protein surface observed by atomic force microscopy." Ultramicroscopy 108(10): 1124-1127.

SANCHEZ, H., KANAAR, R. & WYMAN, C.(2010), Molecular recognition of DNA-protein complexes: a straightforward method combining scanning force and fluorescence microscopy. Ultramicroscopy. 110(7):844-51

VICENTE, N. B., ZAMBONI, J. E. D., ADUR, J. F., PARAVANI, E. V., AND CASCO, V. H. (2007). Photobleaching correction in fluorescence microscopy images. Journal of Physics Conference Series *90*, 012068.

The vertebrate skeleton is a dynamic system which is continually subject to a "remodeling" process which involves the coordinated actions of osteoclasts (cells that resorb bone), osteoblasts (cells that build new bone) and osteocytes (osteoblasts embedded in the bone mineral matrix) (Figure 5.1.1). The combined activity of these cells regulates normal bone function and turnover and enables bone to adapt its structure in response to its mechanical usage; lack of physical activity leads to loss of bone whereas physical activity produces healthy bone, and excessive compressive forces inhibit production of new osteoblasts [244–248].

The conversion of physical forces into biochemical information is fundamental to

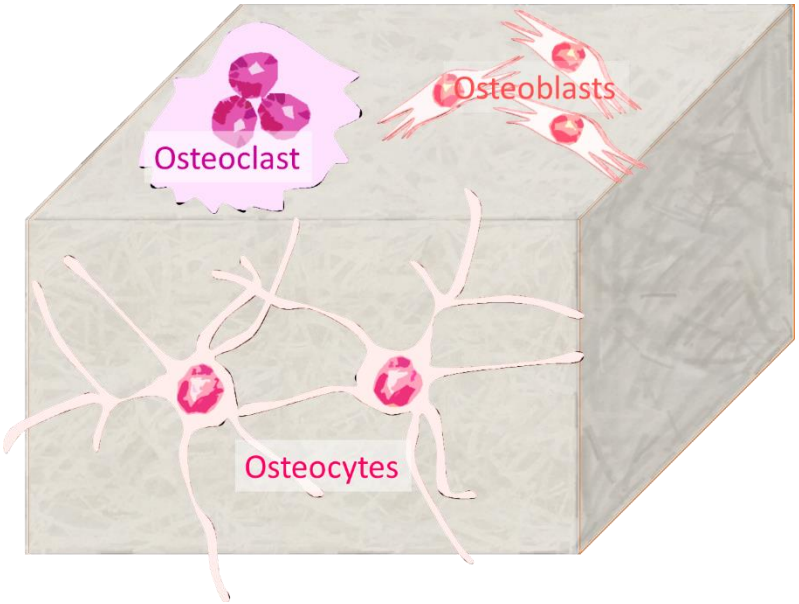

FIGURE 5.1.1. SCHEMATIC OF BONE CELLS IN MINERAL MATRIX

development and normal bone metabolism. This happens through a process called "mechanotransduction". Mechanical loads *in-vivo* cause deformation in bone that stretch the bone cells and create fluid movement. For this reason, bone mechanotransduction *in-vitro* is most commonly stimulated through fluid flow or mechanical stretch [249–251]. However, microdamage also occurs in our bones as a result of repetitive cyclic loading and is thought to play an important role in regulating bone turnover and strength [247,252–254]. Due largely to its abundance throughout the mineralized bone matrix, cells of osteoblastic origin have been assumed to play a role in sensing mechanical stimulus and

damage and in signalling for its repair. However, it is unknown if individual bone cells can differentiate between membrane deformation and micro-injury.

The two most studied mechanisms that transform mechanical loading into a biochemical response are force transduction through stretch-activated ion channels within the cell membrane [126,255,256], and integrin-cytoskeleton-nuclear receptors [99,250,257]. Other explored mechanisms include cell–cell adhesion elements (cadherins, gap junctions), surface processes (primary cilia, stereocilia), other membrane elements (caveolae, surface receptors), cytoskeleton constituents (microfilaments, microtubules and intermediate filaments), extracellular matrix particles (collagen, fibronectin, proteoglycans and basement membrane) and other cell–extracellular matrix adhesions (focal adhesions). All these mechanisms collectively interact [241]. The exact mechanism implicated in mechanotransduction and the following cascade of events may depend on the type of stimulation and is considered to relate to different cellular components [150]. The intricate interaction of these pathways suggests that the entire cell is a mechanosensor and that many different pathways are available to sense the effect of a mechanical signal [250].

When mechanical stimulation is applied and its effect on stretch activated ion channels is to be studied, the activation of the ion channels leads to a calcium influx from the extracellular to the intracellular space. This initial influx of calcium is known to trigger a signaling cascade through inositol trisphosphate (IP_3), which induces release of calcium from intracellular stores. This process is known as calcium-induced-calcium release signaling [59].

In this chapter, we explore the effect of microinjury in single osteoblasts using AFM. We examine how a single cell responds to forces inducing cell membrane deformation or deformation resulting in micro-injury and we analyze the signalling cascade induced by the mechanical stimulation through fluorescence microscopy using calcium-sensitive dye fluo-4 AM as an indicator of intracellular calcium changes.

Local membrane deformation and micro-injury lead to qualitatively different responses in osteoblasts

G. Monserratt Lopez-Ayon[1], Heng-Yen Liu[2,3], Shu Xing[1,2], Osama M. Maria[2], Jeffrey M. LeDue[1], Helene Bourque[1], Peter Grutter[1],and Svetlana V. Komarova[2,3]*

Short Title: ***Osteoblast responses to microindentation***

[1]Center for the Physics of Materials and the Department of Physics, McGill University, 3600 University, Montreal, Quebec, H3A 2T8, Canada.

[2]Faculty of Dentistry, McGill University, 3640 University, Montreal, Quebec, H3A 0C7, Canada

[3]Shriners Hospital for Children – Canada, 1529 Cedar Ave, Montreal, Quebec, Canada, H3G IA6.

e-mail list: lopezm*@physics.mcgill.ca, heng-yen.liu@mail.mcgill.ca, shu.xing@mail.mcgill.ca, osama.maria@hotmail.com, gulzhakhan.sadvakassova@mcgill.ca, jledue@gmail.com, helene.bourque@sympatico.ca, grutter@physics.mcgill.ca, svetlana.komarova@mcgill.ca*

Abstract

Micro-damage of bone tissue is known to regulate bone turnover. However, it is unknown if individual bone cells can differentiate between membrane deformation and micro-injury. We generated osteoblasts from mouse bone marrow or bone morphogenetic protein 2-transfected C2C12 cells. Single cells were mechanically stimulated by indentation with the atomic force microscopy probe with variable force load either resulting in membrane deformation only, or leading to membrane penetration and micro-injury. Changes in the cytosolic free calcium concentration ($[Ca^{2+}]_i$) in fluo4-AM loaded cells were analyzed. When deformation only was induced, it resulted in an immediate elevation of $[Ca^{2+}]_i$ which was localized to the probe periphery. Multiple consecutive local Ca^{2+} responses were induced by sequential application of low level forces, with characteristic recovery time of ~2 s. The duration of $[Ca^{2+}]_i$ elevations was directly proportional to the tip-cell contact time. In contrast, cell micro-injury resulted in transient global elevations of $[Ca^{2+}]_i$, the magnitude of which was independent of the tip-cell contact time. Sequential micro-injury of the same cell did not induce Ca^{2+} response within 30 s of the first stimulation. Both local and global Ca^{2+}elevations were blocked in Ca^{2+}-free media or in the presence of stretch-activated channel blocker Gd^{3+}. In addition, amount of Ca^{2+} released during global responses was significantly reduced in the presence of PLC inhibitor Et-18-OCH_3. Thus, we found qualitative differences in calcium responses to mechanical forces inducing only membrane deformation or deformation leading to micro-injury.

Keywords: ***osteoblast, AFM, mechanical stimulation, deformation, injury***

*Abbreviations****: AFM: Atomic Force Microscopy, $[Ca^{2+}]_i$: Cytosolic free Calcium concentration, MEM: Modified Eagle Medium , DMEM: Dulbecco's Modified Eagle Medium, BMP: Bone morphogenetic protein, HEPES: 4-(2-hydroxyethyl)-1-piperazineethanesulfonic acid***

Introduction

Mechanical stimulation of bone is well-known to regulate bone volume, structure and composition [1, 2]. It was recently suggested that, in addition to deformation forces, microdamage plays an important role in regulating bone turnover and strength [3]. Bone is restructured through the coordinated action of bone cells, osteoblasts responsible for bone formation and osteoclasts responsible for bone resorption. Cells of osteoblastic origin, including osteoblasts, osteocytes and bone lining cells are believed to act as mechanosensors in bone tissue [1, 4]. Understanding how bone cells sense and react to mechanical forces is important for gaining insight into the mechanisms of bone adaptation to its mechanical environment.

Because of the complexity of the bone environment *in vivo*, several models have been developed to understand the effects of mechanical stimulation on bone cells *in vitro* [5]. These models include application of hydrostatic pressure, longitudinal substrate stretch and fluid shear. These studies have established that osteoblastic cells can sense mechanical stimulation through plasma membrane receptors, stretch activated ion channels, as well as focal adhesion sites [6]. Ca^{2+} signaling was shown to be the prominent first response of osteoblastic cells to any type of mechanical stimulation [7-9]. Ca^{2+} signaling induced by mechanical stimulation in turn influences numerous bone cell functions such as cytoskeletal reorganization [7], gene expression [10], proliferation and differentiation [6]. However, these studies also identified significant complex signaling interactions between multiple cells [6], making it difficult to de-convolute the responses of single cells to mechanical stimulation. Moreover, these techniques do not allow exact control of forces applied to individual cells, nor do they report single cell micro-injury.

Local indentation techniques allow characterization of the response to mechanical stimulation at the single-cell level. Pipette microinjection [11], pipette suction [11-13], and atomic force microscopy (AFM) [14, 15] have been used to study responses of individual osteoblasts to mechanical stimulation. From these techniques, only AFM allows application of precisely controlled forces in the nano-Newton scale, as well as provides

readout of the extent of membrane deformation [16]. Moreover, AFM can be used with cantilever tips of different geometries, which allow additional control of the distribution of the force. A spherical tip allows the creation of a high range of membrane strains [17], while a pyramidal tip allows reversible membrane penetration, which does not result in long-term cell damage [18, 19].

The goal of this study was to examine how a single osteoblastic cell responds to forces inducing cell membrane deformation only, or membrane deformation resulting in micro-injury. We used either primary bone marrow cells cultured with ascorbic acid, or C2C12 cells stably transfected with bone morphogenic protein (BMP) 2. C2C12 cells have been shown to undergo osteoblastic differentiation when treated with BMP-2 [20]. Mechanical forces of different magnitude were applied using AFM. To monitor cell responsiveness to mechanical forces, changes in cytosolic free Ca^{2+} concentration ($[Ca^{2+}]_i$) were assessed.

Materials and methods

2.1 Cell cultures

All procedures were approved by McGill University's Animal Care Committee (protocol number 2013-7332) and conformed to the ethical guidelines of the Canadian Council on Animal Care. Six week old male C57/BL6 mice (Charles River) were acclimatized for 1 week, fed ad libitum, and kept on a 12-hour light/dark cycle prior to euthanasia by CO_2 asphyxiation followed by cervical dislocation. Femora and tibiae were isolated and separated from soft tissue. The bones were cut in two, placed in an Eppendorf tube, centrifuged twice at 10^3 rpm for 30 seconds. Cells (~$2x10^7$ cells/mouse) were re-suspended in Minimum Essential Medium (MEM (Eagle), from Invitrogen) supplemented with 2 mM of L-glutamine, 100 IU of penicillin, 100 μg/ml of streptomycin and 10 % of fetal bovine serum (Wisent), and $5x10^6$ cells were plated on round 25 mm No.1 glass coverslips (Matteck Corporation), and cultured with 50 μg/ml of ascorbic acid at 5% CO_2, 37°C for

4-6 days to 50-70% of confluence, which allowed easy identification of individual cells. The media was replaced every third day. The osteoblastic phenotype was confirmed by alkaline phosphatase staining (Fast Red, Sigma).

C2C12 cells stably transfected with BMP2 (kindly provided by Dr M. Murshed, McGill University) were plated at $2.5x10^4$ cells on round 25 mm No.1 glass coverslips (Matteck corporation). Cells were cultured in Dulbecco's Modified Eagle Medium (DMEM, Invitrogen) supplemented with 2 mM of L-glutamine, 100 IU of penicillin and 100 μg/ml of streptomycin and 10% of fetal bovine serum at 5% CO_2, 37°C to 50-70% of confluence. The media was changed every third day. The osteoblastic phenotype was confirmed by alkaline phosphatase staining.

2.2 Intracellular calcium measurements

The cells were loaded with 1.5 μl of Ca^{2+}-sensitive dye fluo4–AM (Molecular Probes, stock solution of 1 mg/ml in DSMO), added to 2 ml of culture media for 40 minutes at room temperature. The cells were washed twice with physiological solution (130 mM NaCl; 5 mM KCl; 1 mM $MgCl_2$; 1 mM $CaCl_2$; 10 mM glucose; 20 mM HEPES, pH 7.4, for Ca^{2+}-containing experiments, or 0 mM $CaCl_2$ and 10 mM EGTA for Ca^{2+}-free experiments) [21], the coverslip was assembled onto the peek fluid chamber (Asylum Research) and physiological buffered solution (1.5 ml) was added after loading with fluo4-AM. Gd^{3+} (Sigma) was dissolved directly in buffer to 50 μM final concentration. 1-O-Octadecyl-2-O-methyl-sn-glycero-3-phosphorylcholine (Et-18-OCH_3, Sigma) stock solution (5 mg/ml) was prepared in ethanol, which was used as a vehicle (0.07%) for corresponding experiments. Et-18-OCH_3 was used at 5 μM final concentration. Cells were pretreated with inhibitors for 45 min at room temperature before mechanical stimulation. The cells were illuminated with 488 nm laser light and the emitted light was collected with the (Cascade II) camera. In each experiment a time-sequence of fluorescence images was acquired with one frame taken every 345 ± 10 ms with 250 ms exposure time. Traces were extracted from the video files using a code for Matlab 2011A provided in [22]. The fluorescence signal in

cells not exposed to mechanical stimulation did not demonstrate associated changes and was used as a reference for signal correction for bleaching and cantilever reflection artifacts using the protocol for data processing for systematic signal recovery that we established and described previously [22].

2.3 Atomic force microscopy

The experiments were conducted using an MFP-3D-BIO AFM (Asylum Research, Santa Barbara CA) mounted on an Olympus IX-71 inverted optical microscope. The sample placed in the closed fluid cell was left undisturbed for 15 min to achieve thermal equilibrium at 37°C. A 60X oil immersion objective with 1.45 NA (Olympus) was put into contact with the coverslip allowing optical access from the bottom and AFM access on top of the sample. The region of interest was located and aligned with the cantilever tip using the bright field and fluorescence images.

2.4 AFM probe preparation

The cantilever tip (NCLAuD, Nanosensors), was etched down to 1 μm^2 contact area with a focused ion beam microscope (FEI DB235). When sharp tips were used, the membrane rupture force event was not distinguishable in the force curve. Using Hooke's law ($F=k \cdot d$), the force exerted by the probe (F) was determined from the cantilever spring constant (k, 39 ± 7.8 N/m) and deflection (d). The net extension of the piezo element, the speed, the time of indentation, the time between indentations and the number of indentations were controlled using the Asylum MFP3D software in IgorPro 6.22 platform.

2.5 Statistical analysis

Data are presented as representative images, representative traces, means ± SE with *n* being the number of experiments analyzed. The normalized amplitude as a function of time, the amplitude decay rate as a function of recovery time and the response duration as a function of the contact time were analyzed using least squares regression and fitted a line or an

exponential as appropriate. Categorical data were analyzed as described previously [23]. Statistical differences were assessed using Fisher Exact Probability test for categorical data or Student's t-test for continuous data and were accepted as significant at $p < 0.05$. Statistical analysis was performed in Microsoft Excel 2007.

Results

3.1 Experimental setup

We employed two cell models to study osteoblast mechanosensitivity: *i*) mouse bone marrow cells cultured in the presence of ascorbic acid (50 mg/ml) for 4-6 days (Fig. 1A) or *ii*) C2C12 cells stably transfected with BMP2 and cultured for 2-6 days (Fig. 1B). Both models represent osteoblastic cells at the early differentiation stage due to the limitation of AFM use in confluent and multilayered cultures. Osteoblastic phenotype was confirmed in fixed cultured by alkaline phosphatase staining. In parallel live cultures, the cells exhibiting osteoblastic morphology (strongly adhered cells with relatively large body and several filopodia) were chosen for mechanical testing. Mechanical stimulation was performed with AFM force spectroscopy indentation (Fig. 1C) using a 1 μm^2 area tip (Fig. 1D). Using AFM allows strict control of the amount of force applied to the cell (Fig. 1E, F). The membrane penetration event is easily identifiable on the force-distance curve as a decrease in the force required to continue to move the probe. The membrane penetration force was found to be similar for osteoblasts obtained in different cultures: 516 ± 200 nN for primary osteoblasts and 672 ± 100 nN for C2C12 osteoblasts. We analyzed two distinct modes of mechanical stimulation: *i)* the maximum force was set below the membrane penetration force (at ~400 nN), leading only to membrane deformation (low-load, Fig. 1E, F, *blue*); and *ii)* the maximum force was set above the membrane penetration force (~2800 nN), inducing membrane rupture and penetration (high-load, Fig. 1E, F, *red*).

3.2 Changes in $[Ca^{2+}]_i$ induced by different indentation regimes

Since $[Ca^{2+}]_i$ elevations are known to be the most common first responses to mechanical stimulation [4, 9, 11, 24], we analyzed the changes in $[Ca^{2+}]_i$ in response to different loading regimes in the osteoblasts loaded with $[Ca^{2+}]_i$ fluorescent indicator fluo4-AM. In the low load indentation regime, where the force exerted on the cell induced membrane deformation (Fig. 2 A), only local $[Ca^{2+}]_i$ transients were observed (Fig. 2B). To analyze the transients, the spatially-averaged intensity over a circle of 5 μm in diameter centered on the point of indentation (*red circle* in Fig. 2B) was normalized to the initial baseline signal and plotted as a function of time (Fig. 2C). When larger circles were taken, the change in averaged intensity was smaller; if the whole cell was selected, the local response was not apparent. When consecutive low load indentations were performed at the same location on the same cell multiple local responses were induced (Fig. 2A, C).

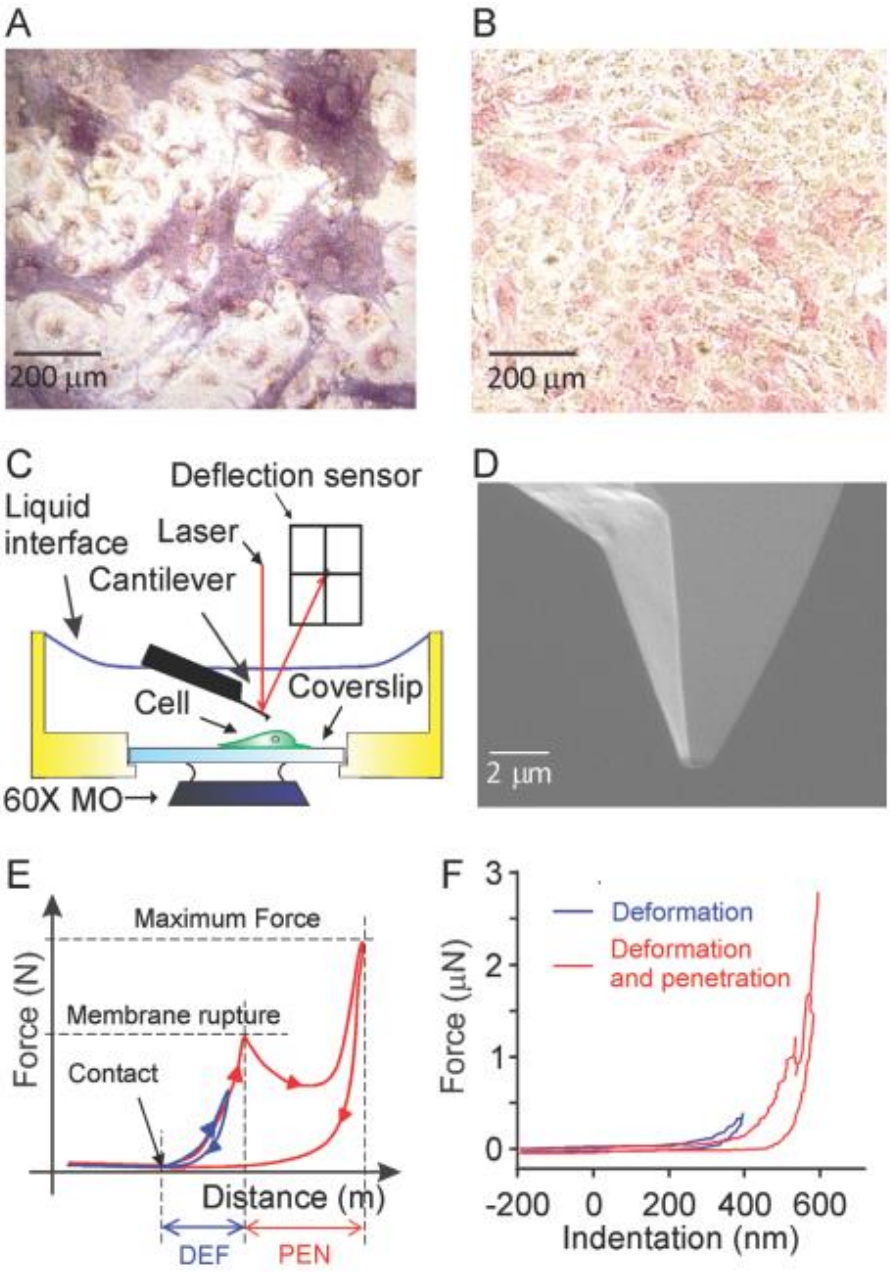

FIGURE 1. **Mechanosensitivity of osteoblastic cells assessed by atomic force microscopy (AFM).** Bone marrow cells were cultured in the presence of ascorbic acid (50 μg/ml) for 4-6 days to induce osteoblast differentiation or C2C12 cells stably transfected with BMP-2 were cultured for 2-6 days to obtain osteoblastic phenotype. A, B) Representative images of bone marrow culture on day 5 (A) and C2C12 culture on day 3 (B) stained for osteoblastic marker, alkaline phosphatase (red). C) Schematic representation of the AFM operation under liquid: the sample and the tip are submerged and changes in the laser reflection signal due to deflection of the cantilever are monitored. D) Experiments were performed using a probe with 1 μm^2 tip area; the tip is etched using focused ion beam. E) Schematic representation of events observed using force-distance curve: *a)* as the AFM tip approaches the cell, the *contact* point is evident as increase in force required to move the probe; *b)* when the probe indents the cell membrane, the force increases until it reaches the *membrane rupture* force and the tip penetrates the cell (apparent by a decrease in the cell resistance); *c)* indentation is continued until a predetermined *maximum force* is reached, and the probe retraction is initiated. The retraction curve commonly deviates from the approach curve, reflecting that energy is required for deformation and penetration of the cell membrane. The maximum force was set to be either below (blue) or above (red) the membrane rupture force. F) The example force-distance curves from the experiments in which deformation only (blue) or deformation plus penetration (red) were induced.

In the high load regime, which resulted in local membrane rupture and penetration of the cell (Fig. 2D), whole cell $[Ca^{2+}]_i$ elevations were observed (Fig. 2E). When the normalized fluorescence intensity was averaged over an ellipse surrounding the whole cell and plotted as a function of time (Fig. 2F), it was apparent that global $[Ca^{2+}]_i$ elevations were transient. When we focused on the membrane level to directly visualize the closure of the membrane micro-injury, we observed that it seals within 40-60 s after the stimulation (Fig. 2G). It is conceivable that high load indentation may affect the cell viability. However, in all our experiments, the cell previously exposed to high load indentation maintained basal calcium levels within normal range for the whole period of observation (5-30 min), and when directly tested using Trypan Blue exclusion test, six out of six cells previously indented were viable ~10 minutes after high load indentation. Taken together, these data strongly suggest that the micro-injury induced by AFM probe is reversible and does not result in the cell death.

Since application of AFM may potentially interfere with fluorescence measurements, we have previously performed in depth analysis of the system performance [22]. We have found that in experiments where local repetitive stimulations were performed, reflection artifacts correlated with cantilever motion represented a significant component of the fluorescent signal. We developed a protocol to correct the fluorescence traces for reflection artifacts, as well as photobleaching, which is described in detail in [22]. The traces were processed as follows: 1) the region of interest was selected in the digital image; 2) the average fluorescence intensity data were extracted and normalized to the initial basal reading to correct for differences in dye loading; 3) the signal was corrected for bleaching and reflection artifacts as described in [22]; 4) the noise was determined as the standard deviation in a linear portion of the trace, and 5) the $[Ca^{2+}]_i$ response was deemed positive when an increase in intensity exceeded four-fold the average noise. Cells exhibiting spontaneous $[Ca^{2+}]_i$ fluctuations [25] were excluded from the study.

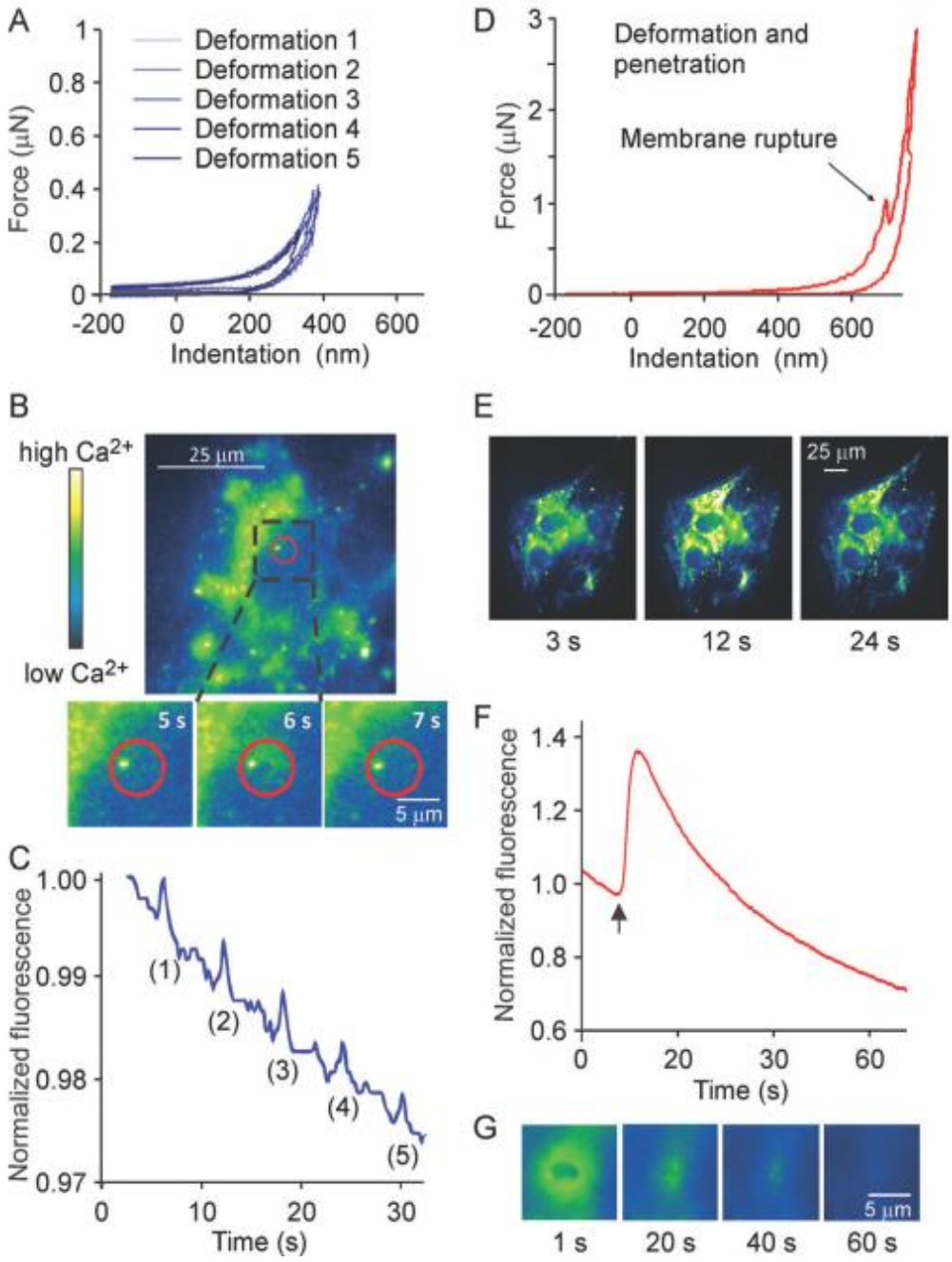

FIGURE 2. **Low level membrane deformation induces local Ca^{2+} response, whereas deformation leading to membrane micro-injury induces global elevations of $[Ca^{2+}]_i$.** Osteoblasts generated from C2C12 cells were loaded with Ca^{2+}-sensitive dye fluo4-AM and changes in $[Ca^{2+}]_i$ in response to mechanical stimulation were assessed. A-C) The maximum force was set below the membrane rupture force. A) Representative force-distance curves depicting multiple local indentations of the cell membrane. B) A single cell exhibiting local $[Ca^{2+}]_i$ elevation in response to membrane deformation. Magnified below is the region of the cell centered at the indentation point, that demonstrates the changes in $[Ca^{2+}]_i$ with time following a single AFM indentation at 5 s. In pseudo-color, black/blue represents low and yellow/white represents high $[Ca^{2+}]_i$ levels. C) Representative trace depicting changes in fluorescence intensity in the region shown in red on B, in response to multiple membrane deformations. D-G) The maximum force was set above the membrane rupture force. D) Force-distance curve demonstrating the membrane deformation and penetration. E) Micrographs demonstrating global increase in fluorescence intensity following a single high-load indentation at 6 s (same color scale as in B). F) Changes in fluorescence intensity in the whole cell shown in E following single indentation with the penetration of cell membrane (indicated by an arrow). G) Magnified region of the cell centered at the high-load indentation point, demonstrating the transient character of membrane damage.

3.3 Characterization of local $[Ca^{2+}]_i$ responses induced by membrane deformation

First, we compared the responses in C2C12-derived and primary osteoblasts. We have found that the low load indentation induced qualitatively similar responses in the primary and C2C12-derived osteoblasts (Fig. 3A). However, when we compared the percentage of cells exhibiting local $[Ca^{2+}]_i$ transients in response to indentation performed at low and high speeds, we found that a higher percentage of C2C12-derived osteoblasts responded to the mechanical stimulation compared to primary osteoblasts (Fig. 3B). In addition, a higher percentage of C2C12-derived osteoblasts exhibited $[Ca^{2+}]_i$ transients when indented at lower speed compared to higher speed (Fig. 3B). In primary osteoblasts a similar trend was observed, however it did not reach statistical significance since the rate of response was low in these cells. We analyzed in depth the $[Ca^{2+}]_i$ responses induced in C2C12-derived osteoblasts by a single low-load indentation performed at different speed (2, 10 and 20 μm/s).The $[Ca^{2+}]_i$ elevations were further characterized by measuring *i*) the relative amplitude of the response (with respect to basal); *ii*) the duration of the response (the width of a transient at the half maximum amplitude); and *iii*) the amount of $[Ca^{2+}]_i$ (duration multiplied by amplitude). The speed of indentation did not significantly affect the amplitude of calcium responses (Fig. 3C). However, indentations performed at low speed induced calcium responses of longer duration (Fig. 3D) and thus resulted in release of greater amount of $[Ca^{2+}]_i$ (Fig. 3E) compared to indentations performed at high speed. To analyze if indenting at different speeds delivered different mechanical stimulation, the force curves were characterized by quantifying *i*) the extent of membrane deformation (the distance between the contact point and the maximum piezo extension) (Fig. 3F), and *ii*) the energy spent to deform the cell (the area between the approach and retraction curves) (Fig. 3F, right scale). No statistically significant difference was observed in these parameters when different indentation speeds were compared.

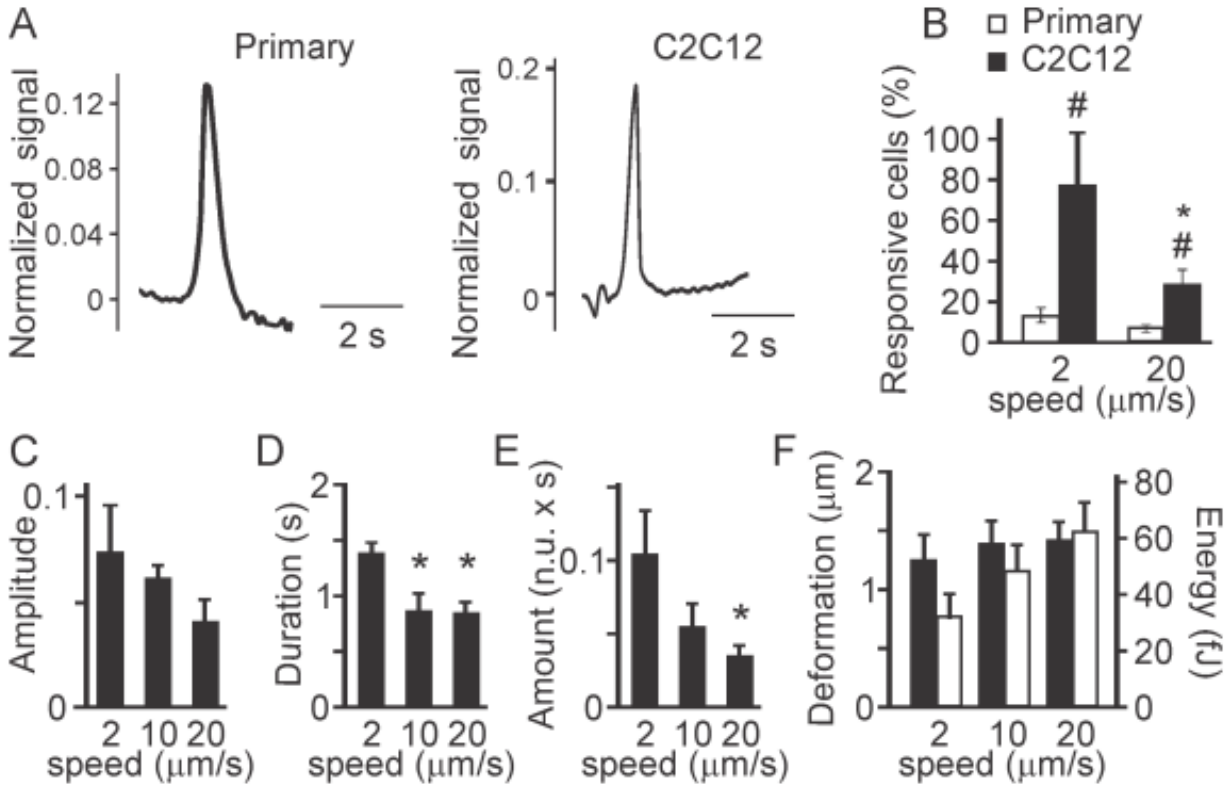

FIGURE 3. **Characteristics of the local Ca^{2+}responses**. Primary or C2C12 derived osteoblasts were loaded with fluo4-AM and single indentations were performed at different speeds (2, 10, 20 mm/s). The maximum force was set below the membrane rupture force. A) The examples of local Ca^{2+} elevations induced by a low level deformation in a primary osteoblast (*left*) and a C2C12-derived osteoblast (*right*). B) The percentage of primary (white) or C2C12-derived (black) osteoblasts responding to deformations with local Ca^{2+} elevations. Data are means ± SE, n = 15 for primary osteoblasts, n=10 and 30 for C2C12 osteoblasts deformed at 2 and 20 μm/s respectively, # indicates $p<0.05$ difference between primary and C2C12-derived osteoblasts,* indicates $p<0.05$ difference between deformation speeds, assessed by Fisher Exact Probability test for categorical data. C-E) Local Ca^{2+} transients in C2C12-derived osteoblasts were analyzed for the amplitude of Ca^{2+} response (C), the duration of Ca^{2+} response (D) and the amount of Ca^{2+} released during the response (E). Data are means ± SE; n is the number of responses from 10 trials: for 2 μm/s n = 6, for 10 μm/s n = 2, for 20 μm/s n = 6, *indicates $p<0.05$ difference as assessed by Student's t-test. F) Force-distance curves were analyzed and the extent of membrane deformation (black, scale on the left) and energy spent to deform the membrane (white, scale on the right) were assessed. Data are means ± SE, n = 5, no significant difference.

We next assessed how the contact time (the net time the probe spent in contact with the cell during stimulation) affects calcium responses to low-load indentations performed at different speeds. We varied the contact time by increasing by 1 s the time that the tip spent in the maximally extended piezo position. The reflection of a cantilever on the calcium fluorescence recording allows achieving exact temporal overlay between the

fluorescence intensity and the force-distance curve (as described in [22]). The $[Ca^{2+}]_i$ signal was initiated when the tip came into contact with the cell and was maximum at the maximum deflection (Fig. 4A,B). When the contact time was increased by 1 s, the comparable increase in calcium response duration was observed (Fig. 4C). The mean of the response duration was plotted as a function of the corresponding contact time demonstrating that the average calcium response duration was directly proportional to the contact time, $R^2 = 0.92$ (Fig. 4D). We next assessed if calcium responses of different duration can be induced in a single cell by varying the contact time (as the piezo extension time) in consecutive indentations (Fig. 4E). We have found that a single cell exhibited $[Ca^{2+}]_i$ elevations of different durations (Fig. 4E, *i-iv, black*) when indentations with different contact times (Fig. 4E, *i-iv, red*) were performed.

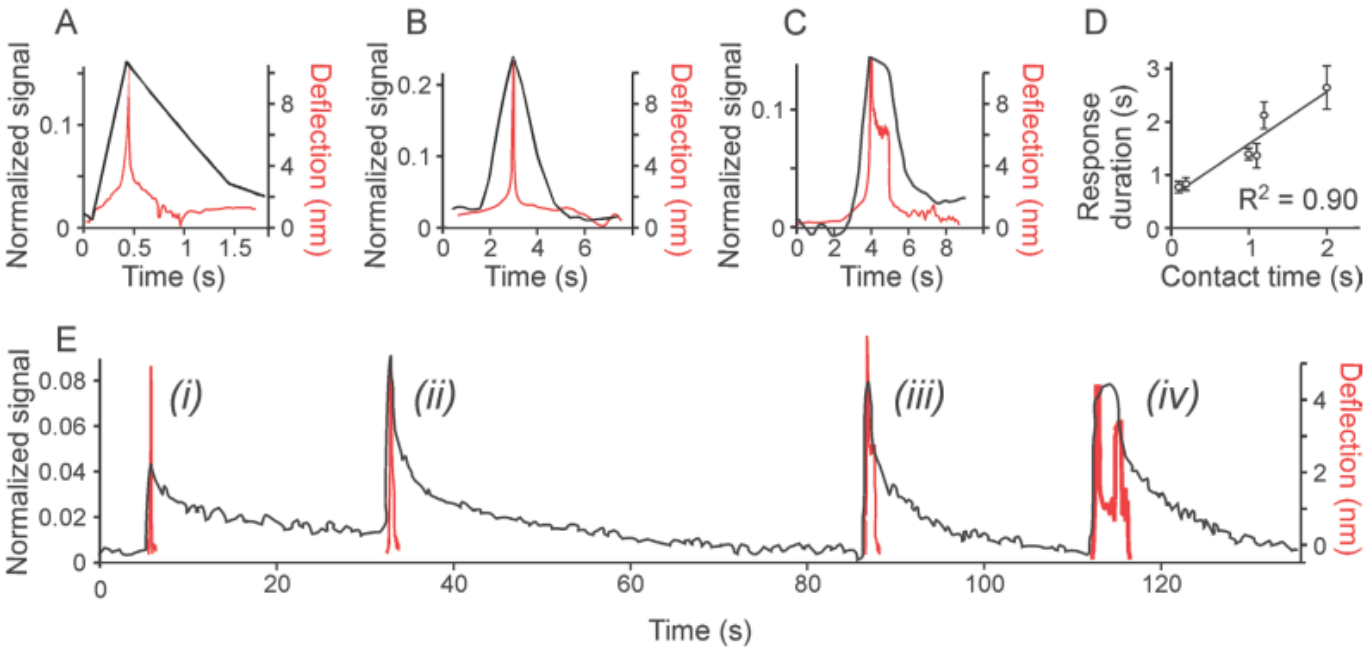

FIGURE 4. **The duration of the low level deformation determines the duration of the Ca^{2+} elevation.** C2C12-derived osteoblasts were loaded with fluo4-AM and responses to single indentation were assessed. The maximum force was set below the membrane rupture force. A-C) Examples of Ca^{2+} transients in black (left scale) in response to indentation performed with different contact time. Overlaid are the cantilever deflection curves in red (right scale). The indentation speed was set to 20 μm/s (A) or 2 μm/s (B, C). For C, the probe was maintained in contact with the cell for additional 1s. D) The Ca^{2+} transient duration is plotted as a function of contact time. Data are means ± SE, for 0.1 s and 1.2 s n = 4, for 0.2 s n = 2, for 1.0, 1.1 and 2.0 s n = 3. Linear fit is $f(x) = 0.98x + 0.60$ with R^2=0.90. E) A single cell exhibited $[Ca^{2+}]_i$ elevations of different duration in response to indentations with different contact times. The indentation speed was 20 μm/s, the probe was maintained in contact with the cell for additional *i*) 0s, *ii*) 0.3s, *iii*) 0.7s and *iv*) 3s.

Since we have found that repeated low level mechanical stimulations can elicit multiple consecutive responses in a single cell, we next examined how the exposure to mechanical stimulation affects subsequent responses of the same cell. Multiple low load indentations were performed on the same cell with different frequencies, and $[Ca^{2+}]_i$ changes in response were assessed (Fig. 5). We have found that when cells were stimulated with higher frequency, the amplitude of the response in consecutive stimulations decreased (Fig. 5A-C). Within each sequence of Ca^{2+} responses to the consecutive indentations, we normalized the amplitudes with respect to the amplitude of Ca^{2+} response to the first

indentation and quantified the amplitude decay rate as a slope (α_i) of the best fit line for the responses. This slope is negative, representing a decrease in the amplitude, and when multiplied by 100, this slope is expressed as percentage decay. We have found that amplitude decay is significantly higher when cells are stimulated with higher frequencies (Fig. 5D). At different frequencies two parameters are changing – the contact time, defined as the time the probe spends in contact with the cell, and recovery time, defined as the time off contact between stimulations. We next specifically varied the recovery time by introducing a delay of 1 s between consecutive stimulations, and plotted the average amplitude decay rates as a function of the recovery time (Fig. 5E). An exponential curve with a characteristic recovery time of 2.00 ± 0.08 s was found to be the best fit for the relationship between the amplitude decay rate and the recovery time. These data suggest that a refractory period of ~10 s is required for complete amplitude recovery after low load mechanical stimulation.

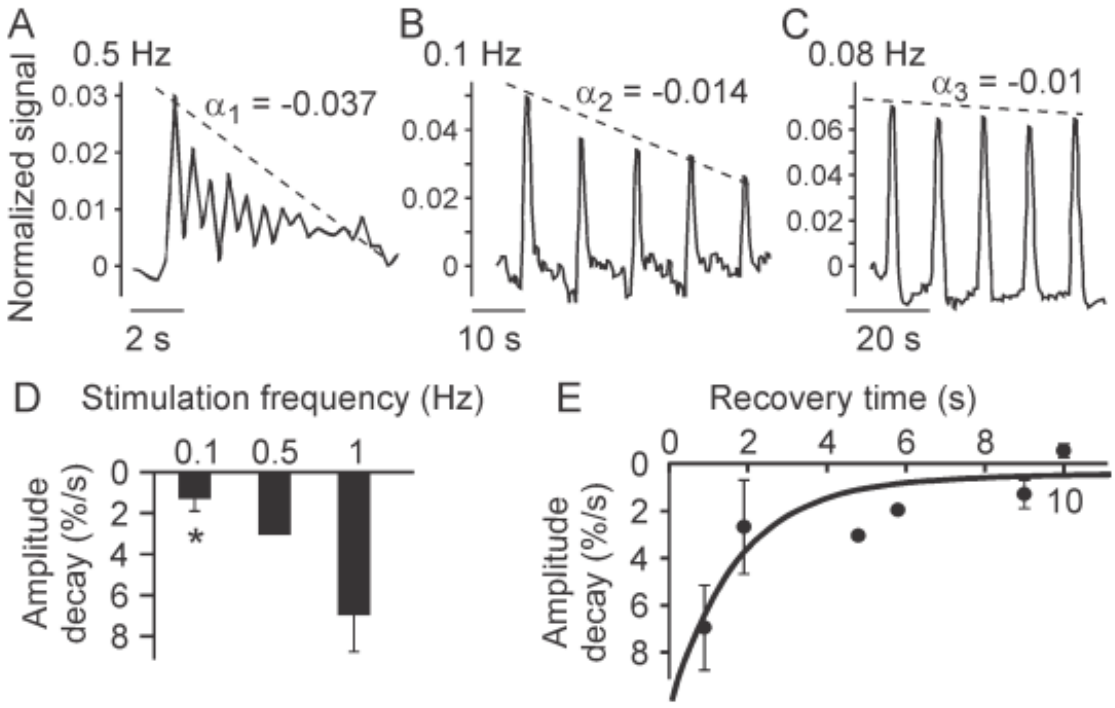

FIGURE 5. **Multiple consecutive low level indentations induce multiple cell responses.** C2C12-derived osteoblasts were loaded with fluo4-AM and changes in $[Ca^{2+}]_i$ in response to multiple indentations were assessed. The maximum force was set below the membrane rupture force. A-C) Examples of multiple Ca^{2+} transients in response to consecutive indentations performed at 10 μm/s, 0.5 Hz (A), 2 μm/s, 0.1 Hz (B) and 2 μm/s, with a 2 s delay between stimulations, 0.08 Hz (C). The amplitudes of the consecutive responses were normalized with respect to the first response and the amplitude decay rate α_i was determined as the slope of a linear fit to the amplitude-time graph (dashed line). D) The amplitude decay rates were plotted as a function of the frequency of indentation. Data are means ± SE (except for 0.5 Hz), n is a number of responses from 5 trials: for 0.1 Hz n = 4, for 0.5 Hz n = 1, for 1 Hz n = 4,*indicates $p<0.05$ difference compared to 1 Hz, assessed by Student's t-test. E) The amplitude decay rates were plotted as a function of the recovery time. Data are means ± SE (except for 4.8 and 5.8 s), n is a number of responses from 5 trials: for 0.9 s n = 3, for 1.9 s n = 4, for 4.8 s and 5.8 s n = 1, for 9 s n = 4 and for 10 s n = 3. The solid line represents an exponential fit: $f(x) = a\ exp(-x\ b)+c$ with a time constant of $b = 0.5s^{-1}$; τ~2s, RMSE = 0.02 s^{-1} (R^2=0.77).

3.4 Characterization of global $[Ca^{2+}]_i$ responses induced by membrane deformation and micro-injury

When the maximum force was set at 2800 nN (three-fold above the membrane penetration force), the force-distance curves confirmed that membrane penetration occurred in all the cells tested. We have found that qualitatively similar responses were induced in primary and C2C12-derived osteoblasts (Fig. 6A, B), however the response rate was significantly lower for the primary osteoblasts (Fig. 6C). When the whole cell average fluorescence intensity and the force-distance curves of individual cells were overlaid in time, we found that, in contrast to low-load indentation, micro-injury-induced global $[Ca^{2+}]_i$ elevations were delayed with respect to the maximum deflection of the probe (which indicates maximum cell penetration), and reached their amplitude after the tip was released from cell contact (Fig. 6A, B). We assessed $[Ca^{2+}]_i$ changes induced in C2C12-derived osteoblasts by a single high-load indentation performed at different speeds (2, 10 and 20 μm/s). There was no significant correlation between the indentation speed and the amplitude (Fig. 6D), duration (Fig. 6E) or amount of Ca^{2+} released (Fig. 6F) during the responses. The force-distance curve analysis did not demonstrate statistically significant differences in the extent of membrane deformation prior to the membrane penetration (Fig. 6G), extent of membrane penetration (Fig. 6H), energy spent in deformation, micro-injury and penetration (Fig. 6I) or membrane rupture force (Fig. 6J).

3.5 Contribution of mechanosensitive channels and calcium stores to elevations in $[Ca^{2+}]_i$ induced by membrane deformation and micro-injury

Since the rise in $[Ca^{2+}]_i$ can be due to influx from the extracellular space as well as to release from intracellular stores, we next investigated the contribution of these pathways to membrane deformation and to micro-injury-induced $[Ca^{2+}]_i$ responses. We analyzed changes in $[Ca^{2+}]_i$ in response to low-load and high-load mechanical stimulations in C2C12 osteoblasts maintained in the control Ca^{2+}-containing buffer or in Ca^{2+}-free, EGTA (10 mM)-containing buffer (Fig. 6A-C). Both local $[Ca^{2+}]_i$ elevations (Fig. 6A,B) and global $[Ca^{2+}]_i$ responses (Fig. 6C) were prevented by the lack of calcium in the extracellular space.

We next inhibited mechanosensitive membrane channels using Gd^{3+} (50 μM) [17]. In the presence of Gd^{3+} both local $[Ca^{2+}]_i$ transients in response to membrane deformation (Fig. 6D) and micro-injury-induced global $[Ca^{2+}]_i$ responses (Fig. 6E) were prevented. To inhibit the phospholipase C (PLC)-inositol triphosphate (IP_3) pathway leading to calcium release from intracellular stores, we used PLC inhibitor Et-18-OCH_3 (5 μM) [17]. In the low-load regime, local $[Ca^{2+}]_i$ transients (Fig. 6F) occurred at the same frequency as in control (Fig. 6G), and the amount of Ca^{2+} released during the responses was not significantly affected (Fig. 6H). However, global $[Ca^{2+}]_i$ transients induced by the high-load stimulation were noticeably smaller in Et-18-OCH_3-treated, but not in vehicle-treated cells compared to control (Fig. 6I). The percentage of cells exhibiting global $[Ca^{2+}]_i$ transients in response to membrane penetration was not significantly affected by Et-18-OCH_3 or vehicle (Fig. 6J). However, the amount of Ca^{2+} released during the response was significantly decreased in cells treated with Et-18-OCH_3 (Fig. 6K). These data indicate that mechanosensitive Ca^{2+} channels mediate both local and global responses, while the intracellular Ca^{2+} stores are important for global responses only.

Discussion

In this study, we have examined the ability of individual osteoblasts to respond to mechanical stimulation applied using AFM. Variable force load was applied resulting in either membrane deformation only or in membrane penetration and micro-injury, and changes in $[Ca^{2+}]_i$ in fluo-4 loaded cells were analyzed. Qualitatively different Ca^{2+} responses were observed in different force loads. In response to membrane deformation only, immediate local $[Ca^{2+}]_i$ elevations limited to the indentation region were observed. Multiple stimulations of a single cell resulted in Ca^{2+} responses of similar amplitude if a recovery time of more than 10 s between the stimulations was allowed. The duration of Ca^{2+} responses to low-load indentation was proportional to the duration of deformation. In contrast, micro-injury induced global Ca^{2+} elevation, which continued to develop after the removal of the probe and was independent of the duration of indentation. These data

demonstrate that Ca^{2+} responses to local membrane deformation exhibit threshold properties when micro-injury is induced.

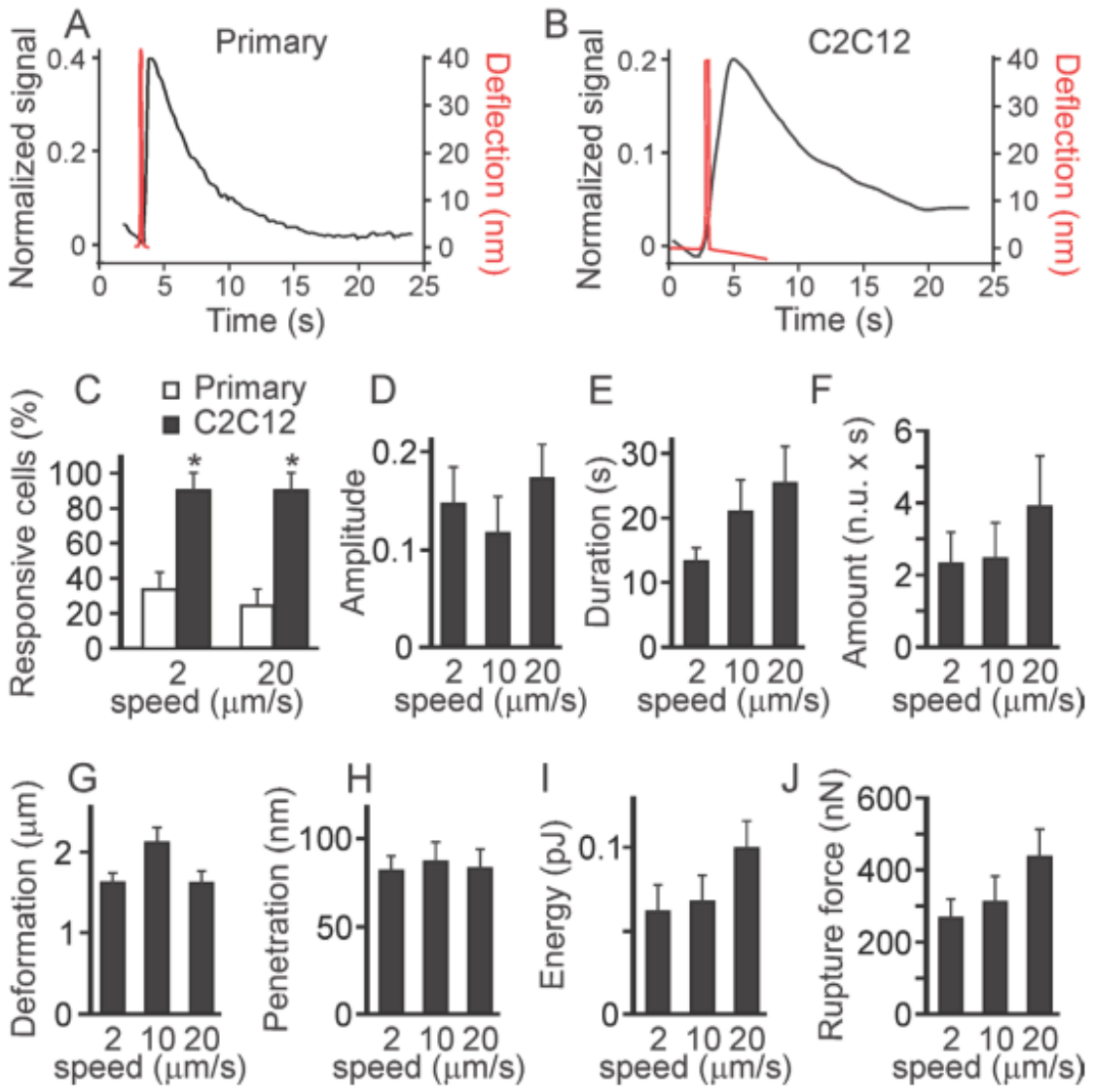

FIGURE 6. **The Ca^{2+} responses to indentation resulting in penetration are not significantly affected by the speed of the indentation or the contact time.** Primary mouse osteoblasts or osteoblasts generated from C2C12 cells were loaded with fluo4-AM and single indentations were performed. The maximum force was set above the membrane rupture force. A,B) Examples of Ca^{2+} transients (left scale) in primary osteoblast (A) or C2C12-derived osteoclast (B) in response to the high-load indentations. Overlaid are the cantilever deflection curves in red (*right scale*). C) The percentage of cells that exhibit global Ca^{2+} elevations in primary (white) or C2C12-generated (black) osteoblasts in response to the high-load indentations performed with different speed of 2 or 20 μm/s. Data are means ± SE, n = 25 for primary osteoblasts and n=10 for C2C12-derived osteoblasts, # indicates a $p<0.05$ difference between primary and C2C12-generated osteoblasts as assessed by Fisher Exact Probability test. D-F) Changes in global Ca^{2+} in response to membrane penetration in C2C12-derived osteoblasts were analyzed for the amplitude of Ca^{2+} response (D), the duration of Ca^{2+} response (E) and the amount of Ca^{2+} released during the response (F). Data are means ± SE, n is the number of response from 10 trials: for 2 μm/s n = 9, for 10 μm/s n = 10, and for 20 μm/s n = 9, no significant difference. G-J) Force-distance curves were analyzed for the extent of membrane deformation (G), penetration depth (H), energy spent to deform and penetrate the membrane (I) and membrane rupture force (J). Data are means ± SE, n= 10, no significant difference.

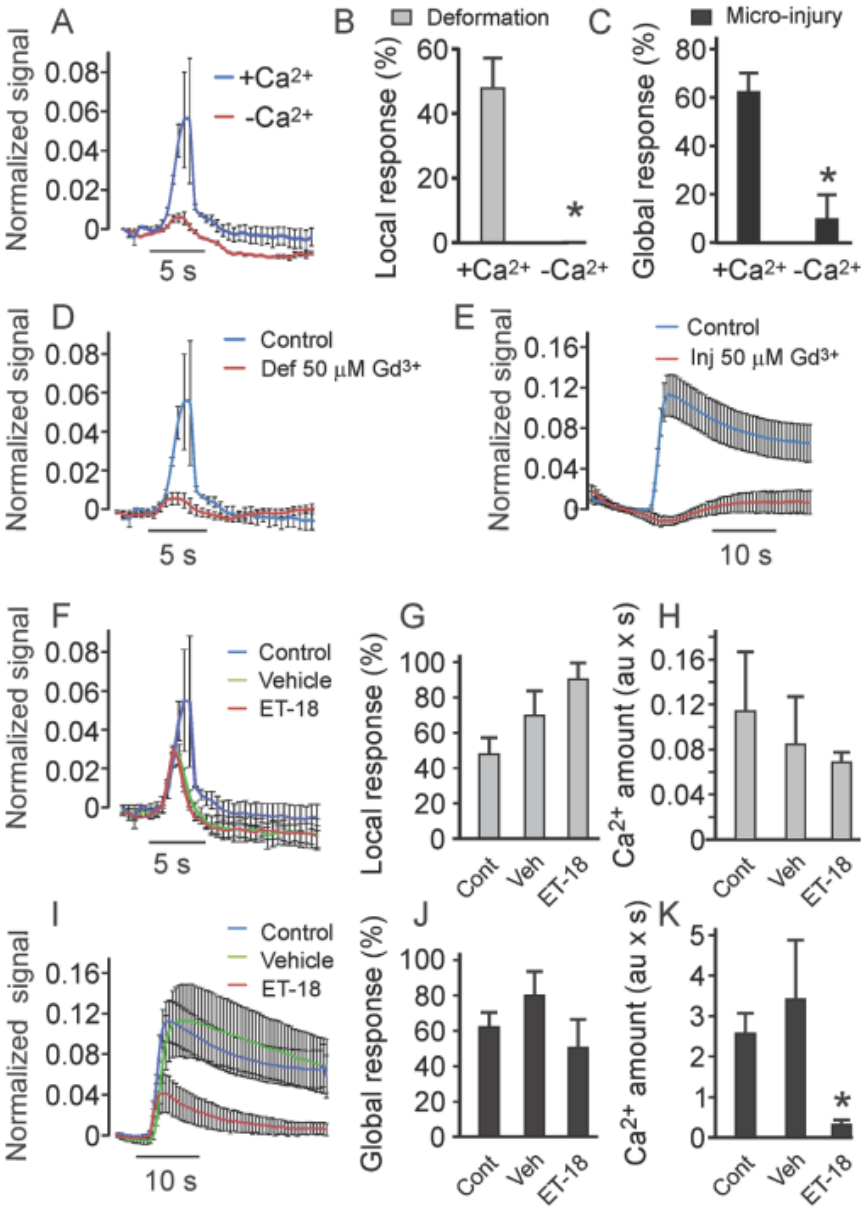

FIGURE 7. **The membrane deformation-induced Ca^{2+} responses are affected by inhibitors of stretch-activated Ca^{2+} channels and phospholipase C.** C2C12-generated osteoblasts were loaded with fluo4-AM, and single indentations were performed at 2 μm/s. A) Average local Ca^{2+} transients in response to low-load indentation in Ca^{2+}-containing (blue) and Ca^{2+}-free (10 mM EGTA, red) buffer. Data are means ± SE. B, C) Percentage of cells exhibiting local (B) and global (C) Ca^{2+} elevations in Ca^{2+}-containing ($+Ca^{2+}$) or Ca^{2+} free ($-Ca^{2+}$) buffer in response to low-load (B) or high-load (C) indentation. Data are means ± SE, for (B) n = 30 for Ca^{2+}-containing, n = 10 for Ca^{2+}-free; for (C) n = 10; *indicates a $p<0.05$ difference as assessed by Fisher Exact Probability test. D) Average local Ca^{2+} transients in response to membrane indentation in control (blue) or mechanosensitive Ca^{2+} channel blocker Gd^{3+} (50 μM)-containing buffer (red). Data are means ± SE. E) Average global Ca^{2+} transients in response to membrane penetration in control (blue) or Gd^{3+}-containing buffer (red). Data are means ± SE. F) Average local Ca^{2+} responses to membrane indentation in control (blue), vehicle (0.07% ethanol)-containing (green) or PLC inhibitor Et-18-OCH_3-containing (red) buffer. Data are means ± SE. G) The percentage of cells that exhibited local Ca^{2+} elevations in response to membrane indentation in control, vehicle- or Et-18-OCH_3-containing buffer. Data are means ± SE, n = 30 for control, n = 10 for vehicle and Et-18-OCH_3-treated cells, no significant difference. H) Average amount of Ca^{2+} released in response to membrane indentation in control, vehicle- or Et-18-OCH_3-containing buffer. Data are means ± SE, n = 4-5, no significant difference. I) Average global Ca^{2+} elevations in response to membrane penetration in control (blue), vehicle-containing (green) or Et-18-OCH_3-containing (red) buffer. Data are means ± SE. J) The percentage of cells that exhibited global Ca^{2+} elevations in response to membrane penetration. Data are means ± SE, n = 33 for control, n = 10 for vehicle and Et-18-OCH_3-treated cells, no significant difference. K) Average amount of Ca^{2+} released in response to membrane penetration Data are means ± SE, n = 8 for control and vehicle, n = 5 for Et-18-OCH_3-treated cells, *indicates a $p<0.05$ difference as assessed by Student's t-test.

In our model, micro-injury was required in order to achieve global elevations of $[Ca^{2+}]_i$ in the majority of cells. Many techniques used to study cell mechanosensitivity, such as fluid flow, substrate strain and pipette indentation, do not allow sufficient resolution to detect membrane micro-injury. However, a number of studies, in which the absence of membrane penetration can be reliably confirmed, demonstrated that global Ca^{2+} responses can be induced by membrane deformation only [11, 17]. Several differences in the experimental setup could account for this discrepancy. Charras and Horton [17] used AFM with spherical tip of 10-30 μm diameter, which would deform a 100-fold larger area compared to the pyramidal tip with 1 μm^2 contact area used in our study. Thus, the extent of horizontal membrane involvement in the deformation may be important for cell mechanosensitivity. While Xia and Ferrier [11] used patch-clamp micropipette with similar dimensions to the pyramidal tip used in our study, it has been shown that pipette suction creates substantially larger strains compared to AFM micro-indentation [14]. Therefore, higher calcium responses observed in the Xia and Ferrier study compared to our study are in keeping with previously demonstrated critical role of vertical membrane deformation in cell mechanosensitivity [17]. We have now shown that the duration of Ca^{2+} responses is directly proportional to time the cell membrane spends in deformation. Therefore, it is likely that cell sensitivity to membrane deformation is related to a combined effect of: *i*) the extent of the horizontal involvement of the membrane, *ii*) the vertical deformation of the membrane and *iii*) the duration of the deformation. Mechanosensitive calcium channels were strongly implicated in generating Ca^{2+} responses to mechanical stimulations in previous studies [11, 17, 25] and were confirmed to provide a critical contribution to both local and global Ca^{2+} responses in our study. Therefore, it is possible that local intracellular Ca^{2+} acts as an integrating signal that increases when open channels are more numerous or are activated longer, until it reaches the threshold Ca^{2+} concentration necessary to induce global Ca^{2+} response. Micro-injury then contributes to increasing local Ca^{2+} levels to threshold concentrations, inducing global response. Once global calcium elevation is triggered, it proceeds independently of the level of mechanical stimulation, as suggested by the lack of correlation between the magnitude of global Ca^{2+} response and mechanical

stimulation in our study and that of Charras and Horton [17]. Our data demonstrate that calcium release from intracellular stores plays an important role in this process.

We identified the refractory periods during which the responses to subsequent mechanical stimulations were either absent or diminished in amplitude. This refractory period following membrane deformation only was relatively short, and the calcium response was fully reestablished after the recovery time of 10 s. In contrast, in experiments where micro-injury and global elevation of calcium were observed, the recovery period was longer than 30 s. Previously, the refractory periods for global Ca^{2+} responses to fluid flow were reported to be in the order of 600-900 s [26]. The presence of refractory periods is of potential importance, since it was shown previously, that in order to induce potent osteogenic response, mechanical loading of bone should be performed as a series of repeated loading periods separated by the periods of rest [27, 28]. Of interest, the rest period of 10 s was found to be sufficient to induce potent bone formation in response to low magnitude mechanical loading [28, 29].

Taken together, our study provides new insights into the complex dynamics of cellular responses to mechanical stimulations. In contrast to many previous studies of cell responses to mechanical forces, atomic force microscopy allows very precise control and monitoring of the physical parameters of the experiment, such as forces and deformations applied at a single cell level. Using a well-established readout of cellular response, calcium signaling, allowed us to identify novel correlates between mechanical stimulation and cell responses. Such knowledge is important for better understanding of the mechanisms of mechanical loading-induced bone formation, as well as micro-damage induced bone remodeling.

Grant information

This work was supported by Natural Sciences and Engineering Research Council of Canada Discovery grants to PHG (RGPIN-223110) and SVK (RGPIN-288253).

Acknowledgements

The authors are grateful to Gulzhakhan Sadvakassova for preparing and characterizing the cells used in this study, Dr M. Murshed, McGill University for the C2C12-BMP-2 cell line. The authors thank DJ Oliver for helpful discussions. GMLA was supported by the Principal's Graduate Fellowship, Chalk-Rowles Fellowship, NSERC Graduate Excellence Fellowship and McGill University. HYL was funded by NSERC Undergraduate Science Research Award. SVK holds Canada Research Chair.

References

[1] Rubin CT. Skeletal strain and the functional significance of bone architecture. Calcif Tissue Int 1984;36 Suppl 1: S11-8.

[2] Suva LJ, Gaddy D, Perrien DS, Thomas RL, Findlay DM. Regulation of bone mass by mechanical loading: microarchitecture and genetics. Curr Osteoporos Rep 2005;3: 46-51.

[3] Burr D. Microdamage and bone strength. Osteoporosis international : a journal established as result of cooperation between the European Foundation for Osteoporosis and the National Osteoporosis Foundation of the USA 2003;14 Suppl 5: S67-72.

[4] Burger EH, Klein-Nulend J. Mechanotransduction in bone--role of the lacuno-canalicular network. FASEB J 1999;13 Suppl: S101-12.

[5] Brown TD. Techniques for mechanical stimulation of cells in vitro: a review. Journal of biomechanics 2000;33: 3-14.

[6] Liedert A, Kaspar D, Blakytny R, Claes L, Ignatius A. Signal transduction pathways involved in mechanotransduction in bone cells. Biochemical and biophysical research communications 2006;349: 1-5.

[7] Chen NX, Ryder KD, Pavalko FM, Turner CH, Burr DB, Qiu J, Duncan RL. Ca(2+) regulates fluid shear-induced cytoskeletal reorganization and gene expression in osteoblasts. Am J Physiol Cell Physiol 2000;278: C989-97.

[8] Hung CT, Allen FD, Pollack SR, Brighton CT. Intracellular Ca2+ stores and extracellular Ca2+ are required in the real-time Ca2+ response of bone cells experiencing fluid flow. Journal of biomechanics 1996;29: 1411-7.

[9] Hung CT, Pollack SR, Reilly TM, Brighton CT. Real-time calcium response of cultured bone cells to fluid flow. Clin Orthop Relat Res 1995: 256-69.

[10] Papachristou DJ, Papachroni KK, Basdra EK, Papavassiliou AG. Signaling networks and transcription factors regulating mechanotransduction in bone. BioEssays : news and reviews in molecular, cellular and developmental biology 2009;31: 794-804.

[11] Xia SL, Ferrier J. Propagation of a calcium pulse between osteoblastic cells. Biochemical and biophysical research communications 1992;186: 1212-9.

[12] Kirber MT, Guerrero-Hernandez A, Bowman DS, Fogarty KE, Tuft RA, Singer JJ, Fay FS. Multiple pathways responsible for the stretch-induced increase in Ca2+ concentration in toad stomach smooth muscle cells. J Physiol 2000;524 Pt 1: 3-17.
[13] Zou H, Lifshitz LM, Tuft RA, Fogarty KE, Singer JJ. Visualization of Ca2+ entry through single stretch-activated cation channels. Proc Natl Acad Sci U S A 2002;99: 6404-9.
[14] Charras GT, Williams BA, Sims SM, Horton MA. Estimating the sensitivity of mechanosensitive ion channels to membrane strain and tension. Biophysical journal 2004;87: 2870-84.
[15] Guo XE, Takai E, Jiang X, Xu Q, Whitesides GM, Yardley JT, Hung CT, Chow EM, Hantschel T, Costa KD. Intracellular calcium waves in bone cell networks under single cell nanoindentation. Mol Cell Biomech 2006;3: 95-107.
[16] Lamontagne C-A, Cuerrier C, Grandbois M. AFM as a tool to probe and manipulate cellular processes. Pflügers Archiv European Journal of Physiology 2008;456: 61-70.
[17] Charras GT, Horton MA. Single cell mechanotransduction and its modulation analyzed by atomic force microscope indentation. Biophysical journal 2002;82: 2970-81.
[18] Cuerrier CM, Lebel R, Grandbois M. Single cell transfection using plasmid decorated AFM probes. Biochemical and biophysical research communications 2007;355: 632-636.
[19] Vakarelski IU, Brown SC, Higashitani K, Moudgil BM. Penetration of Living Cell Membranes with Fortified Carbon Nanotube Tips. Langmuir 2007;23: 10893-10896.
[20] Katagiri T, Yamaguchi A, Komaki M, Abe E, Takahashi N, Ikeda T, Rosen V, Wozney JM, Fujisawa-Sehara A, Suda T. Bone morphogenetic protein-2 converts the differentiation pathway of C2C12 myoblasts into the osteoblast lineage. J Cell Biol 1994;127: 1755-66.
[21] Kemeny-Suss N, Kasneci A, Rivas D, Afilalo J, Komarova SV, Chalifour LE, Duque G. Alendronate affects calcium dynamics in cardiomyocytes in vitro. Vascular pharmacology 2009;51: 350-8.
[22] Lopez-Ayon GM, Oliver DJ, Grutter PH, Komarova SV. Deconvolution of calcium fluorescent indicator signal from AFM cantilever reflection. Microsc Microanal 2012;18: 808-15.
[23] Xu B, Feng X, Burdine RD. Categorical data analysis in experimental biology. Developmental biology 2010;348: 3-11.
[24] Duncan RL, Turner CH. Mechanotransduction and the functional response of bone to mechanical strain. Calcif Tissue Int 1995;57: 344-58.
[25] Nishitani WS, Saif TA, Wang Y. Calcium Signaling in Live Cells on Elastic Gels under Mechanical Vibration at Subcellular Levels. PloS one 2011;6: e26181.
[26] Donahue SW, Donahue HJ, Jacobs CR. Osteoblastic cells have refractory periods for fluid-flow-induced intracellular calcium oscillations for short bouts of flow and display multiple low-magnitude oscillations during long-term flow. Journal of biomechanics 2003;36: 35-43.

[27] Robling AG, Hinant FM, Burr DB, Turner CH. Improved Bone Structure and Strength After Long-Term Mechanical Loading Is Greatest if Loading Is Separated Into Short Bouts. Journal of Bone and Mineral Research 2002;17: 1545-1554.
[28] Srinivasan S, Weimer DA, Agans SC, Bain SD, Gross TS. Low-Magnitude Mechanical Loading Becomes Osteogenic When Rest Is Inserted Between Each Load Cycle. Journal of Bone and Mineral Research 2002;17: 1613-1620.
[29] Srinivasan S, Agans SC, King KA, Moy NY, Poliachik SL, Gross TS. Enabling bone formation in the aged skeleton via rest-inserted mechanical loading. Bone 2003;33: 946-955.

The majority of nervous tissue is made up of two types of cell: neurons and glia. Glial cells surround neurons to protect them. Neurons are electrically excitable cells in the nervous system that process and transmit information through electrical and chemical signals. All neurons share the same basic architecture. They consist of a cell body, which gives rise to one or multiple dendrites, one axon, and multiple synaptic sites (Figure 6.1.1 A). Dendrites branch out in a tree-like fashion and are the main apparatus for receiving incoming synaptic signals from other nerve cells. In contrast, the axon extends away from the cell body, pulled by the growth cone. The growth cone is a dynamic, actin-supported extension of a developing neurite seeking its synaptic target. The axon is the main conducting unit for carrying synaptic signals to other neurons. The signals that the axon conveys are called action potentials; they are rapid, transient all-or-none nerve impulses initiated at a specialized trigger region at the origin of the axon. Neurons connect to each other at synapses and information is transferred from the "presynaptic site" in the axon to the "postsynaptic site" in the dendrites in a unidirectional manner (Figure 6.1.1 B). [224]

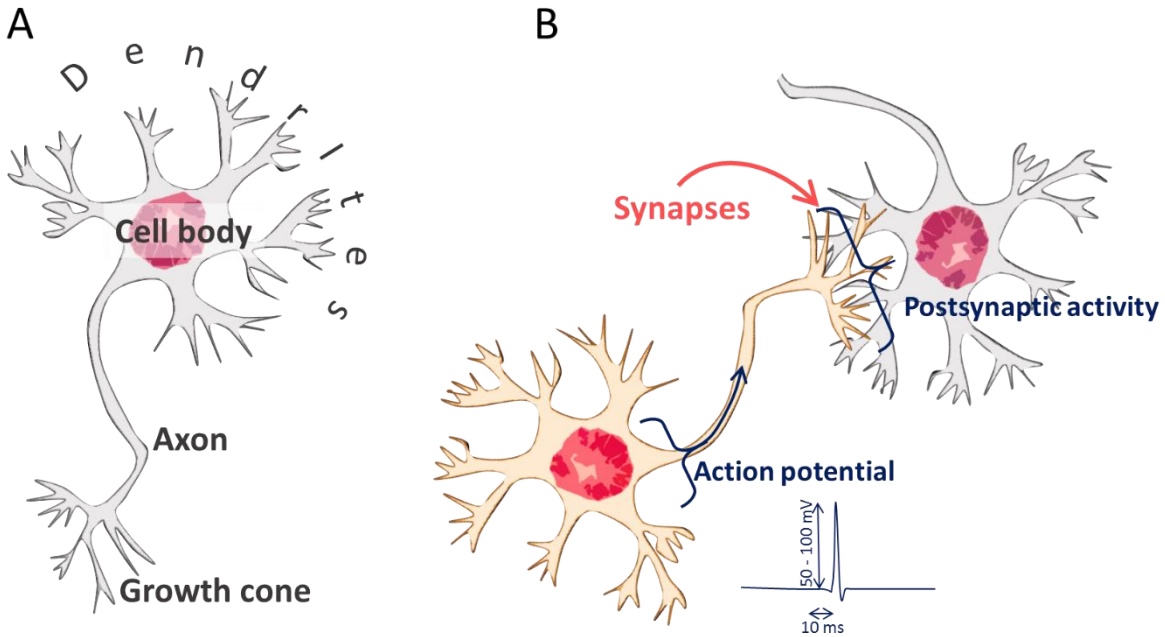

(FIGURE 6.1.1) SCHEMATICS OF: A) NEURON MORPHOLOGY B) ACTION POTENTIAL CONVEYED BY A NEURON THROUGH SYNAPSES RESULTING IN POSTSYNAPTIC ACTIVITY.

During development, neurons send out exploratory tips (filopodia), which are highly mobile structures that possess detectors of chemical guidance cues; they translate cues from the environment into directional movement to grow toward a specific destination [258]. While the axon grows mainly in length, the dendritic tree grows mainly by the addition and elongation of branches [259]. Once the axon reaches its target location, it usually arborizes and establishes synapses with the target cells, assembling the functional neuronal network [260].The final branching pattern of the neuron is not only established by branch addition and maintenance, but also by branch retraction and elimination [261] [239].

Much effort has been put into understanding how guidance of the growth cone occurs. Highly complex interactions are involved in growth cone motility, neuronal process outgrowth and guidance [260]. These interactions involve remodeling of actin, microtubules and their associated proteins [262–265]. It has been shown that synapse formation and axonal branch initiation directly regulate local assembly of the F-actin network [77].

Presynaptic endings that appear strikingly similar to the ones produced in-situ can be triggered when an adhesive contact is locally presented and induce dynamic reorganization of F-actin [208,266]. Thus, presynaptic boutons can selectively form following neurite adhesion to beads coated with poly-D-lysine (PDL). AFM can be used to precisely position a PDL-coated bead on a neurite to initiate adhesive contact formation [208]. Upon adhesion and presynaptic differentiation, when the bead is mechanically pulled away, a branch is initiated extending from the axon to the PDL-bead [267].

In this study we explore different techniques that enable manipulation of a PDL-coated bead to initiate, elongate and connect neurons. We show that the neurites newly extended are not different in structure from naturally grown ones and they retain the capability to transmit electrical signals.

Rewiring neuronal networks using micromanipulation

G. Monserratt Lopez-Ayon[1], Margaret H. Magdesian[1,2]Megumi Mori[1], Dominic Boudreau[3], David Oliver[1], Alexis Goulet-Hanssens[4], William Paul[1], Ricardo Sanz[2], Yoichi Miyahara[1], Christopher J. Barrett[3], Alyson Fournier[2], Yves De Koninck[5], Peter Grütter[1]

[1] Department of Physics, McGill University, Montreal, Quebec, H3A 2T8 Canada.

[2] Montreal Neurological Institute, McGill University, Montreal, Quebec, H3A 2B4 Canada.

[3] Centre de Recherche de l'Institut Universitaire en Santé Mentale de Québec, Québec, Québec G1J 2G3, Canada

[4] Department of Chemistry, McGill University, Montreal, Quebec, H3A 2K6 Canada

Abstract

In mammalian adults, injury to the central nervous system (CNS) typically leads to permanent functional deficits, mainly because it is still not possible to reproduce critical developmental steps: regeneration of axons over long distances and accurate reconnection with the appropriate target [268]**. Here we show that we can initiate a new axon, extend it over long distances and functionally connect it to the desired target cell. We achieve this by approaching a functionalized bead to rat CNS axons using micromanipulation to induce a presynaptic adhesion contact. By pulling the bead a new axonal branch is formed, which can be extended over hundreds of micrometers in less than one hour. The new neurite can be precisely connected to the desired target. Whole cell paired patch clamp recordings revealed that the connection is functional. Our results support previous findings showing that neurite outgrowth can be initiated at any point of an axon, that assembly of growth cones is not a prerequisite for axonal growth and highlight the importance of mechanical cues in fast directing neurite elongation and connection.** [269] **These results challenge the current understanding of the limits of neuronal growth, have direct implications in the study of neural stem cell differentiation, signal propagation and network assembly, and open new avenues for the development of drug discovery platforms, therapies and surgical techniques to achieve functional CNS regeneration.**

Introduction

During development, neurons extend axons over distances exceeding the neuronal cell body diameter by more than a thousand fold to reach targets and build the intricate network that comprise the adult CNS [260]. The growth cone, a highly motile structure at the tip of the axon, continuously explores the spatial environment interacting with guidance cues to accurately select a correct trajectory among multiple possible routes [260,270–272]. Guidance of the growth cone is a complex mechanism orchestrated by several different families of molecules [260]. Once the axon reaches its target location, it usually

arborizes and establishes synapses with the target cells, assembling the functional neuronal network [260]. Proper function of the nervous system depends on the specificity of these neuronal connections.

Injuries to the adult CNS usually lead to permanent disability due to multiple factors that limit axonal regrowth and restoration of synaptic connections [268]. Therapies to promote CNS regeneration after injury have focused on modifying the chemical environment of the scar tissue surrounding CNS lesions [269]. The general idea has been to reproduce the growth stimulatory conditions present during development [268], however, the environment in the adult CNS is strikingly different from that in the developing organism [273]. Following injury, most CNS axons fail to assemble a new growth cone and fail to build an effective regenerative response [269]. In addition, the scar tissue surrounding CNS lesions is inhibitory to axonal growth [260,268–276]. Several strategies have been explored to target different aspects of this process: cellular replacement, neurotrophic factor delivery, axon guidance and removal of growth inhibition, manipulation of intracellular signalling, bridging and artificial substrates, and modulation of the immune response [275]. Nonetheless, regrowth of long axons towards correct targets and the formation of functionally appropriate synapses is still not possible. The current status is still well described by Santiago Ramon y Cajal: "once the development was ended, the founts of growth and regeneration of the axons and dendrites dried up irrevocably. In the adult centres the nerve paths are something fixed, ended and immutable. Everything may die, nothing may be regenerated. It is for the science of the future to change, if possible, this harsh decree" [276].

Previous work in our lab focused on means of stimulating synapse formation using mechano-chemical stimuli [208,277,278]. We showed that presynaptic bouton formation can be induced by the contact of a poly-D-lysine coated bead (PDL-bead) with an axon [208]. When the PDL-bead is mechanically pulled away after presynaptic differentiation, a new axonal branch forms extending from the axon to the PDL-bead [277]. Upon pulling, the synaptic protein cluster follows the bead. Transport of synaptophysin and bassoon were detected in the newly formed neurite [277].

(*The methods section follows after the results*)

Results

Here we introduce the concept of mechanically manipulating PDL-beads to induce the formation and elongation of new neurites to establish functional connection between two neurons. Specifically, we induce new, functional connections between rat hippocampal neurons, which are cultured in Polydimethylsiloxane (PDMS) microdevices. These PDMS devices allow us to perform experiments and connect previously isolated populations of neurons (Fig. 1).

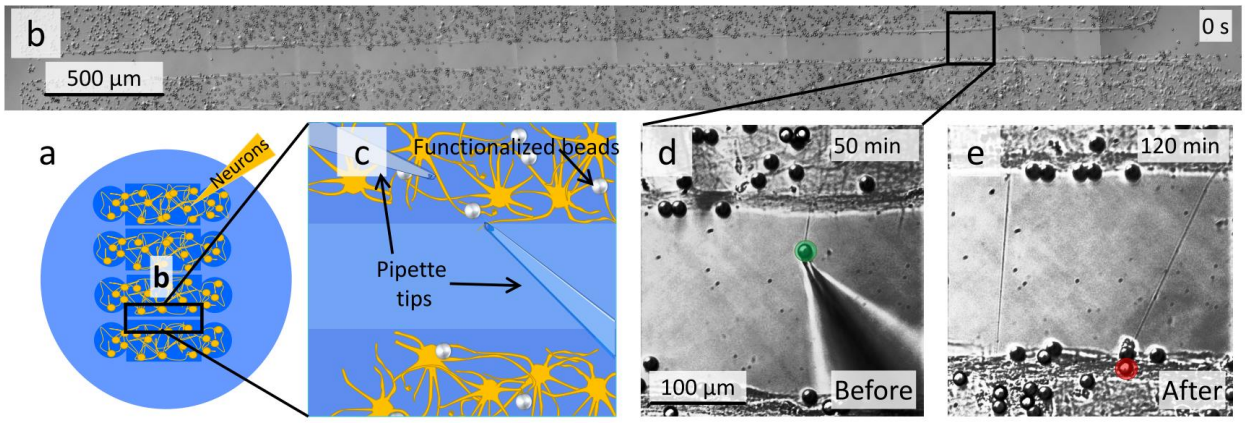

Figure 1. Initiation, elongation and connection of new neurites using pipette micromanipulation. (**a)** Design of the PDMS microfluidic chamber (blue) assembled on a glass coverslip to grow dissociated cultures of rat primary hippocampal neurons in four isolated populations for 14-21 days. One day before experiments were performed the microfluidic chamber was disassembled by removing the PDMS and exposing the gap between neuronal populations (**b)**. Neurons were incubated with PDL-beads for 1 h, schematic representation of the experimental setup shows a zoom in the gap between two isolated neuronal populations (one above and the other one below) as well as the position of the two pipette tips (**c)**. By applying negative pressure to a pipette, a PDL-bead adhered to the neuronal population above the gap is pulled and attaches to the pipette tip, thereby initiating a new neurite (**d)**. By maintaining the negative pressure in the pipette, the PDL-bead (green) with the newly formed neurite can be pulled enabling elongation. (**e)** Pipette micromanipulation guides the extension (250-800 µm) of the new neurite over the gap and the formation of a precise connection with the neuronal population below the gap. To assure physical contact between the pulled neurite and the new population, a second adhesion point is established by positioning a non-adhered PDL-bead (red) (picked with the second pipette) on top of the contact between the new neurite and the second neuronal population. Image shows two newly created filaments guided with micromanipulation to connect two previously isolated neuron populations.

We investigated the maximum rate at which a neurite could be pulled while maintaining its structural integrity using controlled AFM manipulation of the bead (Fig.2). We found that it was crucial to pull at a controlled rate during the initial formation, limiting the neurite extension speed to 0.5 µm/min for the first 5 µm of pulling. Neurites could thus be elongated to lengths >840 µm (limited by instrumentation) at an average speed of 20 ± 10 µm/min. The ability of the filament to sustain such a high growth speed is remarkable considering that the maximum growth rate of neurons in a developing human fetus is ~ 0.8 µm/min [279].

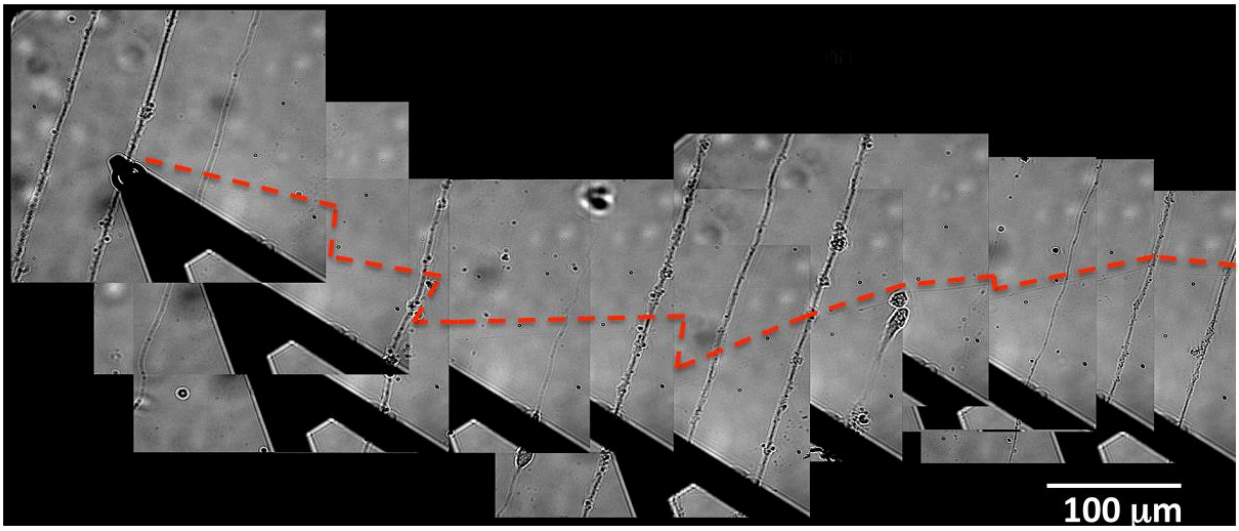

Figure 2. Initiation, elongation and connection of new neurites in primary rat hippocampal neurons using PDL-beads and AFM. Superposition of individual images. Neurons were cultured for 14-21 days in PDMS microfluidic chambers enabling the growth of axons and dendrites in parallel inside the microchannels. PDMS was removed one day before imaging and a PDL-bead attached to the AFM tip was brought in contact with a bundle of neurites. After one hour the bead was pulled, thereby creating and elongating a new neurite, which is extended and precisely connected to the next bundle of neurites. The new neurite remained attached to the bead and was elongated for more than 840 µm in 42 minutes. Neurite elongation was limited by instrumentation restrictions because the experimental setup on the AFM does not allow displacements larger than 1 mm, dashed line highlights the neurite trajectory.

Using an AFM to manipulate the PDL-bead allowed the development of robust protocols for successful initiation of an adhesive contact, as well as investigate the finer

details of the pulling process further discussed in the methods. AFM is however not suitable for manipulation of many contacts, as it is challenging to disconnect the neurite attached to the bead glued to the AFM tip without mechanically destroying the newly formed connection or inducing cell death. We developed a powerful and reliable technique whereby a loose PDL-bead was held by suction at the tip of a micropipette mounted on a micromanipulator. The bead can then be used to initiate and extend filaments following similar protocols to those established by AFM with the advantage that the bead can readily be released from the micropipette by removing the suction. This allows the manipulation apparatus to be removed in order for other analytical techniques to be applied to the intact new connection.

We observed that depending on the bead size, multiple neurites may be initiated and pulled by a single contact. A single axon typically only produced a single neurite, but three neurites or more could be pulled from multi-axon bundles (Fig. 3). Changes in synaptic size, density and dendritic spine morphology have been associated with different pathologies, including mental retardation and autism spectrum disorders [280]. We used three different PDL-beads sizes: 4.5 µm beads (n_{total}: 5) created one neurite in 60% of the experiments and two neurites in 20%, while 10 µm beads (n_{total}: 87) pulled two neurites in 50% of the cases and 20 µm beads (n_{total}: 15) pulled 3 neurites in 67% of the experiments

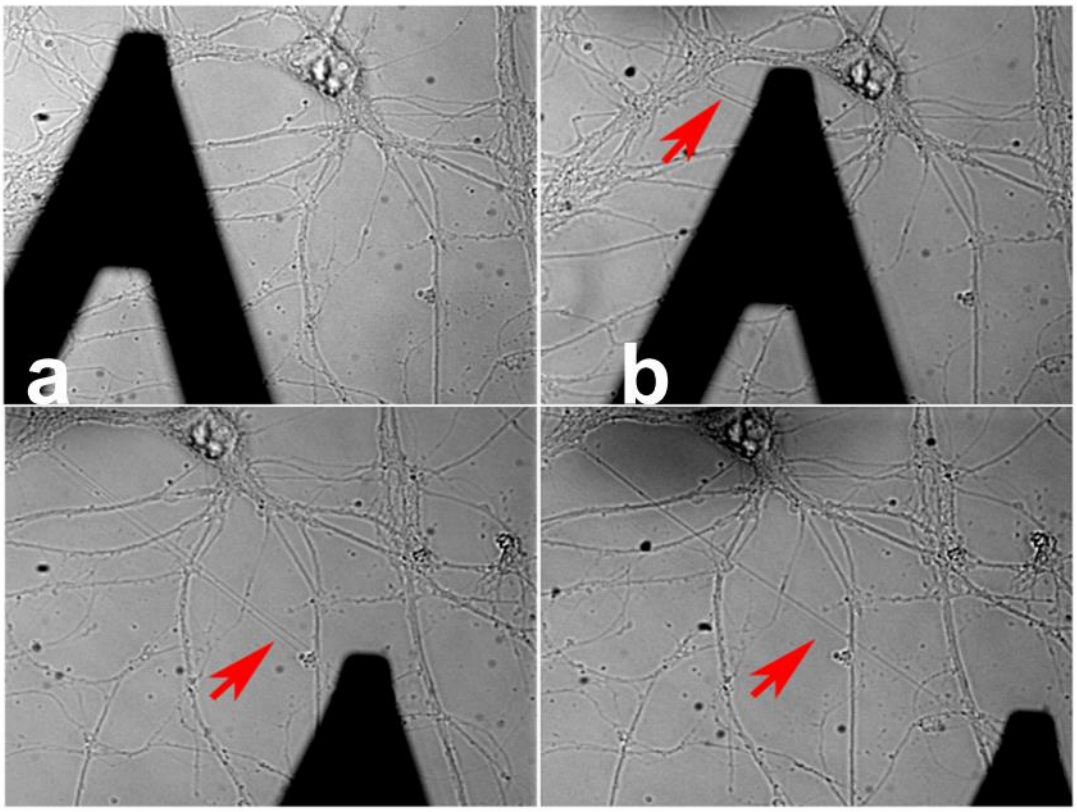

Figure 3. Initiation, elongation and connection of multiple filaments. (a), A PDL-bead attached to the tip of an AFM microscope was brought in contact with bundles of neurites for 30 minutes. (b), next, the AFM tip was moved 15 µm away from the sample enabling the visualization of several neurites attached to the PDL-bead. (c), upon micromanipulation of the AFM tip neurites can be extended over more than 90 µm in less than 5 minutes (d), As the new neurites grow longer they assemble together generating a thicker fiber.

and one neurite in only 11% of the experiments performed.

If the PDL-bead at the end of the extending filament is brought in contact with another neuron it promotes the formation of a new connection. We found that maintaining the bead in contact at the new site for one hour was sufficient to create a mechanically stable connection that lasted for more than 24 hours (Fig. 4). This allows us to bridge two previously unconnected cells (Fig. 1). This simple process of manipulating PDL-beads is robust: new neurites were created and extended in 95% of the experiments performed and the connections were stable for more than 2h in 50% of the experiments performed. We reproduced these experiments both in rat hippocampal (n=80) and cortical (n=23) neurons grown inside microdevices with channels (Fig. 1) as well as in regular dissociated cultures (Fig. 3).

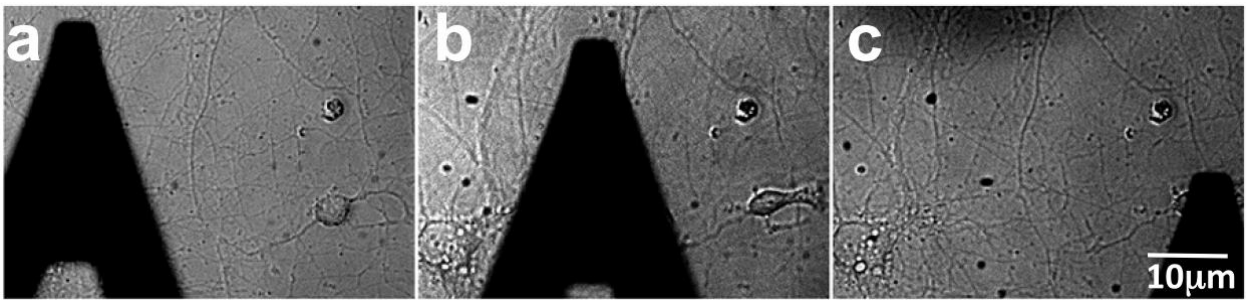

Figure 4. Initiation, elongation and connection of new neurites in rat cortical neurons. (a), A PDL-bead attached to the tip of an AFM microscope was brought in contact with neurites from primary culture of dissociated rat cortical neurons for 30 minutes. (**b)**, next, the AFM tip was moved 15 μm away from the sample enabling the visualization a newly formed neurite attached to the PDL-bead. (**c)**, upon micromanipulation of the AFM tip the neurite was extended over more than 90 μm in less than 5 minutes.

We used immunofluorescence techniques to assess the structural components present in the newly created neurites. The neurites were found to contain actin, tubulin, tau and neurofilament (Fig. 5), establishing the presence of typical chemical components of the cytoskeleton in naturally grown axons and dendrites [281].

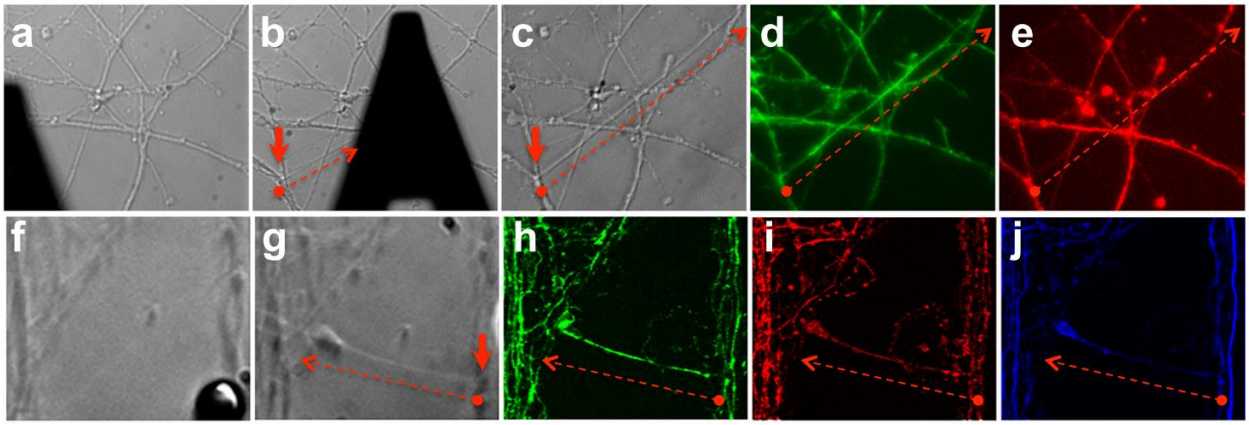

Figure 5. The newly formed neurite contains actin, tubulin, tau and neurofilament. a, A neurite created and extended (**b**) with AFM micromanipulation was fixed 1 h after connection (**c**) and labeled with phalloidin (**d**) and anti-β -tubulin antibody (**e**). **f**, Neurite created and extended (**g**) with pipette micromanipulation was incubated for 18 h at 37 °C with 5% CO_2, fixed and labeled with phalloidin (**h**) and antibodies anti-tau-1 (**i**) and anti-neurofilament 200 (**j**). Arrows indicate the neurite starting point and dashed lines highlight the newly formed neurite.

We also observed the transport of mitochondria along the mechanically created neurites. Structurally, the manipulated neurites do not show any discernible difference as compared to naturally grown ones. Interestingly, in the presence of the Tubulin Tracker™ reagent (Invitrogen), new neurites were created but could not be labeled nor extended for more than 10 µm without breaking (n=3). This reagent contains taxol, a drug that stabilizes microtubules and reduces their dynamicity [282]. These results indicate that tubulin polymerization is essential to new neurite elongation. Moreover, contact of PDL-beads with neurites trigger Ca^{2+} signaling (Fig. 6). The elevation of the free intracellular calcium concentration is involved in several events, including local transformation of the cytoskeleton, activation of long-range retrograde molecular signaling and activation of local protein translation [269].

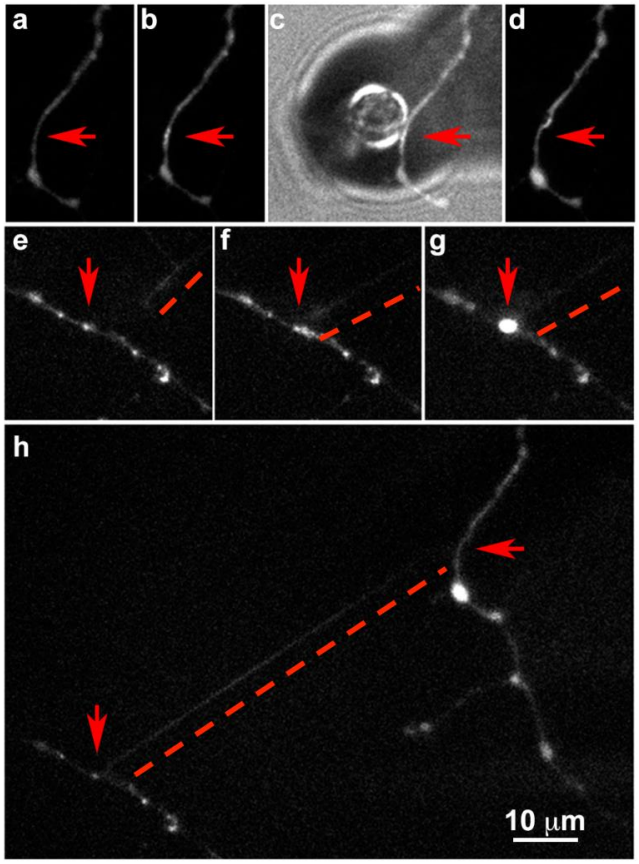

Figure 6. Contact of PDL coated beads with neurites trigger calcium signaling. (**a**), Axons before and after (**b**) contact with a PDL-bead attached to the AFM tip (**c**) show local increase in calcium signaling at the contact point. After 30 min of contact, calcium labeling was observed around the PDL-bead (**d**). As the bead is pulled to the left, the new neurite elongates (**e**) towards a dendrite. Calcium labeling significantly increases as the new micromanipulated neurite touches the dendrite (**f** and **g**). (**h**), Image shows the full length of the new filament. Arrows indicate the PDL-bead-neurite contact and the dashed line highlight the new neurite.

To assess whether the newly created connection was functional (Fig 7a), it was compared to cells naturally connected across the gap (Fig 7b) and cells not connected across the gap (Fig 7c). Paired whole-cell patch clamp recordings were performed for each condition (Fig 7d-f). Firing activity was recorded from a neuron in the population above the gap, where neurite extension was initiated (presynaptic cell), while postsynaptic activity was recorded from a neuron in the population below the gap, where the extended neurite was connected. In the newly formed connection, the excitatory postsynaptic currents appeared correlated to the presynaptic activity. For analysis, both the presynaptic and the postsynaptic peaks were detected and postsynaptic traces were aligned with respect to the presynaptic action potentials. Ten consecutive traces are plotted in what we call a spike triggered activity plot (Fig 7 g-i). Analysis of the spike triggered activity indicates a significant increase in the number of postsynaptic peaks after presynaptic action potential

(PAP) in the ± 100 ms interval for the cases in which the tested neurons are connected (Fig 7g) assessed by McNemar's test ($p < 0.05$).

It is highly likely that the cells patched are not directly connected to each other, but rather indirectly connected through synapses with other neurons, what is called a polysynaptic connection. It has been shown that polysynaptic activity generally exhibits lower transmission probabilities and longer and more variable latencies (>5 ms) because the multiple pathways through which the signal can be successfully transmitted induce a delay and the probability of signal transmission through the network is decreased [234,283,284]. Thus, the correlation observed in the traces suggest that the neurons tested are functionally connected, and the delay and variable latencies observed imply that the connection is polysynaptic.

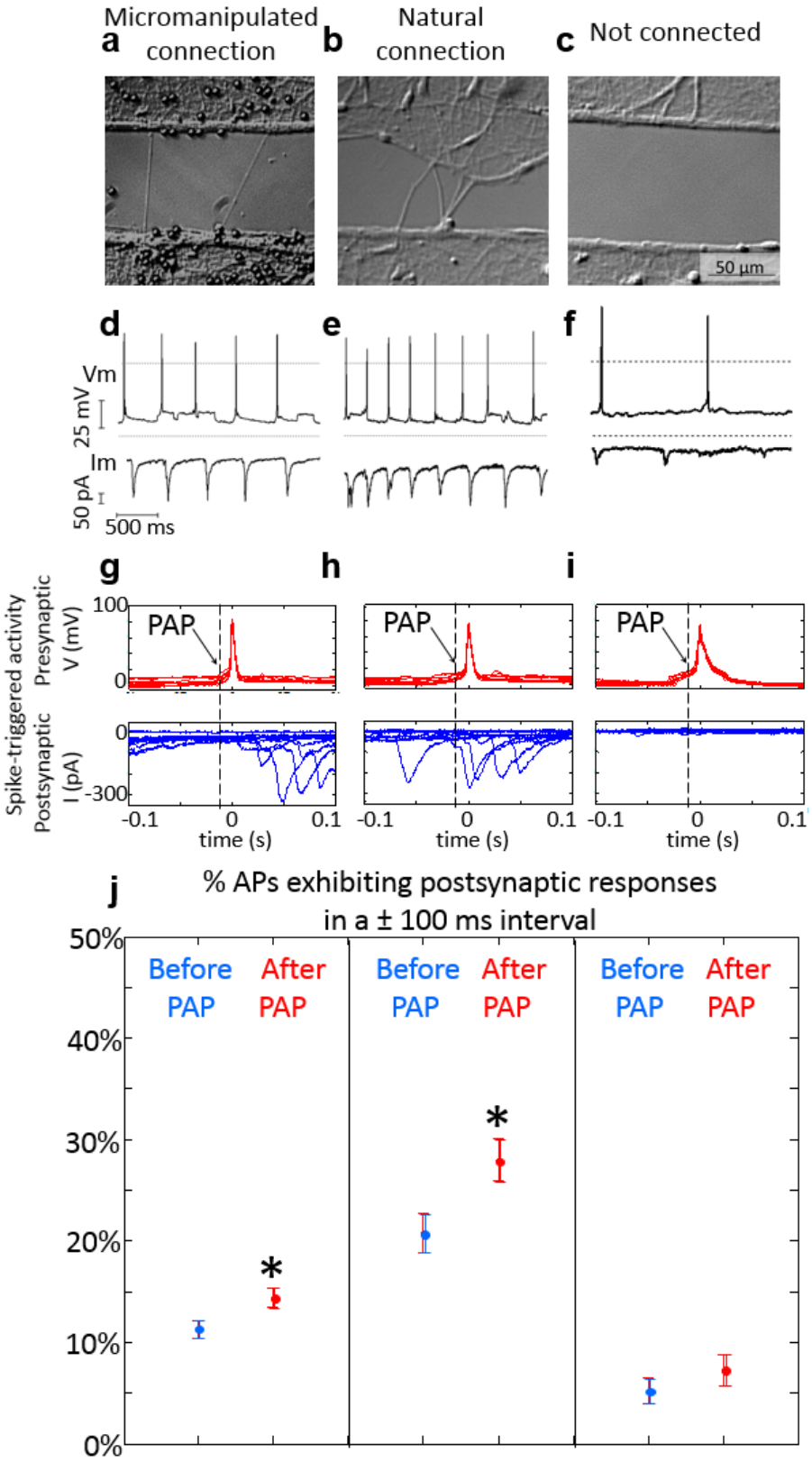

Figure 7. The newly induced, elongated and connected neurite can transfer information between two isolated neuronal populations. Isolated neuronal populations were cultured separated by a 100 µm gap in PDMS microdevices. Paired patch clamp recordings were performed in whole cell configuration from a neuron in population one and a neuron in population two (on the other side of the gap) when the two populations were connected through mechanical manipulation (a), allowed to naturally interconnect across the gap (b) or remain non-connected by maintaining the gap (c). Representative traces of paired recordings (d-f) and spike-triggered activity of 10 consecutive traces for each condition are shown (g-i). Dashed vertical lines (g-i) mark the onset of presynaptic action potential (PAP). The percentage of PAP associated with postsynaptic responses in ± 100 ms intervals for each condition is shown (j). Data are means ± SE, (nTotal_AP=1202, nbefore=136, nafter=173) for the mechanically-induced connection, (nTotal_AP=439, nbefore=91, nafter=123) for neuronal populations naturally connected and (nTotal_AP=304, nbefore=16, nafter=22) for not connected populations. * indicates $p < 0.05$ as assessed by McNemar's t-test (17).

Conclusion

Previous studies have shown that mechanical tension can determine axonal fate and promote extension of existing axons in CNS neurons [129] and in PNS neurons *in-vitro* [19,66,67,128,285]. Extended axons are structurally indistinguishable from those naturally grown [66], suggesting that axonal growth is not limited by cellular components, but rather by a poor growth cone performance, which exerts too little tension to exploit the available capacity for axonal elongation [128]. In addition, naturally connected PNS neurons stretched over several centimeters retain the ability to transmit active electrical signals and present increased density of Na^+ and K^+ channels [67].

However, many therapies for functional recovery after axonal injury have focused on the reproduction of the sequence of developmental events during axonal growth, namely growth cone assembly and development of chemical cues to guide axonal growth and synapse formation [268]. Here we have shown that it is possible to grow axons without following the same order of events that take place during development. In mature neurons, synapse formation can be induced by forming an adhesion contact (e.g. with a PDL coated bead), which can then be mechanically pulled to generate new axonal branches. These new neurites can be extended at unprecedented fast elongation rates by micromanipulation without the need of a growth cone. Given that synaptophysin and bassoon transport are detected in the newly formed neurite, [277] and actin, tubulin, neurofilament and tau are found by immunofluorescence labeling, the structure of the created neurites appears very similar to naturally grown ones.

Several studies have explored ways to initiate and elongate cellular filaments (also known as tethers and membrane nanotubes) [106,112,164,286,287] from living cells to analyze mechanical properties. Using Human Embryonic Kidney cells, one study succeeded in connecting the newly extended tether to other another cell, and the tether was capable of transmitting electrical signals over long distances [17]. To our knowledge, this is the first time that successful micromanipulation of an adhesive contact is used to extend and connect a new functional process between neurons. We show that the new filament

possesses the ability to transmit electrical signals between two separated neuronal populations.

Our results show that it is possible to create new axonal branches and to (re)wire neuronal networks using standard micromanipulation techniques accessible to most laboratories. The techniques presented here opens vast new fields of exploration and points to the importance of mechanical cues to fundamental biological processes of CNS axonal growth and repair. The method can be used to study signal propagation models [288] and transfer functions of neuronal networks, as one can control the diameter of the pulled neurite by varying the manipulation speed, and controllably generate a predefined neuronal topology. It can also be applied to study the connectivity between different cell types, and it might be used to develop robust brain-machine interfaces by connecting functional axons onto inorganic interfaces.

To improve the yield of functional signal transfer between separate cell populations, an immediate future direction is to modify the current protocol to use optical and/or magnetic bead manipulation. These developments, would also enable creating a greater number of filaments and manipulating the filaments in three dimensions which would increase the applicability of the technique to tissues and in-vivo models as opposed to live cultured cells.

This method has the potential to be applied as a discovery platform for drugs and therapies for traumatic CNS and other neurodegenerative diseases. For a start, axotomy can be performed in cells in culture following established procedures that enable axonal regeneration [269]. After regeneration one can attempt to artificially connect the transected cell with another chosen cell by the method developed here and analyze the connectivity.

Methods

Microfluidic Chambers. Microfluidic chambers with microchannels to extend axons or with isolated compartments to grow separated populations of neurons on the same dish were designed and micro fabricated by ANANDA, Advanced Nano-Design Applications,

McGill University, Montreal, QC, Canada. These devices are made of polydimethylsiloxane (PDMS) using Sylgard 184 Silicone elastomer kit (Dow Corning, Midland, MI) as previously described in [148]. PDMS devices were assembled on 25-mm glass coverslips (Warner Instruments, Hamden, CT). The glass surface was coated with 100 µg/ml Poly-D-Lysine (Sigma-Aldrich, St. Louis, MO) and the devices were used to culture neurons.

Neuronal cultures. All procedures were approved by McGill University's Animal Care Committee and conformed to the guidelines of the Canadian Council of Animal Care. Hippocampal neurons from Sprague Dawley rat embryos of either sex (Charles River, Wilmington, MA) were isolated as previously described [208] and added to the microfluidic chambers. Cells were cultured in the microfluidic chambers for 13-20 days in vitro (DIV) and the PDMS devices were removed 1-4 days prior to AFM imaging or micromanipulation experiments as described [148]. During experiments cells were continuously perfused with physiological saline containing 135 mM NaCl (Sigma-Aldrich), 3.5 mM KCl (Sigma-Aldrich), 2 mM $CaCl_2$ (Sigma-Aldrich), 1.3 mM $MgCl_2$ (BDH Inc, UK), 10 mM HEPES (Fisher) and 20 mM D-glucose (Gibco). Osmolarity was 240 - 260 mOsm and pH was adjusted to 7.3 – 7.4 using NaOH (Sigma), with continuous bubbling of O_2 to reduce pH oscillations during experiments.

Atomic Force Microscopy. Experiments were conducted using an MFP-3D-BIO AFM (Asylum Research, Santa Barbara CA) mounted on an Olympus IX-71 inverted optical microscope. The sample was placed in the closed fluid cell, open configuration and was left undisturbed for 15 min to achieve thermal equilibrium at 37 °C. A 40XPH objective with 0.6 NA (Olympus) was used to focus on the sample allowing optical access from the bottom and AFM access from the top of the sample. Triangular MLCT cantilevers (spring constant of 0.01 N/m from Bruker) were used and custom modified as described below. The region of interest was located and aligned with the cantilever tip using bright field illumination.

Beading of the AFM probe. A 50 µl drop of 4 µm, 10 µm or 20 µm beads (Polysciences) diluted in water (1:500) was deposited on a square coverslip and quickly dried at 37°C.

Epoxy adhesive (Loctite®E-30Cl) was added at one edge of another square coverslip and both coverslips are fixed at opposite sides of a microscope slide using vacuum grease 1 cm apart, with the dab of glue facing towards the center of the slide. The slide was positioned in the microscope. The tip of an AFM cantilever was brought in contact with the glue and retracted with a small droplet of glue on the tip. Next, the slide was shifted to the coverslip containing the beads, the AFM tip with glue was brought in contact with the bead, and was lifted away. Bead attachment was optically confirmed and the glue was cured overnight at 37°C.

AFM micromanipulation. Neurons cultured for 1-21 days in microfluidic chambers were positioned in the AFM and a 10X objective was used to find the region of interest. A 40XPH objective with 0.6 NA was used for optical access. The AFM beaded tip was brought in contact with an axon for 30 minutes applying forces between 0.1-0.3 nN [148]. Next, the AFM tip was moved 5 μm away from the sample at a speed of 0.5 μm/min enabling the visualization of one or more neurites attached to the bead. The AFM tip was micromanipulated further at exponentially increasing speeds as long as intermittent periods of rest were allowed. Maximum speeds >100 μm/min were sustained, with average speeds of 20 ± 10 μm/min. We have yet to discover if there is a fundamental limitation to these speeds. After reaching the second target, the bead was brought in contact with the region of interest for 1 h applying forces between 0.1-0.3 nN. After that the AFM was moved away from the sample.

Pipette micromanipulation. 10 μm beads were coated with 100 μM/ml of PDL as described [208], added to 14-21 days neurons grown in microfluidic chambers and incubated for 1 h. Cell medium and non-adherent PDL-beads were removed and cells were positioned on an inverted optical microscope (Olympus IX-71) with perfusion of oxygenated physiological saline solution at room temperature at a rate of 0.5-1 ml/min. Experiments were conducted using two pipette micromanipulators (MX7600R from SD Instruments and PCS-5000-series from Burleigh). Pipettes with a tip outer diameter of approximately 5 μm were prepared from glass capillary tubes (1.5 mm OD, King Precision Glass, Inc). A 40XPH objective with 0.6 NA was brought into focus with the sample,

allowing optical access from below and micromanipulation of the pipettes from above the sample. The region of interest was located using the bright field illumination. The tip of a pipette was optically guided close (2-5 μm) to the PDL-bead attached to an axon in the neuronal population above the gap using the motorized micromanipulators. Negative pressure was applied with a 1 ml syringe connected to the pipette to pull the PDL-bead towards the pipette tip. Negative pressure in the pipette was maintained throughout the whole micromanipulation experiment to keep the PDL-bead attached to the pipette. Next, the beads were moved 5 μm away from the axon at 0.5 μm/min enabling the creation of one or more neurites attached to the bead. Subsequently, the PDL-bead-neurite complex was pulled towards the neuronal population below, extended at exponentially increasing speeds as long as intermittent periods of rest were allowed. Maximum speeds >100 μm/min were sustained. Neurites could thus be elongated to lengths >800 μm (limited by instrumentation) at an average speed of 20 ± 10 μm/min. Upon arrival at the target region, the PDL-bead-neurite complex was put in contact with the chosen cell for 1 h. At the same time, a second pipette was used to pick a non-adhered PDL-bead with suction and placed on top of a second contact point between the neurite and the target cell to assure good physical contact. After 1 h the PDL-beads were released from the pipette tip and the newly created neurite (s) remained attached to the chosen target cell. Saline solution was replaced by Neurobasal medium (Invitrogen) and the sample was incubated overnight at 37° C with 5% CO_2 before electrophysiology tests were performed.

Immunocytochemistry. Immunocytochemistry was performed as previously described [208] with mouse anti-tubulin (The Developmental Studies Hybridoma Bank, University of Iowa, IA), rabbit anti-neurofilament 200 (Sigma-Aldrich), mouse anti-tau-1 antibody clone PC1C6 (Millipore, MA, USA), and Alexa 488 conjugated phalloidin (Invitrogen). The secondary antibodies used were Rhodamine Red anti-mouse IgG (Invitrogen) and Alexa Fluor 647 anti-rabbit IgG (Invitrogen). Samples were imaged with a 40X objective on an inverted optical microscope (Olympus IX-71) or with a Fluoview FV1000 laser scanning confocal microscope (Olympus, Richmond Hill, Ontario) with a 60X PlanApo oil immersion objective on an inverted microscope.

Electrophysiology. Whole cell paired patch clamp recordings were conducted in hippocampal neurons DIV 14-21 perfused with oxygenated physiological saline at room temperature for 30 minutes prior and during patch-clamp experiments. Pipettes were prepared from glass capillary tubes (1.5 mm OD with filament, King Precision Glass, Inc). The pipettes to patch on the postsynaptic cell were filled with internal solution containing 95 mM Cs-methysulfonate (Sigma-Aldrich), 10 mM NaCl (Sigma-Aldrich), 0.15 mM $CaCl_2$ (Sigma-Aldrich), 10 mM HEPES (Fisher) and 10 mM D- glucose (Gibco). The pipettes to patch on the presynaptic cell were filled with internal solution containing 95 mM K-methysulfonate, 4 mM MgCl and 10 mM HEPES. The pH of all internal solutions was adjusted to 7.2 - 7.3 using CsOH (Sigma-Aldrich) or KOH (Sigma-Aldrich) and the osmolarity was adjusted to 230 - 240 mOsml l^{-1}. Pipette resistance in the bath was 3-5 MΩ. Cells were observed using bright field illumination through 10X and 40X objectives. The electrodes were visually guided to the cell of interest using motorized micromanipulators. Images were captured using a cooled Cascade II camera mounted on a side port of the microscope and stored using Image Pro 6.2 software. The exposure time was set to 50 ms and movies were acquired at a rate of 1 image/min. Brightness and contrast were optimized to enable proper observation of the pipette-cell contact during approach and seal formation. Seal formation was achieved by maintaining a high positive pressure in the pipette while approaching the cell and then suddenly switching to negative pressure once the membrane of the cell deflects due to the presence of the pipette. Whole-cell recording was first established on one of the neurons in the population below (postsynaptic cell), then the second pipette was sealed to the neuron in the population above (the presynaptic cell). Once in the whole cell recording mode, the presynaptic cell was switched to current clamp for recording of spontaneous action potentials, while the postsynaptic cell stayed in voltage clamp at a holding potential of -70 mV for recording of excitatory (downward peaks) or 0 mV for recording of inhibitory (upward peaks) postsynaptic activity. Patch-clamp recordings were performed using Axopatch-200A and -200B amplifiers (Axon Instruments). Membrane current and Voltage were digitized via an USB-6218 (National Instruments) coupled to a personal computer running WinWCP V4.7.3 software (from the

University of Strathclyde Faculty of Science). WinWCP controlled the electrical stimuli provided. The signals were filtered at 5 kHz through the amplifier and sampled at 10 KHz. Pre and postsynaptic traces were continuously recorded. The paired recording data was exported as a text file for offline analysis.

Data analysis. Matlab was used to analyze the acquired image stacks as well as the paired recording traces. The total length of the filaments pulled was measured. The paired recordings were divided in intervals with a linear background. A background line was fitted and subtracted and a threshold voltage (for the presynaptic trace, 50 mV) or current (postsynaptic trace, -40 pA) was selected. Peaks in the pre- and post- synaptic activity were detected. Spike triggered activity of ten consecutive traces was plotted; the peak of every action potential was set at zero and the simultaneous postsynaptic trace was aligned. The delay between the onset of the action potential and every postsynaptic peak was calculated within an interval of ± 100 ms to allow detecting events longer than monosynaptic activity (~5ms) and as much as ~3 synaptic delays apart (~20 ms each) since the probability of observing longer latencies is very low [284]. The counts before and after the onset of the action potential were treated as categorical data and differences were assessed for 95% confidence interval using Wilson's method following procedures in [289].The counts after the onset of the action potential in the populations connected were compared to those of the not connected neurons and differences were accepted as significant at $p<0.05$. Statistical significance assessed using Pearson's chi-square test [290] for categorical data as suggested by procedures in [289].

Chapter 7. Conclusions

Mechanical cues are a regulatory parameter that influences the cell behaviour by eliciting a range of physiological, biochemical and electrical responses. This dissertation has explored the influence of local mechanical stimulation in the activity of cells *in-vitro*. We applied localized mechanical stimuli to individual osteoblasts using AFM as a model to study microinjury. We examined the ability of individual osteoblasts to respond to mechanical stimulation. The applied force load was varied and resulted in either membrane deformation or in membrane penetration and micro-injury and the changes in [Ca 2+]i were analyzed. We have discovered that cells respond qualitatively differently to forces inducing membrane deformation only, than to forces resulting in membrane microinjury. Upon cyclic membrane stimulation, we identified refractory periods during which the responses to subsequent mechanical stimulations were either absent or diminished in amplitude. This is significant, since it was previously shown, that macroscopic mechanical loading of bone should be performed as a series of repeated loading periods separated by the periods of rest to induce a potent osteogenic response [291–293]. Importantly, our data demonstrate that Ca2+ responses to local membrane deformation exhibit threshold properties when micro-injury is induced. We proposed that intracellular Ca2+ acts as an integrating signal that increases until it reaches the threshold Ca2+ concentration necessary to induce global Ca2+ response. From our results and others, we suggest that cell sensitivity to membrane deformation is related to a combined effect of: the extent of the membrane area deformed and the duration of the deformation. To confirm this hypothesis, systematic exploration of the influence of a long duration stimulation or a stimulation with a greater horizontal membrane involvement could be useful. Taken together, our study provides new insights into the complex dynamics of cellular responses to mechanical stimulation, which is important for better understanding the mechanisms of mechanical loading-induced bone formation, as well as micro-damage induced bone remodeling.

We also investigated the influence of mechanical cues in the initiation, growth and extension and connection of functional neuronal processes for assembly of neuronal networks. We developed a platform to optimally perform these experiments and we now have instrumentation reliability allowing experiments to be carried out routinely and explore potential biological factors that lead to a strong, mature and stable artificial connection. We investigated the maximum rate at which the mechanically-formed neurites

could be pulled while maintaining structural integrity. The neurites typically supported elongations of up to lengths >840 μm at an average speed of 20 ± 10 μm/min. Such a high growth agrees with maximum values found in the literature for stretch growth [128] and is remarkable considering that the maximum growth rate of neurons in a developing human fetus is ~ 0.8 μm/min [279]. The formation of a new connection was promoted by adhesion of the PDL-bead with another neuron. We found that maintaining the bead in contact at the new site for one hour was sufficient to create a mechanically stable connection for more than 24 hours. Using an AFM tip to pull the PDL-bead allowed the development of robust protocols for successful initiation of an adhesive contact and brought understanding to the details of the pulling process. Using techniques accessible to almost all laboratories, following a similar process as the protocols established using AFM, we developed a powerful and reliable method whereby the bead was temporarily fixed and manipulated by suction at the tip of a micropipette mounted on a micromanipulator. The bead could then be readily released at the site of contact upon attachment. To assess the functionality of the newly created connection paired whole-cell patch clamp recordings were performed. Firing of one neuron in the population where the filament was initiatied, induced postsynaptic activity of a polysynaptic nature in at least one of the neurons in the neuronal population to which the filament was connected. In a fraction of the experiments, postsynaptic currents are correlated with the presynaptic action potentials. To our knowledge, this is the first time that a functional connection between separate populations of neurons is induced by chemical-mechanical micromanipulation.

Both bone cells and neurons contain built-in mechanosensitive mechanisms. Along this thesis it has become evident while bone cells are actually designed to detect mechanical forces and are even thought to be individual mechanotransducers [250,255], neurons are not, though their growth cones possess stretch-sensitive ion channels that mediate their motility [294].

Mechanical cues affect growth and differentiation in both types of cells. Bone cell activity and differentiation is determined by the mechanical stimulation that the cells are subject to. [295,296]. Microgravity has been shown to affect osteoclastogenesis [295]. In the case of neurons, during development, they send filopodia out to sense their environment and the mechanical forces afffect migration and differentiation [281]. It has been shown that uniaxial mechanical stimulation induces differentiation of filopodia into axons and dendrites in a directed manner [129,211,297].

We have mentioned the fact that Ca^{2+} is one of the initial responses to mechanical stimulation in bone cells and many studies including ours haive shown that in the absence of extracellular Ca^{2+}, the cellular response is inhibited [150,298,299]. In neurons, axotomy disrupts the membrane and exposes the axon's interior to external ionic conentrations. The entrance of calcium into an axon is necessary for the formation of a new growth cone [269]. Thus, calcium influx is required to induce recovery after mechanical insult.

Microinjury in bone is an important process in the regulation of bone turnover and strength [252]. We have explored some of the mechanisms in which microinjury is sensed by bone cells. In studies not presented in this thesis, we have analyzed the axonal resistance to local mechanical compression by AFM. We have shown that neurons from the CNS are more sensitive than those of the peripheral NS and that if affected by a local compression of high force and long duration, the axon will degenerate and the cell will irrevocably die [210]. In vivo, peripheral neurons that suffer an injury will generally not reform their previous connections, presumably due to the prohibitive chemical environment of the mature body and also the complex architecture of neural connections. This is in marked contrast to the considerable powers of recovery of injured bone.

Chapter 8. Outlook

Although the study of the mechanical properties of the cell is useful and provides certain insights, it does not provide the whole picture. Throughout this dissertation it has become clear that mechanical stimulation influences cells in many different ways.

In Chapter 5 we proposed that cell sensitivity to membrane deformation is related to a combined effect of: the extent of the membrane area deformed and the duration of the deformation. More systematic analysis of the influence of these parameters would enable better understanding of the elements involved in the mechanotransduction of the Ca^{2+} response. In addition to this, other mechanisms of mechanotransduction (such as integrin receptors) could be investigated.

Our studies were limited to the effect of mechanical stimulation on the Ca^{2+} response of a single cell. Studies have shown that this response can be propagated when the cells are physically connected [300]. Some of our group's experiments (not included in this thesis) suggest that the response can be evoked even in cells that are **not** physically connected. We have thought the propagation could occur by the diffusion of some released molecule through the media. It would be interesting to better understand whether and how this mechanism of communication arises.

Following the methods developed for the extension of neurites, measurement and characterization of the forces experienced by the filament under extension and during retraction could lead to a better understanding of the viscoelastic properties of the filament itself. It would also be interesting to better understand how is it that the structural elements present in the naturally grown processes come to be present in the pulled neurite. Does this happen overnight? Do these structural elements grow as fast as we pull? What is the timing of the synapse formation?

This method presents a phenomenal platform for studies related to synapse formation and has the potential application to be a drug discovery platform for neurodegenerative diseases related to synaptic malfunction such as Alzheimer's disease [301].

I suggest that it would be interesting to culture neurons *in-vitro*, perform axotomy in an axon following established procedures, [269] and following recovery, try to reconnect the axotomized neuron to another cell.

An obvious future direction for the neural rewiring work is in vivo implementation. One possible initial test platform would be to try to ablate and re-wire neuronal connections in the optic nerve, which is relatively easy to access. Alternately a system in a simple animal could be used as a first proof of principle, such as the tongue of the aplysia sea slug which is controlled by only two neurons. It would be interesting to see whether this approach could work to reconnect one of the neurons after transection of the other. Further into the future, these developments could have impact in therapies for regeneration traumatic brain injury and other CNS disorders.

Appendix A. Whole cell patch clamp equivalent circuit.

Now that we have an understanding of the electronics of the cell membrane, we can proceed with the schematics of the equivalent circuit for a cell under whole cell patch clamp conditions [302].

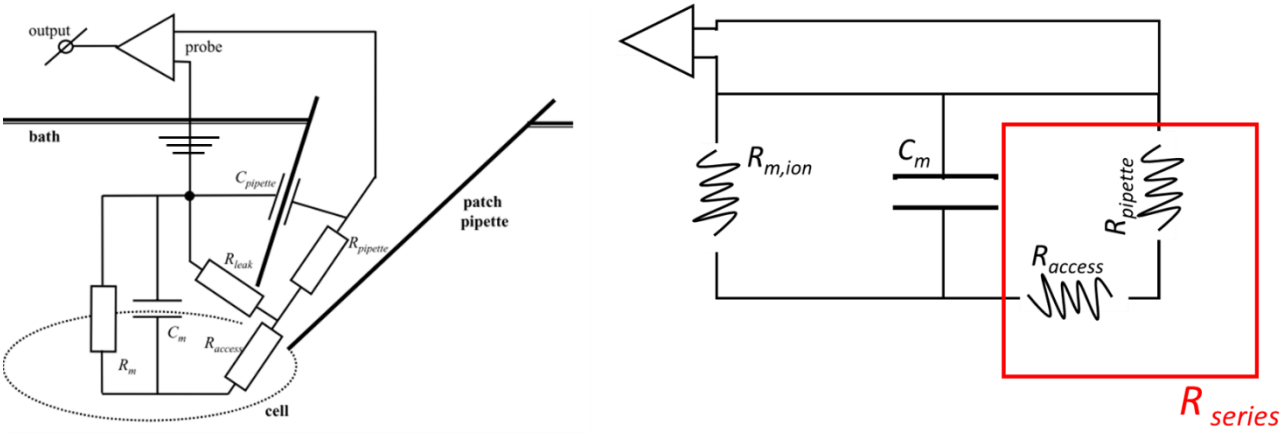

(Figure A1.) Equivalent circuit for the whole cell configuration and its simplification.

In this circuit, important new features appear which merit introduction and can greatly simplify the equivalent circuit for the above configuration:

Pipette resistance (R pipette): The small size of the tip of the micropipette creates a resistance to the current. Typical values for whole cell configuration range between 3-10MΩ.

Pipette capacitance (C pipette): The pipette glass is an insulator between the bath solution and the pipette solution, thus, it forms a capacitor. This capacitance is ideally very small due to the glass thickness and for the purpose of our recordings has been neglected.

Leak resistance (R leak): From time to time, the pipette inflicts damage the plasma membrane while sealing and opening the patch. This effectively creates a "short circuit" from the cytosol to ground. If this resistance is low (i.e., the hole in the membrane is large), then there will be a considerable load on the membrane potential that the cell might not be able to sustain and will end up dying. Damage must be kept to a minimum, in order to maximize this resistance.

References

[1] O. P. Hamill and B. Martinac, Physiol Rev **81**, 685 (2001).

[2] D. W. Thompson, *On Growth and Form* (London: Cambridge University Press, Cambridge [Eng.] University, 1917).

[3] Y.-K. Wang and C. S. Chen, Journal of Cellular and Molecular Medicine **17**, 823 (2013).

[4] D. E. Discher, D. J. Mooney, and P. W. Zandstra, Science (New York, N.Y.) **324**, 1673 (2009).

[5] N. Basso and J. N. M. Heersche, Bone **30**, 347 (2002).

[6] S. Judex, X. Lei, D. Han, and C. Rubin, Journal of Biomechanics **40**, 1333 (2007).

[7] A. Stuart, *Three Lectures on Muscular Motion, Read Before the Royal Society in the Year 1738 (Croonean Lectures).* (1739).

[8] A. E. Pelling and M. A. Horton, Pflügers Archiv : European Journal of Physiology **456**, 3 (2008).

[9] D. Erickson, S. Mandal, A. H. J. Yang, and B. Cordovez, Microfluidics and Nanofluidics **4**, 33 (2008).

[10] a Fuhrmann, J. R. Staunton, V. Nandakumar, N. Banyai, P. C. W. Davies, and R. Ros, Physical Biology **8**, 015007 (2011).

[11] Y.-W. Chiou, H.-K. Lin, M.-J. Tang, H.-H. Lin, and M.-L. Yeh, PloS One **8**, e77384 (2013).

[12] M. Li, L. Liu, N. Xi, Y. Wang, Z. Dong, X. Xiao, and W. Zhang, Science China. Life Sciences **55**, 968 (2012).

[13] Y.-R. Liou, W. Torng, Y.-C. Kao, K.-B. Sung, C.-H. Lee, and P.-L. Kuo, PloS One **9**, e89767 (2014).

[14] J. Condeelis and J. E. Segall, Nature Reviews. Cancer **3**, 921 (2003).

[15] A. Liedert, D. Kaspar, R. Blakytny, L. Claes, and A. Ignatius, Biochemical and Biophysical Research Communications **349**, 1 (2006).

[16] T. K. Berdyyeva, C. D. Woodworth, and I. Sokolov, Physics in Medicine and Biology **50**, 81 (2005).

[17] P. Pascoal, D. Kosanic, M. Gjoni, and H. Vogel, Lab on a Chip **10**, 2235 (2010).

[18] P. Lamoureux, S. Heidemann, and K. E. Miller, Journal of Visualized Experiments : JoVE 3 (2011).

[19] D. Bray, Developmental Biology **102**, 379 (1984).

[20] Y. Wang, Y. Yang, L. Yan, S. Y. Kwok, W. Li, Z. Wang, X. Zhu, G. Zhu, W. Zhang, X. Chen, and P. Shi, Nature Communications **5**, 4466 (2014).

[21] C. M. Cuerrier, R. Lebel, and M. Grandbois, Biochemical and Biophysical Research Communications **355**, 632 (2007).

[22] A. Vaziri and M. R. K. Mofrad, Journal of Biomechanics **40**, 2053 (2007).

[23] K. V Upadhye, J. E. Candiello, L. a Davidson, and H. Lin, Cellular and Molecular Bioengineering **4**, 270 (2011).

[24] G. Binnig and C. F. Quate, Physical Review Letters **56**, 930 (1986).

[25] N. V Bukoreshtliev, K. Haase, and A. E. Pelling, Cell and Tissue Research **352**, 77 (2013).

[26] J. Howard, *Mechanics of Motor Proteins and the Cytoskeleton* (Sinauer Associates, Incorporated, 2001), p. 367.

[27] B. Alberts, A. Johnson, J. Lewis, M. Raff, K. Roberts, and P. Walter, *Molecular Biology of the Cell*, 4th ed. (Garland Science, 2002).

[28] N. Caille, O. Thoumine, Y. Tardy, and J.-J. Meister, Journal of Biomechanics **35**, 177 (2002).

[29] S. B. Zimmerman and A. P. Minton, 27 (1993).

[30] D. A. Fletcher and R. D. Mullins, Nature **463**, 485 (2010).

[31] H. Delanoë-Ayari, R. Al Kurdi, M. Vallade, D. Gulino-Debrac, and D. Riveline, Proceedings of the National Academy of Sciences of the United States of America **101**, 2229 (2004).

[32] J. L. Ross, M. Y. Ali, and D. M. Warshaw, Current Opinion in Cell Biology **20**, 41 (2008).

[33] R. De, A. Zemel, and S. A. Safran, Methods in Cell Biology **98**, 143 (2010).

[34] K. Haase and A. E. Pelling, Communicative & Integrative Biology **6**, e26714 (2013).

[35] K. Haase and A. E. Pelling, Cytoskeleton (Hoboken, N.J.) **70**, 494 (2013).

[36] H. Lodish, A. Berk, S. L. Zipursky, P. Matsudaira, D. Baltimore, and J. Darnell, (2000).

[37] D. S. Fudge, K. H. Gardner, V. T. Forsyth, C. Riekel, and J. M. Gosline, Biophysical Journal **85**, 2015 (2003).

[38] H. de Forges, A. Bouissou, and F. Perez, The International Journal of Biochemistry & Cell Biology **44**, 266 (2012).

[39] F. Pampaloni and E.-L. Florin, Trends in Biotechnology **26**, 302 (2008).

[40] C. P. Brangwynne, F. C. MacKintosh, S. Kumar, N. A. Geisse, J. Talbot, L. Mahadevan, K. K. Parker, D. E. Ingber, and D. A. Weitz, The Journal of Cell Biology **173**, 733 (2006).

[41] S. R. Heidemann and D. Wirtz, Trends in Cell Biology **14**, 160 (2004).

[42] N. X. Chen, K. D. Ryder, F. M. Pavalko, C. H. Turner, D. B. Burr, J. Qiu, and R. L. Duncan, American Journal of Physiology Cell Physiology **278**, C989 (2000).

[43] E. Schordan, S. Welsch, S. Rothhut, A. Lambert, M. Barthelmebs, J.-J. Helwig, and T. Massfelder, Journal of the American Society of Nephrology : JASN **15**, 3016 (2004).

[44] A. Goulet-Hanssens, K. Lai Wing Sun, T. E. Kennedy, and C. J. Barrett, Biomacromolecules **13**, 2958 (2012).

[45] K. Haase, Z. Al-Rekabi, and A. E. Pelling, Progress in Molecular Biology and Translational Science **126**, 103 (2014).

[46] Y. Sugawara, R. Ando, H. Kamioka, Y. Ishihara, S. A. Murshid, K. Hashimoto, N. Kataoka, K. Tsujioka, F. Kajiya, T. Yamashiro, and T. Takano-Yamamoto, Bone **43**, 19 (2008).

[47] F. R. Bueno and S. B. Shah, Tissue Engineering. Part B, Reviews **14**, 219 (2008).

[48] S. Menon and K. A. Beningo, PloS One **6**, e17277 (2011).

[49] E. Simard, J. J. Kovacs, W. E. Miller, J. Kim, M. Grandbois, and R. J. Lefkowitz, PloS One **8**, e80532 (2013).

[50] M. L. Rodriguez, P. J. McGarry, and N. J. Sniadecki, Applied Mechanics Reviews **65**, 60801 (2013).

[51] S. S. K. J. Van Vliet, G. Bao, Acta Mater., **51**, 5881 (2003).

[52] T. D. Brown, Journal of Biomechanics **33**, 3 (2000).

[53] D. B. Jones, H. Nolte, J.-G. Scholübbers, E. Turner, and D. Veltel, Biomaterials **12**, 101 (1991).

[54] S. Higgins, J. S. Lee, L. Ha, and J. Y. Lim, BioResearch Open Access **2**, 212 (2013).

[55] M. D. Frame and I. H. Sarelius, Microcirculation (New York, N.Y. : 1994) **2**, 377 (1995).

[56] E. M. Redmond, P. A. Cahill, and J. V Sitzmann, In Vitro Cellular & Developmental Biology. Animal **31**, 601 (1995).

[57] G. Helmlinger, B. C. Berk, and R. M. Nerem, Journal of Vascular Research **33**, 360 (n.d.).

[58] C. R. Jacobs, C. E. Yellowley, B. R. Davis, Z. Zhou, J. M. Cimbala, and H. J. Donahue, Journal of Biomechanics **31**, 969 (1998).

[59] C. T. Hung, F. D. Allen, S. R. Pollack, and C. T. Brighton, Journal of Biomechanics **29**, 1411 (1996).

[60] T. Donahue, T. Haut, C. Yellowley, H. Donahue, and C. Jacobs, Journal of Biomechanics **36**, 1363 (2003).

[61] C. T. Brighton, J. R. Fisher, S. E. Levine, J. R. Corsetti, T. Reilly, A. S. Landsman, J. L. Williams, and L. E. Thibault, The Journal of Bone and Joint Surgery. American Volume **78**, 1337 (1996).

[62] P. M. Freeman, R. N. Natarajan, J. H. Kimura, and T. P. Andriacchi, Journal of Orthopaedic Research : Official Publication of the Orthopaedic Research Society **12**, 311 (1994).

[63] H. Ozawa, K. Imamura, E. Abe, N. Takahashi, T. Hiraide, Y. Shibasaki, T. Fukuhara, and T. Suda, Journal of Cellular Physiology **142**, 177 (1990).

[64] J. A. Ryan, E. A. Eisner, G. DuRaine, Z. You, and A. H. Reddi, Journal of Tissue Engineering and Regenerative Medicine **3**, 107 (2009).

[65] X. L. Lu and V. C. Mow, Medicine and Science in Sports and Exercise **40**, 193 (2008).

[66] B. J. Pfister, A. Iwata, D. F. Meaney, and D. H. Smith, The Journal of Neuroscience : The Official Journal of the Society for Neuroscience **24**, 7978 (2004).

[67] B. J. Pfister, D. P. Bonislawski, D. H. Smith, and A. S. Cohen, FEBS Letters **580**, 3525 (2006).

[68] O. Thoumine and A. Ott, Journal of Cell Science **110 (Pt 1**, 2109 (1997).

[69] N. D. Leipzig and K. A. K. A. Athanasiou, Journal of Biomechanics **38**, 77 (2005).

[70] K. . Van Vliet, G. Bao, and S. Suresh, Acta Materialia **51**, 5881 (2003).

[71] A. Ashkin and J. M. Dziedzic, Science (New York, N.Y.) **235**, 1517 (1987).

[72] A. Ashkin, J. M. Dziedzic, and T. Yamane, Nature **330**, 769 (1987).

[73] C. T. Lim, E. H. Zhou, A. Li, S. R. K. Vedula, and H. X. Fu, Materials Science and Engineering: C **26**, 1278 (2006).

[74] S. M. Block, Nature **360**, 493 (1992).

[75] K. Svoboda and S. M. Block, Annual Review of Biophysics and Biomolecular Structure **23**, 247 (1994).

[76] K. C. Neuman and S. M. Block, The Review of Scientific Instruments **75**, 2787 (2004).

[77] P. H. Chia, B. Chen, P. Li, M. K. Rosen, and K. Shen, Cell **156**, 208 (2014).

[78] D. McGloin, Philosophical Transactions. Series A, Mathematical, Physical, and Engineering Sciences **364**, 3521 (2006).

[79] J. Guck, R. Ananthakrishnan, H. Mahmood, T. J. Moon, C. C. Cunningham, and J. Käs, Biophysical Journal **81**, 767 (2001).

[80] S. Suresh, J. Spatz, J. P. Mills, A. Micoulet, M. Dao, C. T. Lim, M. Beil, and T. Seufferlein, Acta Biomaterialia **1**, 15 (2005).

[81] J. Guck, S. Schinkinger, B. Lincoln, F. Wottawah, S. Ebert, M. Romeyke, D. Lenz, H. M. Erickson, R. Ananthakrishnan, D. Mitchell, J. Käs, S. Ulvick, and C. Bilby, Biophysical Journal **88**, 3689 (2005).

[82] L. M. Walker, Å. Holm, L. Cooling, L. Maxwell, Å. Öberg, T. Sundqvist, and A. J. El Haj, FEBS Letters **459**, 39 (1999).

[83] I. Titushkin and M. Cho, Biophysical Journal **90**, 2582 (2006).

[84] C. Bustamante, Z. Bryant, and S. B. Smith, Nature **421**, 423 (2003).

[85] S. M. Block, L. S. Goldstein, and B. J. Schnapp, Nature **348**, 348 (1990).

[86] S. Suresh, C. T. Lim, and M. Dao, in *Advances in Bioengineering* (ASME, 2003), pp. 357–357.

[87] M. Dao, C. T. Lim, and S. Suresh, Journal of the Mechanics and Physics of Solids **51**, 2259 (2003).

[88] A. Ehrlicher, T. Betz, B. Stuhrmann, D. Koch, V. Milner, M. G. Raizen, and J. Kas, Proceedings of the National Academy of Sciences of the United States of America **99**, 16024 (2002).

[89] I. Guido, M. S. Jaeger, and C. Duschl, European Biophysics Journal : EBJ **40**, 281 (2011).

[90] J. Chen, M. Abdelgawad, L. Yu, N. Shakiba, W.-Y. Chien, Z. Lu, W. B. Geddie, M. A. S. Jewett, and Y. Sun, in *2011 IEEE 24th International Conference on Micro Electro Mechanical Systems* (IEEE, 2011), pp. 1119–1122.

[91] M. Kopycinska-Müller, R. H. Geiss, and D. C. Hurley, Ultramicroscopy **106**, 466 (2006).

[92] A. Bussonnière, Y. Miron, M. Baudoin, O. Bou Matar, M. Grandbois, P. Charette, and A. Renaudin, Lab on a Chip **14**, 3556 (2014).

[93] O. Feinerman, A. Rotem, and E. Moses, Nature Physics **4**, 967 (2008).

[94] A. R. Bausch, F. Ziemann, A. A. Boulbitch, K. Jacobson, and E. Sackmann, Biophysical Journal **75**, 2038 (1998).

[95] N. Wang and D. E. Ingber, Biochemistry and Cell Biology = Biochimie et Biologie Cellulaire **73**, 327 (n.d.).

[96] D.-H. Kim, P. K. Wong, J. Park, A. Levchenko, and Y. Sun, Annual Review of Biomedical Engineering **11**, 203 (2009).

[97] P. Gehr, J. D. Brain, S. B. Bloom, and P. A. Valberg, Nature **302**, 336 (n.d.).

[98] P. A. Valberg, Science (New York, N.Y.) **224**, 513 (1984).

[99] N. Wang, J. P. Butler, and D. E. Ingber, Science (New York, N.Y.) **260**, 1124 (1993).

[100] B. D. Matthews, D. R. Overby, F. J. Alenghat, J. Karavitis, Y. Numaguchi, P. G. Allen, and D. E. Ingber, Biochemical and Biophysical Research Communications **313**, 758 (2004).

[101] M. a Hemphill, B. E. Dabiri, S. Gabriele, L. Kerscher, C. Franck, J. a Goss, P. W. Alford, and K. K. Parker, PloS One **6**, e22899 (2011).

[102] T. R. Strick, J. F. Allemand, D. Bensimon, A. Bensimon, and V. Croquette, Science (New York, N.Y.) **271**, 1835 (1996).

[103] V. Heinrich and R. E. Waugh, Annals of Biomedical Engineering **24**, 595 (n.d.).

[104] R. J. Mannix, S. Kumar, F. Cassiola, M. Montoya-Zavala, E. Feinstein, M. Prentiss, and D. E. Ingber, Nature Nanotechnology **3**, 36 (2008).

[105] F. H. C. Crick, Experimental Cell Research **1**, 505 (1950).

[106] B. G. Hosu, M. Sun, F. Marga, M. Grandbois, and G. Forgacs, Physical Biology **4**, 67 (2007).

[107] D. E. Ingber, Progress in Biophysics and Molecular Biology **97**, 163 (2008).

[108] S. Nakamura and Y. Hiramoto, Development, Growth and Differentiation **20**, 317 (1978).

[109] W. R. Trickey, F. P. T. Baaijens, T. A. Laursen, L. G. Alexopoulos, and F. Guilak, Journal of Biomechanics **39**, 78 (2006).

[110] I. Obataya, C. Nakamura, S. Han, N. Nakamura, and J. Miyake, Biosensors & Bioelectronics **20**, 1652 (2005).

[111] E. A. Evans, Biophysical Journal **13**, 941 (1973).

[112] J. Y. Shao and R. M. Hochmuth, Biophysical Journal **71**, 2892 (1996).

[113] Y.-S. Chu, O. Eder, W. A. Thomas, I. Simcha, F. Pincet, A. Ben-Ze'ev, E. Perez, J. P. Thiery, and S. Dufour, The Journal of Biological Chemistry **281**, 2901 (2006).

[114] E. Neher and B. Sakmann, Scientific American **266**, 44 (1992).

[115] M. B. Jackson, Current Protocols in Neuroscience / Editorial Board, Jacqueline N. Crawley ... [et Al.] **Chapter 6**, Unit 6.6 (2001).

[116] G. Stuart, Current Protocols in Neuroscience / Editorial Board, Jacqueline N. Crawley ... [et Al.] **Chapter 6**, Unit 6.7 (2001).

[117] T. W. Secomb, Cell Biophysics **18**, 231 (1991).

[118] J. Z. Wu, W. Herzog, and M. Epstein, Journal of Biomechanics **32**, 563 (1999).

[119] J. Z. Wu and W. Herzog, Annals of Biomedical Engineering **28**, 318 (2000).

[120] M. A. Haider and F. Guilak, Journal of Biomechanical Engineering **122**, 236 (2000).

[121] B. Daily, E. L. Elson, and G. I. Zahalak, Biophysical Journal **45**, 671 (1984).

[122] S. Felder and E. L. Elson, The Journal of Cell Biology **111**, 2513 (1990).

[123] D. Shin and K. Athanasiou, Journal of Orthopaedic Research : Official Publication of the Orthopaedic Research Society **17**, 880 (1999).

[124] G. I. Zahalak, W. B. McConnaughey, and E. L. Elson, Journal of Biomechanical Engineering **112**, 283 (1990).

[125] E. J. Koay, A. C. Shieh, and K. A. Athanasiou, Journal of Biomechanical Engineering **125**, 334 (2003).

[126] G. T. Charras, B. a Williams, S. M. Sims, and M. a Horton, Biophysical Journal **87**, 2870 (2004).

[127] K. Hayakawa, H. Tatsumi, and M. Sokabe, Journal of Cell Science **121**, 496 (2008).

[128] P. Lamoureux, R. E. Buxbaum, and S. R. Heidemann, Journal of Cell Science **111 (Pt 2**, 3245 (1998).

[129] P. Lamoureux, G. Ruthel, R. E. Buxbaum, and S. R. Heidemann, The Journal of Cell Biology **159**, 499 (2002).

[130] M. O'Toole, P. Lamoureux, and K. E. Miller, Biophysical Journal **94**, 2610 (2008).

[131] J. Krayer, S. Tatic-Lucic, and S. Neti, Sensors and Actuators B: Chemical **118**, 20 (2006).

[132] P. P. Lehenkari, G. T. Charras, A. Nykänen, and M. A. Horton, Ultramicroscopy **82**, 289 (2000).

[133] K. D. Costa, Methods in Molecular Biology (Clifton, N.J.) **319**, 331 (2006).

[134] J. K. Hörber, W. Häberle, F. Ohnesorge, G. Binnig, H. G. Liebich, C. P. Czerny, H. Mahnel, and A. Mayr, Scanning Microscopy **6**, 919 (1992).

[135] T. Fukuma, M. J. Higgins, and S. P. Jarvis, Biophysical Journal **92**, 3603 (2007).

[136] Y. F. Dufrêne, D. Martínez-Martín, I. Medalsy, D. Alsteens, and D. J. Müller, Nature Methods **10**, 847 (2013).

[137] D. J. Muller, J. Helenius, D. Alsteens, and Y. F. Dufrene, Nat Chem Biol **5**, 383 (2009).

[138] M. Radmacher, J. P. Cleveland, M. Fritz, H. G. Hansma, and P. K. Hansma, Biophysical Journal **66**, 2159 (1994).

[139] E. Florin, V. Moy, and H. Gaub, Science **264**, 415 (1994).

[140] Y. F. Dufrêne and A. E. Pelling, Nanoscale **5**, 4094 (2013).

[141] C. Heu, A. Berquand, C. Elie-caille, and L. Nicod, Journal of Structural Biology **178**, 1 (2012).

[142] C. M. Cuerrier, A. Gagner, R. Lebel, F. Gobeil, and M. Grandbois, Journal of Molecular Recognition : JMR **22**, 389 (2009).

[143] E. A-Hassan, W. F. Heinz, M. D. Antonik, N. P. D'Costa, S. Nageswaran, C. a Schoenenberger, and J. H. Hoh, Biophysical Journal **74**, 1564 (1998).

[144] J. Wang and A. E. Pelling, Medical & Biological Engineering & Computing **48**, 1015 (2010).

[145] C. M. Cuerrier, M. Benoit, G. Guillemette, F. Gobeil, and M. Grandbois, Pflügers Archiv : European Journal of Physiology **457**, 1361 (2009).

[146] A. E. Pelling, F. S. Veraitch, C. P.-K. Chu, C. Mason, and M. A. Horton, Cell Motility and the Cytoskeleton **66**, 409 (2009).

[147] Z. Al-Rekabi, K. Haase, and A. E. Pelling, Experimental Cell Research **322**, 21 (2014).

[148] M. H. Magdesian, F. S. Sanchez, M. Lopez, P. Thostrup, N. Durisic, W. Belkaid, D. Liazoghli, P. Grütter, and D. R. Colman, Biophysical Journal **103**, 405 (2012).

[149] Y. R. Silberberg, A. E. Pelling, G. E. Yakubov, W. R. Crum, D. J. Hawkes, and M. A. Horton, 1335 (2008).

[150] G. T. Charras and M. a Horton, Biophysical Journal **82**, 2970 (2002).

[151] G. T. Charras, B. a Williams, S. M. Sims, and M. a Horton, Biophysical Journal **87**, 2870 (2004).

[152] J. G. McGarry, P. Maguire, V. a Campbell, B. C. O'Connell, P. J. Prendergast, and S. P. Jarvis, Journal of Orthopaedic Research : Official Publication of the Orthopaedic Research Society **26**, 513 (2008).

[153] P. Maguire, J. McGarry, V. Campbell, B. O'Connell, P. Prendergast, and S. Jarvis, Microscopy and Microanalysis **11**, 952 (2005).

[154] L. Guolla, M. Bertrand, K. Haase, and A. E. Pelling, Journal of Cell Science **125**, 603 (2012).

[155] Y. R. Silberberg, L. Guolla, A. E. Pelling, N. Signalling, and M. Hall, 1 (2009).

[156] T. Osada, H. Uehara, H. Kim, and A. Ikai, Journal of Nanobiotechnology **1**, 2 (2003).

[157] C. M. Cuerrier, R. Lebel, and M. Grandbois, Biochemical and Biophysical Research Communications **355**, 632 (2007).

[158] C. T. Lim, E. H. Zhou, and S. T. Quek, Journal of Biomechanics **39**, 195 (2006).

[159] G. Mitchell, C.-A. Lamontagne, R. Lebel, M. Grandbois, and F. Malouin, Biochemical and Biophysical Research Communications **364**, 595 (2007).

[160] M. Kocun, M. Grandbois, and L. A. Cuccia, Colloids and Surfaces. B, Biointerfaces **82**, 470 (2011).

[161] M. Grandbois, W. Dettmann, M. Benoit, and H. E. Gaub, The Journal of Histochemistry and Cytochemistry : Official Journal of the Histochemistry Society **48**, 719 (2000).

[162] M. Grandbois, M. Beyer, M. Rief, H. Clausen-Schaumann, and H. Gaub, Science (New York, N.Y.) **283**, 1727 (1999).

[163] B. D. Sattin, A. E. Pelling, and M. C. Goh, Nucleic Acids Research **32**, 4876 (2004).

[164] M. Sun, J. S. Graham, B. Hegedüs, F. Marga, Y. Zhang, G. Forgacs, and M. Grandbois, Biophysical Journal **89**, 4320 (2005).

[165] K. He, X. Shi, X. Zhang, S. Dang, X. Ma, F. Liu, M. Xu, Z. Lv, D. Han, X. Fang, and Y. Zhang, Cardiovascular Research **92**, 39 (2011).

[166] K. A. Addae-Mensah and J. P. Wikswo, Experimental Biology and Medicine (Maywood, N.J.) **233**, 792 (2008).

[167] D. J. Muller and Y. F. Dufrêne, (2008).

[168] D. J. Muller, Imaging 7986 (2008).

[169] Y. F. Dufrene, E. Evans, A. Engel, J. Helenius, H. E. Gaub, and D. J. Muller, Nat Methods **8**, 123 (2011).

[170] G. U. Lee, D. A. Kidwell, and R. J. Colton, Langmuir **10**, 354 (1994).

[171] B. B. Pittenger, N. Erina, and C. Su, (1993).

[172] T. Aoki, M. Hiroshima, K. Kitamura, M. Tokunaga, and T. Yanagida, Ultramicroscopy **70**, 45 (1997).

[173] V. Lulevich, Y.-P. Shih, S. H. Lo, and G.-Y. Liu, The Journal of Physical Chemistry. B **113**, 6511 (2009).

[174] Y. J. Oh, W. Jo, J. Lim, S. Park, Y. S. Kim, and Y. Kim, Ultramicroscopy **108**, 1124 (2008).

[175] E. Florin, V. Moy, and H. Gaub, Science **264**, 415 (1994).

[176] W. F. Heinz and J. H. Hoh, Trends in Biotechnology **17**, 143 (1999).

[177] M. Radmacher, Biophysical Journal **64**, 735 (1993).

[178] R. E. Mahaffy, C. K. Shih, F. C. MacKintosh, and J. Käs, Physical Review Letters **85**, 880 (2000).

[179] B. M. J. Puttock, E. G. Thwaite, and C. Scientific, Industrial Research (1969).

[180] A. R. Harris and G. T. Charras, Nanotechnology **22**, 345102 (2011).

[181] K. E. Petersen, Proceedings of the IEEE **70**, 420 (1982).

[182] J. A. Kent, editor, *Kent and Riegel's Handbook of Industrial Chemistry and Biotechnology* (Springer US, Boston, MA, 2007).

[183] E. K. Dimitriadis, F. Horkay, J. Maresca, B. Kachar, and R. S. Chadwick, Biophysical Journal **82**, 2798 (2002).

[184] E. K. Dimitriadis, F. Horkay, J. Maresca, B. Kachar, and R. S. Chadwick, Biophysical Journal **82**, 2798 (2002).

[185] F. Rico, P. Roca-Cusachs, N. Gavara, R. Farré, M. Rotger, and D. Navajas, Physical Review E **72**, 1 (2005).

[186] D. a Fletcher and R. D. Mullins, Nature **463**, 485 (2010).

[187] S. Yamada, D. Wirtz, and S. C. Kuo, Biophysical Journal **78**, 1736 (2000).

[188] M. T. Kim, Thin Solid Films **283**, 12 (1996).

[189] J. Domke and M. Radmacher, Langmuir **14**, 3320 (1998).

[190] B. B. Akhremitchev and G. C. Walker, Langmuir **15**, 5630 (1999).

[191] B. Oommen and K. J. Van Vliet, Thin Solid Films **513**, 235 (2006).

[192] R. Mahaffy, S. Park, E. Gerde, J. Kas, and C. Shih, Biophysical Journal **86**, 1777 (2004).

[193] E. M. Darling, S. Zauscher, J. a Block, and F. Guilak, Biophysical Journal **92**, 1784 (2007).

[194] E. M. D. P. D, S. Z. P. D, and F. G. P. D, Osteoarthritis and Cartilage (2006).

[195] P. Pravincumar, D. L. Bader, and M. M. Knight, PloS One **7**, e43938 (2012).

[196] S. Gupta, F. Carrillo, C. Li, L. Pruitt, and C. Puttlitz, Materials Letters **61**, 448 (2007).

[197] C. Rotsch, K. Jacobson, and M. Radmacher, Proceedings of the National Academy of Sciences of the United States of America **96**, 921 (1999).

[198] S. Nawaz, P. Sánchez, K. Bodensiek, S. Li, M. Simons, and I. A. T. Schaap, PloS One **7**, e45297 (2012).

[199] B. A. Smith, B. Tolloczko, J. G. Martin, and P. Grütter, Biophysical Journal **88**, 2994 (2005).

[200] T. G. Kuznetsova, M. N. Starodubtseva, N. I. Yegorenkov, S. A. Chizhik, and R. I. Zhdanov, Micron (Oxford, England : 1993) **38**, 824 (2007).

[201] K. M. Abdel-Hamid and M. Tymianski, J. Neurosci. **17**, 3538 (1997).

[202] C. Ceccarini and H. Eagle, Proceedings of the National Academy of Sciences **68**, 229 (1971).

[203] G. Bernhardt, A. Dist�che, R. Jaenicke, B. Koch, H.-D. L�demann, and K.-O. Stetter, Applied Microbiology and Biotechnology **28**, 176 (1988).

[204] G. Giordano, S. Hong, E. M. Faustman, and L. G. Costa, Methods in Molecular Biology (Clifton, N.J.) **758**, 171 (2011).

[205] M. E. Morris, J. Leblond, N. Agopyan, and K. Krnjević, Journal of Neurophysiology **65**, 157 (1991).

[206] R. M. Robertson and T. G. a Money, Current Opinion in Neurobiology **22**, 724 (2012).

[207] E. Spedden, D. L. Kaplan, and C. Staii, Physical Biology **10**, 056002 (2013).

[208] A. L. Lucido, F. Suarez Sanchez, P. Thostrup, A. V Kwiatkowski, S. Leal-Ortiz, G. Gopalakrishnan, D. Liazoghli, W. Belkaid, R. B. Lennox, P. Grutter, C. C. Garner, and D. R. Colman, The Journal of Neuroscience : The Official Journal of the Society for Neuroscience **29**, 12449 (2009).

[209] F. Suarez, P. Thostrup, D. Colman, and P. Grutter, Developmental Neurobiology **73**, 98 (2013).

[210] M. H. Magdesian, F. S. Sanchez, M. Lopez, P. Thostrup, N. Durisic, W. Belkaid, D. Liazoghli, P. Grütter, and D. R. Colman, Biophysical Journal **103**, 405 (2012).

[211] D. H. Smith, J. A. Wolf, and D. F. Meaney, Tissue Engineering **7**, 131 (2001).

[212] A. Goulet-Hanssens and C. J. Barrett, Journal of Polymer Science Part A: Polymer Chemistry **51**, 3058 (2013).

[213] J. M. Bélisle, J. P. Correia, P. W. Wiseman, T. E. Kennedy, and S. Costantino, Lab on a Chip **8**, 2164 (2008).

[214] M. Muyskens, Journal of Chemical Education **83**, 765 (2006).

[215] G. G. Stokes, Philosophical Transactions of the Royal Society of London **142**, 463 (1852).

[216] I. C. Ghiran, Methods in Molecular Biology (Clifton, N.J.) **689**, 93 (2011).

[217] P. Ellinger, Biological Reviews **15**, 323 (1940).

[218] E. T. Whittaker, *A History of the Theories of Aether and Electricity from the Age of Descartes to the Close of the Nineteenth Century / by E.T. Whittaker* ... (Longmans, Green [etc., etc.],, London ;, 1910), pp. 1 – 502.

[219] A. L. Hodgkin and A. F. Huxley, 500 (1952).

[220] D. Colquhoun, BMJ (Clinical Research Ed.) **303**, 938 (1991).

[221] O. P. Hamill, A. Marty, E. Neher, B. Sakmann, and F. J. Sigworth, Pflügers Archiv : European Journal of Physiology **391**, 85 (1981).

[222] P. Clamp, (1992).

[223] P. Clamp, (1999).

[224] E. R. Kandel, *Principles of Neural Science* (2000).

[225] B. Hille, (2001).

[226] A. Molleman, (2003).

[227] Sutter Instruments, (2011).

[228] E. W. Weisstein, From MathWorld--A Wolfram Web Resource. (n.d.).

[229] W. Nernst, in *Cell Membrane Permeability and Transport GR Kepner Ed.* (1988), pp. 174–183.

[230] D. E. Goldman, The Journal of General Physiology **27**, 37 (1943).

[231] A. L. Hodgkin and B. Katz, The Journal of Physiology **108**, 37 (1949).

[232] G. M. Hughes and L. Tauc, The Journal of Physiology **197**, 511 (1968).

[233] R. Miles and J.-C. Poncer, Current Opinion in Neurobiology **6**, 387 (1996).

[234] P. Pavlidis and D. V. Madison, J Neurophysiol **81**, 2787 (1999).

[235] D. Debanne, S. Boudkkazi, E. Campanac, R. H. Cudmore, P. Giraud, L. Fronzaroli-Molinieres, E. Carlier, and O. Caillard, Nature Protocols **3**, 1559 (2008).

[236] J. M. Montgomery, P. Pavlidis, and D. V Madison, Neuron **29**, 691 (2001).

[237] D. Stellwagen, E. C. Beattie, J. Y. Seo, and R. C. Malenka, The Journal of Neuroscience : The Official Journal of the Society for Neuroscience **25**, 3219 (2005).

[238] P. Vincent and A. Marty, The Journal of Physiology **494 (Pt 1**, 183 (1996).

[239] R. Shi and J. Whitebone, Journal of Neurophysiology **95**, 3384 (2006).

[240] S. W. Donahue, H. J. Donahue, and C. R. Jacobs, Journal of Biomechanics **36**, 35 (2003).

[241] P. Pascoal, D. Kosanic, M. Gjoni, and H. Vogel, Lab Chip **10**, 2235 (2010).

[242] R. J. Barfoot, K. H. Sheikh, B. R. G. Johnson, J. Colyer, R. E. Miles, L. J. C. Jeuken, R. J. Bushby, and S. D. Evans, Langmuir : The ACS Journal of Surfaces and Colloids **24**, 6827 (2008).

[243] M. Lang, P. Fordyce, and S. Block, Journal of Biology **2**, 6 (2003).

[244] C. T. Rubin, Calcified Tissue International **36 Suppl 1**, S11 (1984).

[245] K. K. Papachroni, D. N. Karatzas, K. a Papavassiliou, E. K. Basdra, and A. G. Papavassiliou, Trends in Molecular Medicine **15**, 208 (2009).

[246] N. Baecker, A. Tomic, C. Mika, A. Gotzmann, P. Platen, R. Gerzer, and M. Heer, Journal of Applied Physiology (Bethesda, Md. : 1985) **95**, 977 (2003).

[247] M. Doblaré, J. M. Garcia, and T. R Eberg, Archives of Physiology and Biochemistry **112**, 83 (2004).

[248] N. Mitsui, N. Suzuki, M. Maeno, M. Yanagisawa, Y. Koyama, K. Otsuka, and N. Shimizu, Life Sciences **78**, 2697 (2006).

[249] C. T. Hung, S. R. Pollack, T. M. Reilly, and C. T. Brighton, Clinical Orthopaedics and Related Research **313**, 256 (1995).

[250] C. H. T. R. L. Duncan, Calcif Tissue Int **57**, 344 (1995).

[251] L. Tang, Z. Lin, and Y. Li, Biochemical and Biophysical Research Communications **344**, 122 (2006).

[252] D. Burr, Osteoporosis International : A Journal Established as Result of Cooperation between the European Foundation for Osteoporosis and the National Osteoporosis Foundation of the USA **14 Suppl 5**, S67 (2003).

[253] E. R. David Burr, Bruce Martin, Mitchell Schafler, Strain (1985).

[254] T. Mashiba, Clinical Calcium **15**, 931 (2005).

[255] J. Rubin, C. Rubin, and C. R. Jacobs, Gene **367**, 1 (2006).

[256] J. Rubin, C. Rubin, and C. R. Jacobs, Gene **367**, 1 (2006).

[257] C. Huang and R. Ogawa, FASEB Journal : Official Publication of the Federation of American Societies for Experimental Biology **24**, 3625 (2010).

[258] L. A. Lowery and D. Van Vactor, Nature Reviews. Molecular Cell Biology **10**, 332 (2009).

[259] R. O. L. Wong and A. Ghosh, Nature Reviews. Neuroscience **3**, 803 (2002).

[260] M. Tessier-Lavigne and C. S. Goodman, Science (New York, N.Y.) **274**, 1123 (1996).

[261] L. Luo and D. D. M. O'Leary, Annual Review of Neuroscience **28**, 127 (2005).

[262] E. W. Dent and F. B. Gertler, Neuron **40**, 209 (2003).

[263] P. C. Georges, N. M. Hadzimichalis, E. S. Sweet, and B. L. Firestein, Molecular Neurobiology **38**, 270 (2008).

[264] F. J. Ahmad, J. Hughey, T. Wittmann, A. Hyman, M. Greaser, and P. W. Baas, Nature Cell Biology **2**, 276 (2000).

[265] S. Geraldo and P. R. Gordon-Weeks, Journal of Cell Science **122**, 3595 (2009).

[266] A. L. Lucido, (2009).

[267] F. Suarez, P. Thostrup, D. Colman, and P. Grutter, Dev Neurobiol **73**, 98 (2013).

[268] D. J. Chew, J. W. Fawcett, and M. R. Andrews, Progress in Brain Research **201**, 253 (2012).

[269] F. Bradke, J. W. Fawcett, and M. E. Spira, Nature Reviews. Neuroscience **13**, 183 (2012).

[270] B. J. Dickson, Science (New York, N.Y.) **298**, 1959 (2002).

[271] P. Carmeliet and M. Tessier-Lavigne, Nature **436**, 193 (2005).

[272] H. Song and M. Poo, Nature Cell Biology **3**, E81 (2001).

[273] A. J. Aguayo, G. M. Bray, M. Rasminsky, T. Zwimpfer, D. Carter, and M. Vidal-Sanz, The Journal of Experimental Biology **153**, 199 (1990).

[274] G. Yiu and Z. He, Nature Reviews. Neuroscience **7**, 617 (2006).

[275] P. J. Horner and F. H. Gage, Nature **407**, 963 (2000).

[276] S. Ramon y Cajal, Journal of Neurology and Psychopathology **9**, 750 (1928).

[277] F. Suarez, P. Thostrup, D. Colman, and P. Grutter, (2012).

[278] J. S. Goldman, M. A. Ashour, M. H. Magdesian, N. X. Tritsch, S. N. Harris, N. Christofi, R. Chemali, Y. E. Stern, G. Thompson-Steckel, P. Gris, S. D. Glasgow, P. Grutter, J.-F. Bouchard, E. S. Ruthazer, D. Stellwagen, and T. E. Kennedy, The Journal of Neuroscience : The Official Journal of the Society for Neuroscience **33**, 17278 (2013).

[279] A. Hughes, Journal of Anatomy **87**, 150 (1953).

[280] M. Kuwajima, J. Spacek, and K. M. Harris, Neuroscience **251**, 75 (2013).

[281] K. Franze and J. Guck, Reports on Progress in Physics **73**, 094601 (2010).

[282] P. W. Baas and F. J. Ahmad, Brain : A Journal of Neurology **136**, 2937 (2013).

[283] G. Bi and M. Poo, Nature **401**, 792 (1999).

[284] T. H. Muller, D. Swandulla, and H. U. Zeilhofer, J Neurophysiol **77**, 3218 (1997).

[285] P. Lamoureux, S. Heidemann, and K. E. Miller, Journal of Visualized Experiments : JoVE e2509 (2011).

[286] W. E. Brownell, F. Qian, and B. Anvari, Biophysical Journal **99**, 845 (2010).

[287] J. Dai and M. P. Sheetz, Biophysical Journal **68**, 988 (1995).

[288] P. D. Maia and J. N. Kutz, Journal of Computational Neuroscience **36**, 141 (2014).

[289] B. Xu, X. Feng, and R. D. Burdine, Developmental Biology **348**, 3 (2010).

[290] K. Pearson, Philosophical Magazine Series 5 **50**, 157 (1900).

[291] A. E. Goodship, T. J. Lawes, and C. T. Rubin, Journal of Orthopaedic Research : Official Publication of the Orthopaedic Research Society **27**, 922 (2009).

[292] E. Ozcivici, Y. K. Luu, C. T. Rubin, and S. Judex, PloS One **5**, e11178 (2010).

[293] S. Srinivasan, S. C. Agans, K. A. King, N. Y. Moy, S. L. Poliachik, and T. S. Gross, Bone **33**, 946 (2003).

[294] M. Pellegrino, M. Pellegrini, and B. Calabrese, Archives Italiennes de Biologie **135**, 319 (1997).

[295] R. Tamma, G. Colaianni, C. Camerino, A. Di Benedetto, G. Greco, M. Strippoli, R. Vergari, A. Grano, L. Mancini, G. Mori, S. Colucci, M. Grano, and A. Zallone, FASEB Journal : Official Publication of the Federation of American Societies for Experimental Biology **23**, 2549 (2009).

[296] J. R. Mauney, S. Sjostorm, J. Blumberg, R. Horan, J. P. O'Leary, G. Vunjak-Novakovic, V. Volloch, and D. L. Kaplan, Calcified Tissue International **74**, 458 (2004).

[297] S. Gomis-Ruth, C. J. Wierenga, and F. Bradke, Curr Biol **18**, 992 (2008).

[298] G. M. Lopez-Ayon, H.-Y. Liu, S. Xing, O. M. Maria, J. M. LeDue, H. Bourque, P. Grutter, and S. V. Komarova, F1000Research 1 (2014).

[299] S. L. Xia and J. Ferrier, Journal of Cellular Physiology **167**, 148 (1996).

[300] S. L. Xia and J. Ferrier, Journal of Cellular Physiology **167**, 148 (1996).

[301] E. Marcello, R. Epis, C. Saraceno, and M. Di Luca, Advances in Experimental Medicine and Biology **970**, 573 (2012).

[302] A. Molleman, 13 (2003).